Electrospun Polymer Nanofiber Scaffolds for Functionalized Long Sub-Micron Diameter Cables

Citation

Aydin, Aykut. 2019. Electrospun Polymer Nanofiber Scaffolds for Functionalized Long Sub-Micron Diameter Cables. Doctoral dissertation, Harvard University, Graduate School of Arts & Sciences.

Permanent link

http://nrs.harvard.edu/urn-3:HUL.InstRepos:42029599

Terms of Use

Share Your Story

Accessibility

Electrospun Polymer Nanofiber Scaffolds for Functionalized Long Sub-Micron Diameter Cables

A dissertation presented

by

Aykut Aydin

to

The Department of Chemistry and Chemical Biology

in partial fulfillment of the requirements
for the degree of
Doctor of Philosophy
in the subject of
Chemistry

Harvard University
Cambridge, Massachusetts
April 2019

Dissertation Advisor: Roy G. Gordon   Aykut Aydin

Electrospun Polymer Nanofiber Scaffolds for Functionalized Long Sub-Micron Diameter Cables

Abstract

Utilization of thin, flexible, and conductive wires that are twisted in a bundle has significantly improved the performance of communication devices operating at MHz frequencies. For GHz frequency applications, available wires are too large in diameter, and development of new synthetic methodologies are required to shrink such wires to sub-micron scale while retaining their mechanical strength, along with electrical conductivity and insulation from neighboring wires. We present a new method for the preparation of strong, flexible and centimeter-long insulated nanocables on a high-strength polymer nanofiber scaffold. Single strands of poly(*m*-phenylene isophthalamide) nanofibers with diameters in the range of 300 - 600 nm were prepared via electrospinning onto a rotating collector. Coaxial coatings of a variety of metals and insulators were performed to illustrate the materials generality of the methodology. The flexibility and compatibility with extreme deposition conditions (up to 350 °C) offered by this nanofiber scaffold paves the way for the improvement of communication devices in the GHz range.

Table of Contents

Acknowledgements

I would like to express my gratitude toward all my colleagues, friends, and family who supported me during my graduate studies.

First, I would like to thank Professor Roy Gordon for being a very kind, supportive, and insightful mentor. I feel really fortunate to have gotten the chance to learn how to be a researcher from Roy. He has a very positive attitude towards science and always knows how to derive understanding from seemingly complicated or unsuccessful experiments. I really appreciate the many helpful suggestions he had when my experiments were not producing the results we wanted, and I am always impressed by his creativity and breadth of knowledge in a large variety of fields. Roy has an amazing record of translating science to real-world technologies, and I feel truly honored to have learned from him while working on a project with such technological potential.

I would also like to thank my defense committee members Professor Jennifer Lewis and Professor Vinothan N. Manoharan. They both participated in my graduate advising committee and provided many helpful suggestions over the years. Professor Manoharan is our collaborator on the Nano Litz project, and I have had many interesting discussions with him and his students during our project meetings. Professor Lewis's research has been very inspiring to me, and we routinely discuss and learn from her papers in our group. I really appreciate her presence and feedback on our project.

particular have provided me with much needed support, feedback and guidance, and they continuously inspire me as scientists and role models. I would also like to thank my friends from the Department of Chemistry: Guiping Wang, Jeep Veerasak Srisuknimit, Dr. Jennifer Wei, Dr. Siheng (Sean) You, Dr. Andrew Mayfield, and Dr. Amymarie Bartholomew. It has been truly wonderful that we maintained our friendship and frequent get-togethers since the beginning of our graduate studies.

Finally, I would like to express my deepest gratitude towards my family. My parents, Ayşe Berrin Aydin and Zafer Aydin, have always enabled me in pursuing my interests and helped me achieve my dreams. I would like to thank my partner Tim Catala for always making me feel like the luckiest person. I could not have asked for a more supportive and kinder partner to share my life with over the past few years.

Table of Figures

Chapter 1   Introduction

1.1 The NanoLitz Project

The Internet of Things (IoT) continues to spread across all different industries and household systems. According to one projection, while the number of non-IoT devices (such as laptops, handhelds, and PCs) will continue to grow modestly, the number of IoT devices will more than double in the next 5 years.[1] This growth will bring with it an increased demand to better share the limited telecommunication bands. While many advances have been made in the field of MEMS inductors that operate in the GHz frequency range, their performance remains limited by ohmic losses.[2] These losses contribute to signal broadening when such devices emit signals to communicate, and broader emissions lead to increased interference between devices. Developing strategies to lower ohmic losses would lead to better performance and fewer problems due to crowding for telecommunication devices that connect the Internet of Things.
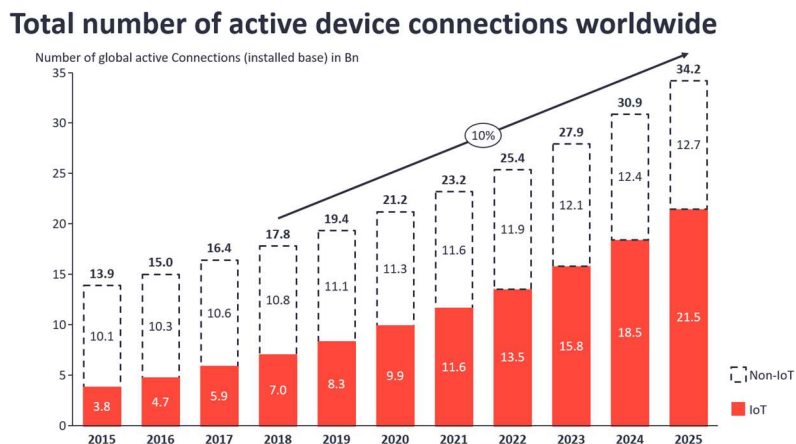
Figure 1.1. Growth projection for the number of devices connected to the Internet. [1]

As high frequency alternating current (AC) flows through a wire, it tends to crowd the outer shell of the wire with decreasing coward density toward the center. The higher the frequency of the current, the thinner this region of electron flow becomes. As the area the current can flow through decreases with increasing AC frequency, the effective resistance current experiences increases. This phenomenon is described as the skin effect since the current flows through the outer "skin" of a wire, and it causes ohmic losses in power transmission or widening of emissions in the case of a radio frequency transmitter, leading to low quality factors (a figure of merit for inductors). Wider emission bands contribute to spectral crowding and interference between devices.

Skin effect is caused by the alternating current in a wire causing an alternating magnetic field around it. This magnetic field induces concentric eddy currents that oppose the flow the main current at the center of the wire while enhancing it at the outer region (Figure 1.2).
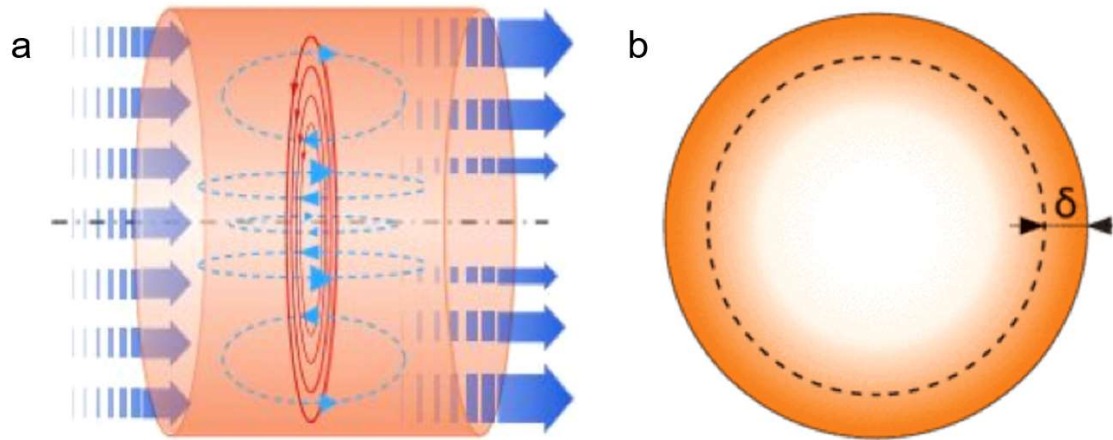
Figure 1.2. Skin effect. (a) Representation of the mechanism behind skin effect. Blue

arrows indicate the alternating current flow. Red circles represent the alternating

magnetic field this generates. Light blue loops show the eddy currents that oppose current

flow at the center of the wire. (b) Cross section profile of the current flow distribution at

high frequency, with darker orange corresponding to the highest density of current flow.

Skin effect can be characterized by skin depth (δ) that corresponds to the distance

from a conductor's surface where the current has dropped to 1/e of its value near the

surface. It can be approximated as follows:

$$\delta = \sqrt{\frac{\rho}{\pi f \mu}}$$

In this equation, ρ is resistivity of the conductor, f is the frequency of the AC, and μ is the

magnetic permeability of the conductor.
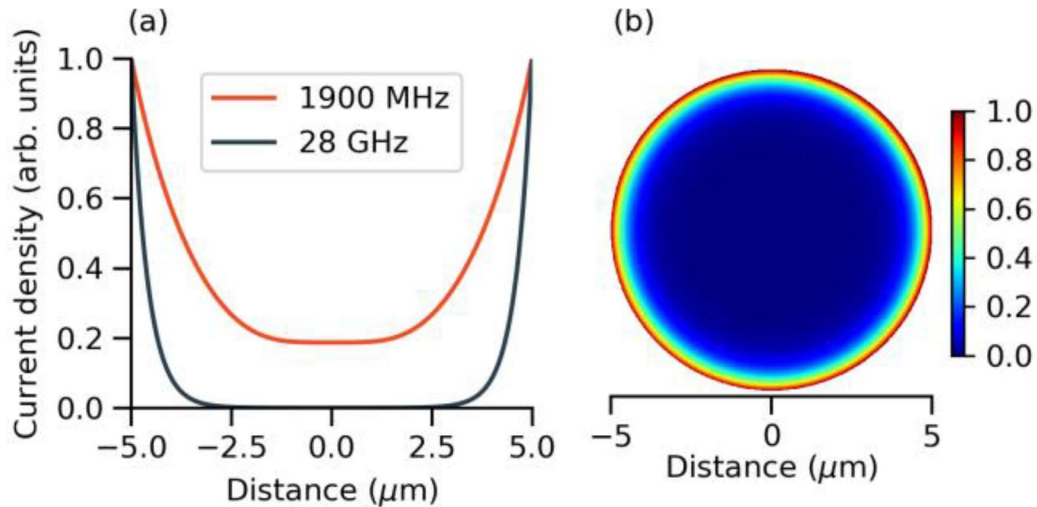
Figure 1.3. Current distribution profile along the cross section of a 10 μm wire. (a-b) Finite element model simulations of current density in a commercial copper wire (58 AWG, ~ 10 μm in diameter). (a) Normalized current density profile at two different AC frequencies. (b) Normalized current density map at 28 GHz. (Reproduced from Russel et al. 2018)[2]

Litz wires are structures consisting of many thin insulated wires bundled in a symmetrical fashion through twisting or braiding, and they are commonly used in devices that operate with less than MHz frequencies. As high frequency AC flows through a litz wire, instead of having the skin depth-limited area of one single large wire, it can flow through the outer shell of each of the thin wires in the bundle, which increases the area it can effectively flow through, improving the quality factor. In a bundle of wires, the resistance a wire experiences is highest at the center due to so called proximity effects, formed through a similar mechanism with skin effect where the magnetic field generated

by the current flowing through an outer wire counters the electron flow at the center of the wire. To minimize the losses due to proximity effects, a litz bundle needs to be symmetrically arranged such that each wire has equal length at the center and the periphery of the bundle as the others, which can e.g. be achieved by making hierarchical twists (twists, twists of twists, etc.).[2]

The smaller wires that constitute a litz wire ideally need to be comparable in diameter to the skin depth of its material for the device frequency, which for 1 GHz for a copper wire is about 2 µm and even thinner for higher frequencies.[2] While litz wires could provide many benefits by lowering ohmic losses in GHz frequency devices, existing methods of making conductive wires (often drawing) do not scale down to micron or submicron diameters needed to form the litz wires at these frequencies. Even if such thin insulated wires were available, existing manipulation methods to make twists or braids would not be gentle enough to handle such thin wires without breaking them. Overarching goal of the NanoLitz project is to develop such methods for making and manipulating ~ 1 m diameter insulated conductive wires to form a litz wire, and to show their electrical performance for GHz frequency applications.[2]

1.2 Overview of Electrospinning

Electrospinning is a polymer processing method for making polymer nanofibers with nanometer or micrometer diameters. It was invented in 1990 and popularized in 1990s.[3-4] In electrospinning, a high potential is applied to a polymer solution being extruded through a nozzle, and a collector is placed across from it that is typically grounded or

held at a high potential of opposite polarity to the solution (Figure 1.4).[5] High potential to

the solution can be applied through a conductive nozzle or an electrode can be immersed

in the polymer solution.
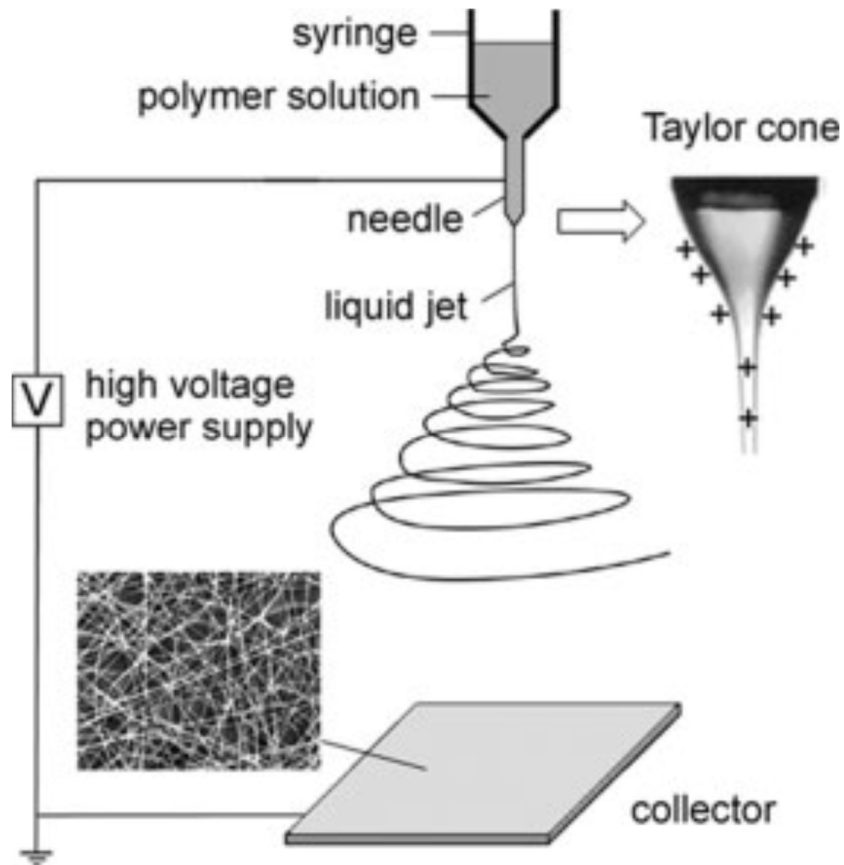
Figure 1.4. Diagram of an electrospinning setup with a spinning jet. At the tip of the

needle (or nozzle), the solution gets polarized and forms a Taylor cone when high

potential is applied, ejecting a jet of solution that eventually dries into polymer fibers that

get deposited at the collector. (Reprinted with permission from reference 5. Copyright

2004 John Wiley and Sons.)

Application of electrospinning has been reviewed for many fields: tissue engineering scaffolds,[6-8] air filtration,[9] water purification,[10-15] energy,[10, 16-17] and others.[10, 18-19] Most of these applications leverage the nanoporous nature of electrospun polymer mats in one way or another. They can also be functionalized with drugs or additives.[20-21] The polymer fibers can be pyrolyzed to make porous carbon electrodes.[22-23] Alternatively, the polymer solution could be preloaded with inorganic precursors for added functionality,[24] and optionally the polymer can be burnt away after the spinning to leave behind inorganic nanofibers.[17, 25-26]

Most existing applications of electrospinning focus on making non-woven mats of fibers as the one shown in the inset in Figure 1.4. For the purpose of making single suspended nanofibers, there needs to be much greater control over the control of the fiber deposition. There are some reports of single nanofibers being tested mechanically, and occasional single nanofibers form or can generated in various setups, but a method of making single nanofibers consistently and with high throughput has not been shown. Nevertheless, aligning such fibers could well follow existing literature protocols for aligning nanofibers in non-woven mats, e.g. for improved cell adhesion in a tissue scaffold or for better flow characteristics in membranes. We ultimately use a spoked-drum collector that is rotating at a high speed[27] which combines both mechanical and electrostatic means of improving fiber alignment, but there are multiple strategies for aligning nanofibers in electrospinning. Typical strategies include some form of a rotating

7

collector for mechanical alignment,[28-32] collector arrangements that have a hole or a gap for electrostatic control over alignment,[33-35] adding auxiliary electrodes[36] or a combination of multiple of these elements.[37] Compared to the strategies that end up with the nanofibers on a flat substrate, the wired-drum is particularly useful for developing single nanofibers, because their alignment and separation can be readily evaluated by eye under bright illumination after each experiment.
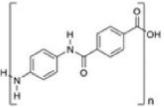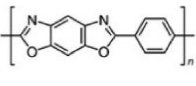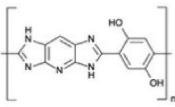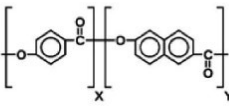
1.3 PMIA and Other High Temperature Stable Polymers

In this project, we are interested in developing polymer nanofibers that serve as a deposition methods-general scaffold for making insulated nanocables. The deposition methods generality includes both physical vapor deposition methods, which can be carried at large scale at Draper to support their high demand for metalized nanocables, as well as atomic layer deposition (ALD) and chemical vapor deposition (CVD) methods that our group has developed. We are particularly interested in applying conformal metal coatings using CVD, and these often require deposition temperatures at or above 200 °C.[38-40] This requirement guided us towards studying the electrospinning behavior for polymers with thermal stability that exceeds 200 °C.

Another property we could seek in the polymer is high strength, and high strength polymers such as Kevlar would be most ideal for making strong polymer nanofiber backbone. Park and Rutledge recently shared a perspective on high strength fibers where they list the major high performance fibers as shown in Table 1.1.[41] As can be seen from this table, they all require highly corrosive concentrated acid solvents. Furthermore, they

note that high strength fiber-forming chemistries are relatively well explored, with the last major chemistry (M5) coming almost 20 years ago, and that they expect "greater opportunity lies in manipulating polymer architecture or processing" going forward.[41-42]

Table 1.1. Properties of high performance fibers. (Reprinted with permission from reference 41. Copyright 2017 American Chemical Society.)[41, 43]

Type		Lyotropic Liquid Crystal		Thermotropic Liquid Crystal
Trade name	Kevlar®	Zylon®	M5	Vectran®
Monomer structure				
Polymer	PPTA	PBO	PIPD	Vectra
Solvent	sulfuric acid	polyphosphoric acid	polyphosphoric acid	N/A (Melt)
Fiber density (g/cm3)	1.44 - 1.47	1.56	1.7	1.4
Young's modulus (GPa)	130-185	270	330	65
Tensile strength (GPa)	3.6-4.1	5.8	3.5-4.5	2.9
$T_{melt} < T_{decompose}$?	No	No	No	No
Decomposition temp. (°C)	550	650	500	400

There exists literature in electrospinning Kevlar, however it seems the morphology is difficult to control, and the high boiling point sulfuric acid solvent either requires heating the solution during electrospinning to 80-90 °C and/or removing via a dry-jet-wet-electrospinning approach.[44] These requirements discouraged us from pursuing Kevlar directly, and we expect similar challenges to be present for the rest of these high strength polymers which require concentrated acid solvents. An exception to that is PBO (Zylon), which can be dissolved in a lower boiling mixture of

methanesulfonic acid and trifluoroacetic acid. Our experiences with attempting to spin PBO is described in Section 4.3.

Because of the difficulty of spinning from a concentrated acid solution, we next considered polymers that can be solubilized in common organic solvents that would still have adequate thermal stability. We investigated the electrospinning behavior of these polymers towards making single nanofibers. Polymers we studied include Nomex, polyetherimide, Kapton, Nova Clear, CP1, and P84. Many of these polymers have thermal stabilities beyond 400°C and yield strength values around a few hundred MPa.

Poly(*m*-phenylene isophthalamide) (PMIA, commercially known as Nomex) is one of the first polymers we tested, and it ultimately supported the development of the nanowires described in this work in Chapters 2, 3 and 5. Our findings from electrospinning experiments with the other polymers are discussed in Chapter 4.

1.4 Overview of the Coated Nanofiber Fabrication Process

This section and parts of Chapter 2, 3 and Appendix A are reproduced with permission from ACS Applied Polymer Materials, in press. Unpublished work copyright 2019 American Chemical Society.

To make a NanoLitz bundle, we need insulated nanowires with sub-micron diameter as described in Figure 1.5. Sub-micron diameter wires, pillars, and similar structures are finding increasing applications in biology,[45-48] photonics,[49] electronics,[50-52] and other related fields.[53-57] Various processes for preparing such nanowires have been

developed.[53-62] Existing methods can offer excellent control over phase purity, diameter, spatial position and electrical properties, but nanowire length is often limited, with some of the longest nanowires prepared by vapor-liquid-solid processes being reported in the millimeter scale.[63] Such short lengths would be exceedingly difficult to manipulate into symmetrical twist or braid in the form of a litz wire, and such short litz wires would be likely be too short to further package into an inductor. Thus, we set out to develop a new method for making insulated nanowires that are >1 cm. Beyond the NanoLitz wires, a material-agnostic method to fabricate centimeter-length nanowires will enable a host of other applications, such as stable electrodes for neural integration.[64]
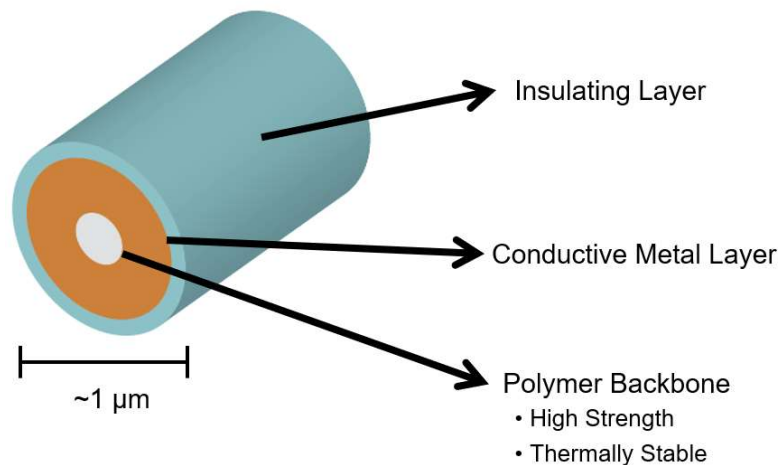
Figure 1.5. Target structure for making NanoLitz wires.

In Chapters 2 and 3, we present a method to fabricate centimeter-long nanowires from a wide variety of materials via deposition on a nanofiber. We first fabricated nanofiber scaffolds by electrospinning a solution containing poly(*m*-phenylene

isophthalamide) (PMIA, commercial names: Nomex or Teijinconex). Centimeter lengths of individual PMIA nanofibers were then suspended across customized fixtures and coated with a range of different materials via a variety of deposition processes. We chose PMIA for the scaffold material because of its high thermal stability that allows high temperature vapor depositions to be applied, demonstrated here up to 350 °C, as well as its relatively high mechanical strength[65-66] which allows the nanofiber core to serve as a strong backbone for supporting the nanowires. We have additionally demonstrated the ability to create multilayer coaxial nanostructures including submicron-scale, electrically insulated metal wires and micron-scale coaxial and triaxial wires. Such multilayered wire structures have potential photonic[67] and X-ray focusing applications.[68-75]

Figure 1.6 describes the various stages of the coated fiber preparation process. First, electrospinning is used to make PMIA fibers out of a polymer solution as described in Chapter 2. A rotating collector is used to align the fibers, and the nozzle from which the

solution ejects is translated during the experiment to distribute the fibers along the
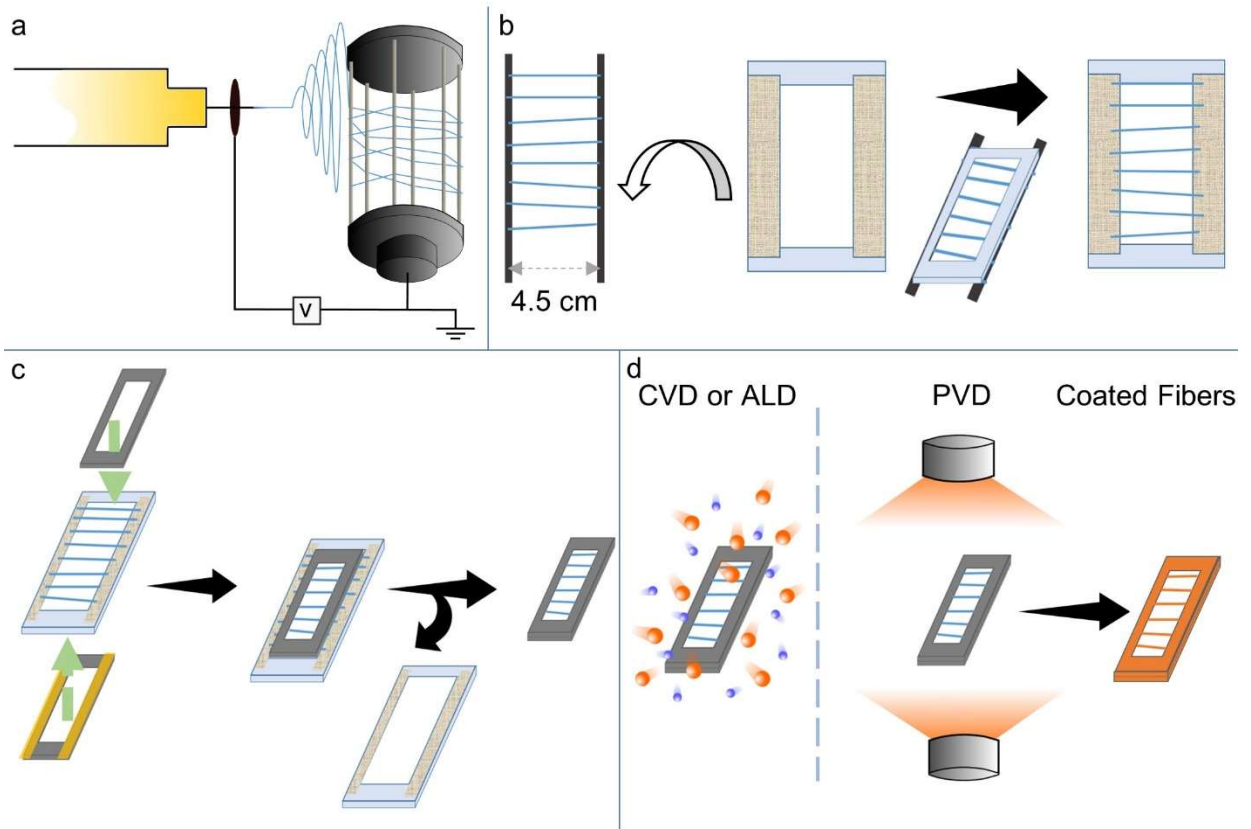
Figure 1.6. Electrospinning and fiber transfer protocol. (a) Diagram of the electrospinning experiment. (b) Schematic of fiber transfer steps from the spoked drum onto a holder with double-sided tape. The final holder can be used directly for sputter coating or as an intermediate holder to transfer for CVD/ALD holders. (c) Transfer of fibers onto metal holder for deposition experiments. The top frame can be attached using screws, avoiding any tape that might interfere with CVD or ALD experiments. (d) Scheme of metal coating onto polymer nanofibers with different methods.

collector. Both solution and electrospinning parameters were optimized to attain aligned single fibers. Solution parameters involve the composition of the polymer solution, and the electrospinning parameters refer to settings such as solution feed rate, spinning voltage, and rotation speed of the collector. Two kinds of rotating collectors were used in this work: a rotating drum collector[29-30] covered with a removable Al-foil substrate for initial solution parameter optimization, and a spoked-drum collector[27] for producing free standing fibers (Figure 1.6-a). Fibers are visible to naked eye under bright illumination (Figure 1.7), which allows for more facile optimization of the electrospinning parameters needed to align fibers. PMIA fibers suspended between the spokes are also more conveniently transferable onto fixtures used for fiber coating, compared to fibers on an Al-foil.

After the fibers were collected on the spoked-drum collector, they were transferred onto fixtures that hold the fibers in suspended form. The exact dimensions of the fixtures used varied and depended on factors such as size constraints of various deposition chambers. Fibers were first transferred from the spoked-drum collector to a fixture with double-sided tape affixed to its long edges (Figure 1.6-b). For chemical vapor deposition (CVD) and atomic layer deposition (ALD), fibers were then transferred to a second fixture that anchored fibers between two steel frames with a gasket of polyimide film (Figure 1.6-c).
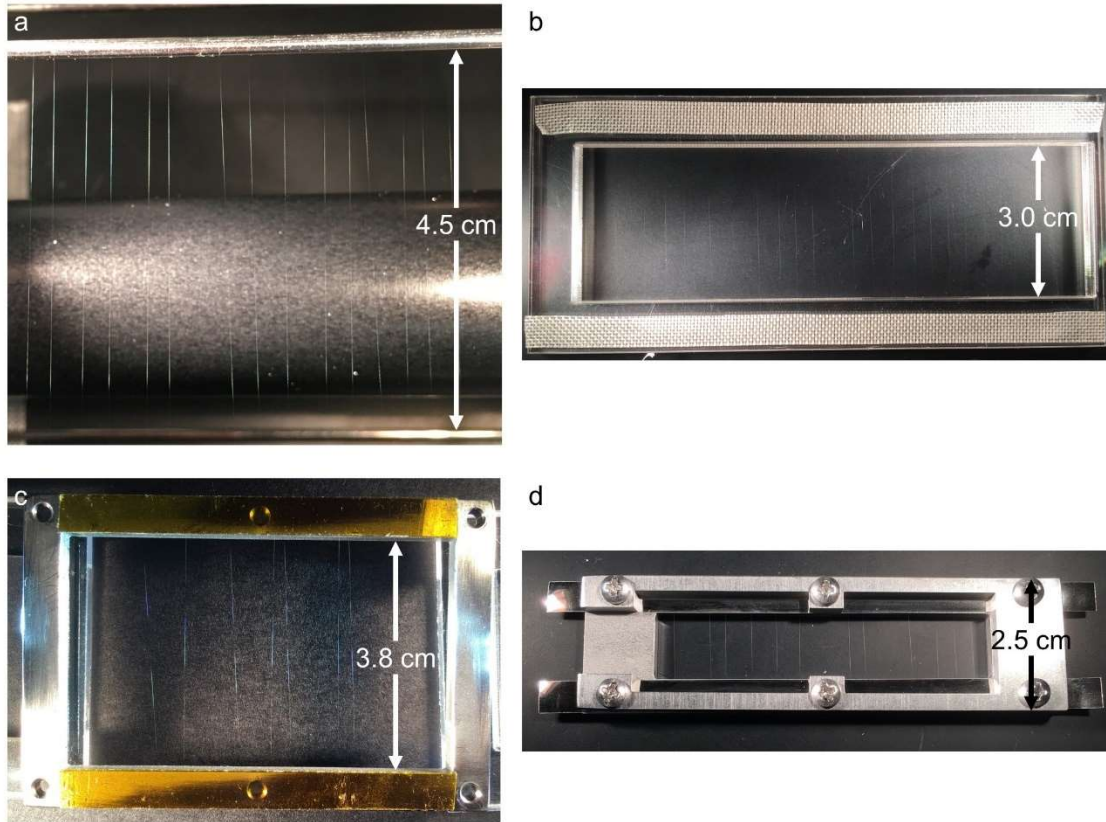
Figure 1.7. Photographs of fibers. (a) Photograph of aligned fibers on part of the rotating spoked-drum collector. (b) Photograph of aligned fibers on a transfer holder. (c) Photograph of our widest holder with some single fibers attached by double-sided tape that is suitable for PVD. (d) Photograph of Co coated fibers with CVD. Bright illumination from the side results in scattered light from the submicron fibers, making them visible to the naked eye.

Once the fibers were suspended in the appropriate fixture, they were coated with functional materials (Figure 1.6-d) as described in Chapter 3. For line-of-sight deposition processes such as PVD, the fixture was typically inverted at least once during the

deposition process to improve conformality. For conformal coatings by ALD or CVD, only one coating step gave coatings with uniform thickness all around the fibers.

1.5 Thesis outline

The thesis is organized in the following way:

- Chapter 1 introduces the NanoLitz project, electrospinning method, and overview of the choice of polymer for nanowire scaffolds, and an overview of the long nanowire fabrication method.

- Chapter 2 describes the development of PMIA electrospinning of single long and suspended nanofibers as well as their properties.

- Chapter 3 describes how PMIA nanofibers were coated with various metals and insulators.

- Chapter 4 overviews our progress on electrospinning other thermally stable polymers for the Nano Litz project.

- Chapter 5 describes the development of a reel-to-reel manufacture of polymer nanofiber scaffold based nanocables.

- Chapter 6 provides an overview of our conclusions and possible future research directions.

1.6 References

1.   State of the IoT 2018: Number of IoT devices now at 7B - Market accelerating. https://iot-analytics.com/state-of-the-iot-update-q1-q2-2018-number-of-iot-devices-now-7b/ (accessed 4/3/2019).

2.   Russell, K. J.; Aydin, A.; Carter, D. J. D.; Kim, E.; Lewis, P. H.; Sun, L.; Gong, X.; Chang, C.; Gordon, R.; Duwel, A., Fabrication of sub-micron metal wires for high-frequency litz wire. In *Hilton Head Workshop 2018*, 2018.

3.   Cooley, J. F. Electrical method of dispersing fluids. US745276A, 1903/11/24/, 1903.

4.   Tucker, N.; Stanger, J. J.; Staiger, M. P.; Razzaq, H.; Hofman, K., The History of the Science and Technology of Electrospinning from 1600 to 1995:. *https://doi.org/10.1177/155892501200702S10* **2012**.

5.   Li, D.; Xia, Y., Electrospinning of Nanofibers: Reinventing the Wheel? *Advanced Materials* **2004,** *16* (14), 1151-1170.

6.   Khorshidi, S.; Solouk, A.; Mirzadeh, H.; Mazinani, S.; Lagaron, J. M.; Sharifi, S.; Ramakrishna, S., A review of key challenges of electrospun scaffolds for tissue-engineering applications. *Journal of Tissue Engineering and Regenerative Medicine* **2016,** *10* (9), 715-738.

7.   Cipitria, A.; Skelton, A.; Dargaville, T. R.; Dalton, P. D.; Hutmacher, D. W., Design, fabrication and characterization of PCL electrospun scaffolds—a review. *Journal of Materials Chemistry* **2011,** *21* (26), 9419-9453.

8.   Rieger, K. A.; Birch, N. P.; Schiffman, J. D., Designing electrospun nanofiber mats to promote wound healing – a review. *Journal of Materials Chemistry B* **2013,** *1* (36), 4531-4541.

9.   Sundarrajan, S.; Tan, K. L.; Lim, S. H.; Ramakrishna, S., Electrospun Nanofibers for Air Filtration Applications. *Procedia Engineering* **2014,** *75*, 159-163.

10.   *Electrospun Nanofibers for Energy and Environmental Applications*. Springer Berlin Heidelberg: Berlin, Heidelberg, 2014.

11.   Feng, C.; Khulbe, K. C.; Matsuura, T.; Tabe, S.; Ismail, A. F., Preparation and characterization of electro-spun nanofiber membranes and their possible applications in water treatment. *Separation and Purification Technology* **2013,** *102*, 118-135.

12.   Wang, X.; Yu, J.; Sun, G.; Ding, B., Electrospun nanofibrous materials: a versatile medium for effective oil/water separation. *Materials Today* **2016,** *19* (7), 403-414.

13.   Liao, Y.; Loh, C.-H.; Tian, M.; Wang, R.; Fane, A. G., Progress in electrospun polymeric nanofibrous membranes for water treatment: Fabrication, modification and applications. *Progress in Polymer Science* **2018,** *77*, 69-94.

14.   Tijing, L. D.; Choi, J.-S.; Lee, S.; Kim, S.-H.; Shon, H. K., Recent progress of membrane distillation using electrospun nanofibrous membrane. *Journal of Membrane Science* **2014,** *453*, 435-462.

15.   Ahmed, F. E.; Lalia, B. S.; Hashaikeh, R., A review on electrospinning for membrane fabrication: Challenges and applications. *Desalination* **2015,** *356*, 15-30.

16.   Jung, J.-W.; Lee, C.-L.; Yu, S.; Kim, I.-D., Electrospun nanofibers as a platform for advanced secondary batteries: a comprehensive review. *J. Mater. Chem. A* **2016,** *4* (3), 703-750.

17.   Ludwig, T.; Bohr, C.; Queraltó, A.; Frohnhoven, R.; Fischer, T.; Mathur, S., Chapter One - Inorganic Nanofibers by Electrospinning Techniques and Their Application in Energy Conversion and Storage Systems. In *Semiconductors and Semimetals*, Mokkapati, S.; Jagadish, C., Eds. Elsevier: 2018; Vol. 98, pp 1-70.

18.   Panthi, G.; Park, M.; Kim, H.-Y.; Lee, S.-Y.; Park, S.-J., Electrospun ZnO hybrid nanofibers for photodegradation of wastewater containing organic dyes: A review. *Journal of Industrial and Engineering Chemistry* **2015,** *21*, 26-35.

19.   Ding, B.; Wang, M.; Yu, J.; Sun, G., Gas Sensors Based on Electrospun Nanofibers. *Sensors* **2009,** *9* (3), 1609-1624.

20.   Zeng, J.; Xu, X.; Chen, X.; Liang, Q.; Bian, X.; Yang, L.; Jing, X., Biodegradable electrospun fibers for drug delivery. *Journal of Controlled Release* **2003,** *92* (3), 227-231.

21.   Hu, X.; Liu, S.; Zhou, G.; Huang, Y.; Xie, Z.; Jing, X., Electrospinning of polymeric nanofibers for drug delivery applications. *Journal of Controlled Release* **2014,** *185*, 12-21.

22.   Sun, J.; Zeng, L.; Jiang, H. R.; Chao, C. Y. H.; Zhao, T. S., Formation of electrodes by self-assembling porous carbon fibers into bundles for vanadium redox flow batteries. *Journal of Power Sources* **2018,** *405*, 106-113.

23.   Zhang, L.; Aboagye, A.; Kelkar, A.; Lai, C.; Fong, H., A review: carbon nanofibers from electrospun polyacrylonitrile and their applications. *Journal of Materials Science* **2014,** *49* (2), 463-480.

24.   Jain, N.; Chakraborty, J.; Tripathi, S. K.; Nasim, M., Fabrication and characterization of in situ synthesized iron oxide-modified polyimide nanoweb by needleless electrospinning. *Journal of Applied Polymer Science* **2014,** *131* (12), n/a-n/a.

25.   Khalil, A.; Hashaikeh, R.; Jouiad, M., Synthesis and morphology analysis of electrospun copper nanowires. *Journal of Materials Science* **2014,** *49* (8), 3052-3065.

26.   Choi, S.-S.; Lee, S. G.; Im, S. S.; Kim, S. H.; Joo, Y. L., Silica nanofibers from electrospinning/sol-gel process. *Journal of Materials Science Letters* **2003,** *22* (12), 891-893.

27.   Katta, P.; Alessandro, M.; Ramsier, R. D.; Chase, G. G., Continuous Electrospinning of Aligned Polymer Nanofibers onto a Wire Drum Collector. *Nano Letters* **2004,** *4* (11), 2215-2218.

28.   Kim, K. W.; Lee, K. H.; Khil, M. S.; Ho, Y. S.; Kim, H. Y., The effect of molecular weight and the linear velocity of drum surface on the properties of electrospun poly(ethylene terephthalate) nonwovens. *Fibers and Polymers* **2004,** *5* (2), 122-127.

29.   Sundaray, B.; Subramanian, V.; Natarajan, T. S.; Xiang, R.-Z.; Chang, C.-C.; Fann, W.-S., Electrospinning of continuous aligned polymer fibers. *Applied Physics Letters* **2004,** *84* (7), 1222-1224.

30.   Chen, W.; Weng, W., Continuous aligned poly(*meta*-phenylene isophthalamide) fibers via stable jet electrospinning. *Journal of Applied Polymer Science* **2016,** *133* (29), 43690.

31.   Moon, S.; Choi, J.; Farris, R. J., Preparation of aligned polyetherimide fiber by electrospinning. *Journal of Applied Polymer Science* **2008,** *109* (2), 691-694.

32.   Edmondson, D.; Cooper, A.; Jana, S.; Wood, D.; Zhang, M., Centrifugal electrospinning of highly aligned polymer nanofibers over a large area. *Journal of Materials Chemistry* **2012,** *22* (35), 18646-18652.

33.   Dan Li; Yuliang Wang, a.; Xia*, Y., Electrospinning of Polymeric and Ceramic Nanofibers as Uniaxially Aligned Arrays. **2003**.

34.   Zhong, W.; Li, F.; Chen, L.; Chen, Y.; Wei, Y., A novel approach to electrospinning of pristine and aligned MEH-PPV using binary solvents. *Journal of Materials Chemistry* **2012,** *22* (12), 5523-5530.

35.   Rafique, J.; Yu, J.; Yu, J.; Fang, G.; Wong, K. W.; Zheng, Z.; Ong, H. C.; Lau, W. M., Electrospinning highly aligned long polymer nanofibers on large scale by using a tip collector. *Applied Physics Letters* **2007,** *91* (6), 063126.

36.   Arras, M. M. L.; Grasl, C.; Bergmeister, H.; Schima, H., Electrospinning of aligned fibers with adjustable orientation using auxiliary electrodes. *Science and Technology of Advanced Materials* **2012,** *13* (3), 035008.

37.   Afifi, A. M.; Nakajima, H.; Yamane, H.; Kimura, Y.; Nakano, S., Fabrication of Aligned Poly(L-lactide) Fibers by Electrospinning and Drawing. *Macromolecular Materials and Engineering* **2009,** *294* (10), 658-665.

38.   Yang, J.; Li, K.; Feng, J.; Gordon, R. G., Direct-liquid-evaporation chemical vapor deposition of smooth, highly conformal cobalt and cobalt nitride thin films. *J. Mater. Chem. C* **2015,** *3* (46), 12098-12106.

39.   Feng, J.; Gong, X.; Lou, X.; Gordon, R. G., Direct-Liquid-Evaporation Chemical Vapor Deposition of Nanocrystalline Cobalt Metal for Nanoscale Copper Interconnect Encapsulation. *ACS Applied Materials & Interfaces* **2017,** *9* (12), 10914-10920.

40.   Li, Z.; Gordon, R. G.; Pallem, V.; Li, H.; Shenai, D. V., Direct-Liquid-Injection Chemical Vapor Deposition of Nickel Nitride Films and Their Reduction to Nickel Films. **2010**.

41.   Park, J. H.; Rutledge, G. C., 50th Anniversary Perspective: Advanced Polymer Fibers: High Performance and Ultrafine. *Macromolecules* **2017,** *50* (15), 5627-5642.

42.   Park, J. H.; Rutledge, G. C., Ultrafine high performance polyethylene fibers. *Journal of Materials Science* **2018,** *53* (4), 3049-3063.

43.   Chae, H. G.; Kumar, S., Rigid-rod polymeric fibers. *Journal of Applied Polymer Science* **2006,** *100* (1), 791-802.

44.   Yao, J.; Jin, J.; Lepore, E.; Pugno, N. M.; Bastiaansen, C. W. M.; Peijs, T., Electrospinning of p-Aramid Fibers. *Macromolecular Materials and Engineering* **2015,** *300* (12), 1238-1245.

45.   Patolsky, F.; Zheng, G.; Lieber, C. M., Nanowire sensors for medicine and the life sciences. *Nanomedicine* **2006,** *1* (1), 51-65.

46.   Zhang, A.; Lieber, C. M., Nano-Bioelectronics. *Chemical Reviews* **2016,** *116* (1), 215-257.

47.   Zhou, W.; Dai, X.; Lieber, C. M., Advances in nanowire bioelectronics. *Rep. Prog. Phys.* **2017,** *80* (1), 016701.

48.   He, B.; Morrow, T. J.; Keating, C. D., Nanowire sensors for multiplexed detection of biomolecules. *Current Opinion in Chemical Biology* **2008,** *12* (5), 522-528.

49.   Yan, R.; Gargas, D.; Yang, P., Nanowire photonics. *Nature Photonics* **2009,** *3* (10), 569-576.

50.   Lu, W.; Lieber, C. M., Semiconductor nanowires. *Journal of Physics D: Applied Physics* **2006,** *39* (21), R387-R406.

51.   Li, Y.; Qian, F.; Xiang, J.; Lieber, C. M., Nanowire electronic and optoelectronic devices. *Materials Today* **2006,** *9* (10), 18-27.

52.   Tian, B.; Kempa, T. J.; Lieber, C. M., Single nanowire photovoltaics. *Chemical Society Reviews* **2009,** *38* (1), 16-24.

53.   Dasgupta, N. P.; Sun, J.; Liu, C.; Brittman, S.; Andrews, S. C.; Lim, J.; Gao, H.; Yan, R.; Yang, P., 25th Anniversary Article: Semiconductor Nanowires - Synthesis, Characterization, and Applications. *Advanced Materials* **2014,** *26* (14), 2137-2184.

54.   Patolsky, F.; Lieber, C. M., Nanowire nanosensors. *Materials Today* **2005,** *8* (4), 20-28.

55.   Hu, J.; Odom, T. W.; Lieber, C. M., Chemistry and Physics in One Dimension: Synthesis and Properties of Nanowires and Nanotubes. *Accounts of Chemical Research* **1999,** *32* (5), 435-445.

56.   Lieber, C. M., Nanoscale Science and Technology: Building a Big Future from Small Things. *MRS Bulletin* **2003,** *28* (7), 486-491.

57.   Xia, Y.; Yang, P.; Sun, Y.; Wu, Y.; Mayers, B.; Gates, B.; Yin, Y.; Kim, F.; Yan, H., One‐Dimensional Nanostructures: Synthesis, Characterization, and Applications. *Advanced Materials* **2003,** *15* (5), 353-389.

58.   Hulteen, J. C.; Martin, C. R., A general template-based method for the preparation of nanomaterials. *Journal of Materials Chemistry* **1997,** *7* (7), 1075-1087.

59.   Shankar, K. S.; Raychaudhuri, A. K., Fabrication of nanowires of multicomponent oxides: Review of recent advances. *Materials Science and Engineering: C* **2005,** *25* (5-8), 738-751.

60.   Fu, Y. Q.; Colli, A.; Fasoli, A.; Luo, J. K.; Flewitt, A. J.; Ferrari, A. C.; Milne, W. I., Deep reactive ion etching as a tool for nanostructure fabrication. *Journal of Vacuum Science & Technology B: Microelectronics and Nanometer Structures* **2009,** *27* (3), 1520.

61.   Ozel, T.; Zhang, B. A.; Gao, R.; Day, R. W.; Lieber, C. M.; Nocera, D. G., Electrochemical Deposition of Conformal and Functional Layers on High Aspect Ratio Silicon Micro/Nanowires. *Nano Letters* **2017,** *17* (7), 4502-4507.

62.   Hyun, J. K.; Zhang, S.; Lauhon, L. J., Nanowire Heterostructures. *Annual Review of Materials Research* **2013,** *43* (1), 451-479.

63.   Hu, P.; Dong, S.; Zhang, X.; Gui, K.; Chen, G.; Hu, Z., Synthesis and characterization of ultralong SiC nanowires with unique optical properties, excellent thermal stability and flexible nanomechanical properties. *Scientific Reports* **2017,** *7* (1), 3011.

64.   Luan, L.; Wei, X.; Zhao, Z.; Siegel, J. J.; Potnis, O.; Tuppen, C. A.; Lin, S.; Kazmi, S.; Fowler, R. A.; Holloway, S., Ultraflexible nanoelectronic probes form reliable, glial scar–free neural integration. *Science Advances* **2017,** *3* (2), e1601966.

65.   Chen, K.; Zhang, S.; Liu, B.; Mao, X.; Sun, G.; Yu, J.; Al-Deyab, S. S.; Ding, B., Large-scale fabrication of highly aligned poly(m-phenylene isophthalamide) nanofibers with robust mechanical strength. *RSC Adv.* **2014,** *4* (86), 45760-45767.

66.   Zhang, S.; Liu, H.; Yin, X.; Li, Z.; Yu, J.; Ding, B., Tailoring Mechanically Robust Poly(*m*-phenylene isophthalamide) Nanofiber/nets for Ultrathin High-Efficiency Air Filter. *Scientific Reports* **2017,** *7*, 40550.

67.   Kim, K.-H.; No, Y.-S.; Chang, S.; Choi, J.-H.; Park, H.-G., Invisible Hyperbolic Metamaterial Nanotube at Visible Frequency. *Scientific Reports* **2015,** *5*, 16027.

68.   Saitoh, K.; Inagawa, K.; Kohra, K.; Hayashi, C.; Iida, A.; Kato, N., Fabrication and Characterization of Multilayer Zone Plate for Hard X-Rays. *Jpn. J. Appl. Phys.* **1988,** *27* (11A), L2131.

69.   Kamijo, N.; Tamura, S.; Suzuki, Y.; Handa, K.; Takeuchi, A.; Yamamoto, S.; Ando, M.; Ohsumi, K.; Kihara, H., Fabrication of a hard x-ray sputtered-sliced Fresnel phase zone plate. *Review of Scientific Instruments* **1997,** *68* (1), 14-16.

70.   Tamura, S., High-Energy X-ray Microprobe by Multilayer Zone Plate and Microscopy at SPring-8. **2004,** *716*, 144-147.

71.   Koyama, T.; Takano, H.; Konishi, S.; Tsuji, T.; Takenaka, H.; Ichimaru, S.; Ohchi, T.; Kagoshima, Y., Circular multilayer zone plate for high-energy x-ray nano-imaging. *Review of Scientific Instruments* **2012,** *83* (1), 013705.

72.   Mayer, M.; Grévent, C.; Szeghalmi, A.; Knez, M.; Weigand, M.; Rehbein, S.; Schneider, G.; Baretzky, B.; Schütz, G., Multilayer Fresnel zone plate for soft X-ray microscopy resolves sub-39 nm structures. *Ultramicroscopy* **2011,** *111* (12), 1706-1711.

73.   Mayer, M.; Keskinbora, K.; Grévent, C.; Szeghalmi, A.; Knez, M.; Weigand, M.; Snigirev, A.; Snigireva, I.; Schütz, G., Efficient focusing of 8 keV X-rays with multilayer Fresnel zone plates fabricated by atomic layer deposition and focused ion beam milling. *J Synchrotron Radiat* **2013,** *20* (Pt 3), 433-440.

74.   Keskinbora, K.; Robisch, A.-L.; Mayer, M.; Sanli, U. T.; Grévent, C.; Wolter, C.; Weigand, M.; Szeghalmi, A.; Knez, M.; Salditt, T.; Schütz, G., Multilayer Fresnel zone plates for high energy radiation resolve 21 nm features at 1.2 keV. *Opt. Express* **2014,** *22* (15), 18440-18453.

75.   Sanli, U. T.; Keskinbora, K.; Grevent, C.; Szeghalmi, A.; Knez, M.; Schiitz, G., Multilayer Fresnel Zone Plates for X-ray Microscopy. *Microscopy and Microanalysis* **2015,** *21* (S3), 1987-1988.

Chapter 2   Electrospinning of PMIA Nanofibers

2.1 Introduction

PMIA was chosen because of its superior thermal stability and relatively high mechanical strength (Chapter 1).[1-2] Electrospinning of PMIA has previously demonstrated.[1-11] PMIA can be dissolved in the presence of various high-boiling organic solvents in the presence of LiCl or $CaCl_2$. This chapter describes the development of the PMIA electrospinning process for making single aligned nanofibers, challenges encountered along the way, and their solutions. PMIA nanofiber protocol we developed is adequately robust and has been the basis of nanowires being used by our collaborators for the Nano Litz development.

2.2 Electrospun PMIA Fibers and Their Properties

For the solution used in electrospinning, PMIA was dissolved in *N,N*-dimethylacetamide (DMAc) in the presence of a chloride salt that increases its solubility and the solution's electrical conductivity.[1-11] The electrospinning process was initially developed on a rotating drum collector with aluminum foil wrapping. It was found that using LiCl often leads to a self-bundling phenomenon[12-20] where by the jet forms 3D structures extending from the collector instead of steadily depositing fibers onto the collector's surface (Figure 2.1), and this makes it challenging to produce single fibers. Using $CaCl_2$ instead of LiCl,[21] keeping the electrospinning chamber at low humidity (below 20% RH),[20] and using a sufficiently high polymer concentration in the solution all

contribute to the elimination of self-bundling. Furthermore, at low polymer concentration, we also frequently observe branched fibers due to jet-splitting.[22-26]

Figure 2.1. Self-bundling of PMIA nanofibers dissolved in DMAc/LiCl.

By doing long depositions and using a lower polymer concentration to accelerate the fiber deposition rate, a thick non-woven mat of PMIA can be obtained, though the alignment gets worse due to repulsion from charges on previously deposited fibers (Figure 2.2-a). This thick mat was used in thermal gravimetric analysis (TGA) experiments to verify the chemical stability of the fibers at increased temperatures (Figure 2.2-b). Due to water absorbed by the $CaCl_2$, direct TGA of the mat gives a solvent loss signal starting at 100°C. However, if the fibers are first dried at 110°C for one hour, this mass loss starts at 300°C, presumably corresponding to the decomposition of $CaCl_2 \cdot xH_2O$. If the mat is washed with water, $CaCl_2$ is removed and the nanofiber mat shows thermally induced mass loss behavior equivalent to the bulk starting material, PMIA.
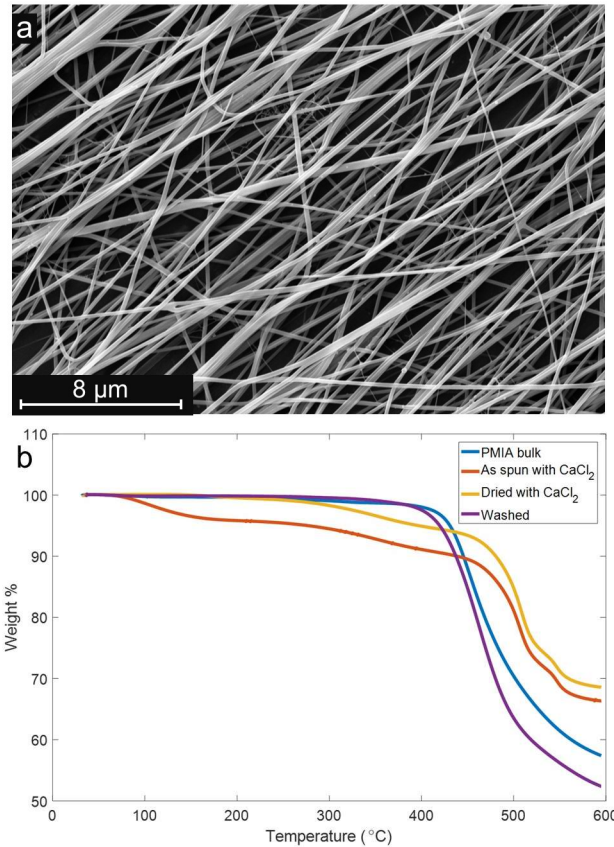
Figure 2.2. PMIA nanofibers and their thermal stability. (a) SEM image of a mat of PMIA fibers. (b) TGA results for PMIA bulk starting material, electrospun fibers containing hydrated CaCl2, CaCl2-containing fibers that were dried inside the TGA instrument, and fibers that were washed by immersion in water. (A 12 wt. % PMIA and 8 wt. % CaCl2 in DMAc was used to generate the thick mat used in TGA.)

With the spoked-drum collector (Figure 1.6-a),[27] aligned PMIA fibers that are ~1 cm apart can be obtained. A bright light source allows one to see where the sub-micron fibers are located even without a microscope. Fiber generation speed needs to match the rotation speed of the drum in order to obtain single nanofibers. Since our collector's

rotation speed is limited to 2500 rpm, fiber generation speed was reduced to match its speed by using high polymer concentration (typically at 17.5 wt. % PMIA) and low spinning voltage (down to 5 kV). For most general applicability, we sought to make the fibers round and smooth, but we also encountered various other morphologies. To observe the fiber morphology, fibers were coated with a metal layer as described in Chapter 3 and cross-sectioned using a focused ion beam (FIB). (Trying to cut the fibers with FIB without a metal coating often yielded cross-sections that are much less well-defined.) For fibers spun at room temperature and low nozzle voltage, a strong dependence of the fiber cross-section morphology on the chamber humidity was found (Figure 2.3-b): Round fibers only form when the chamber is at low humidity (<10%).

Ribbon formation being linked to chamber humidity suggests a mechanism where water diffusion into the spinning jet leads to phase separation since water is a non-solvent for PMIA.[1, 28] Subsequently, a solid shell is formed around the spinning jet, fixing its diameter, while the solution inside keeps evaporating (Figure 2.4). As the solution in the core dries up, it forms a porous structure which collapses under ambient pressure to form ribbons.[22, 29-32] Pores sometimes found within PMIA fibers spun at high humidity further support this hypothesis (Figure 2.4).
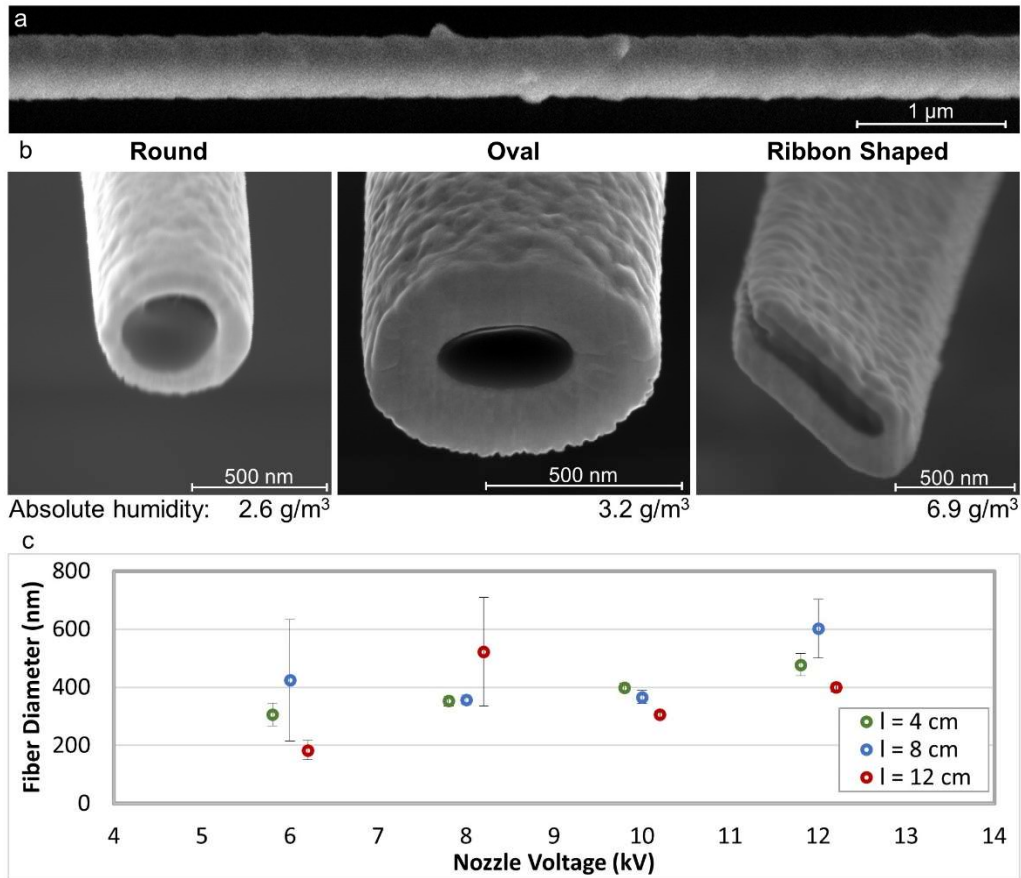
Figure 2.3. PMIA single fibers and their morphology. (a) Typical uncoated fiber SEM image. (b) Dependence of fiber morphology on absolute humidity of the electrospinning chamber (given in g/m3 below the images) when spun at low voltage. Fibers were sputter coated with a layer of metal from all sides to yield sharp cross-sections. (c) Fiber diameter dependence on the spinning voltage at the nozzle (with a grounded collector) for different nozzle-to-collector distances (l). (Error bars correspond to standard deviation from diameter measurements taken from multiple fibers. Voltage values for 4 and 12 cm points were shifted slightly to reduce overlapping points.)

Higher nozzle voltage seems to favor forming round fibers even at high chamber humidity (tested up to 20% RH), but the jet tends to become faster, making alignment more difficult, and fiber diameter slightly increases (Figure 2.3-c). At high voltage, the jet attains its equilibrium diameter rapidly before drying into a fiber, and this time is too short for polymer precipitation to occur by water diffusion. Another factor that can cause ribbon formation is the aging of the electrospinning solution droplet at the nozzle. If the droplet has been left to stand for too long prior to initiating the jet, the solution can partially dry out, lowering its cloud point. Then even lower humidity can cause it to precipitate and form occasional ribbon shaped fibers, even at the high voltage and low humidity conditions described above. Occasional ribbons formed this way account for the larger error bars in three of the data points in Figure 2.3-c. Otherwise, the diameter distribution is much narrower for the single fibers spun on the spoked-drum collector compared to fibers in a non-woven mat formed under similar conditions but with much longer spinning time (Figure 2.2-a). For the latter case, static charges from the previously deposited fibers likely alter the forces on the jet and widen the distribution.
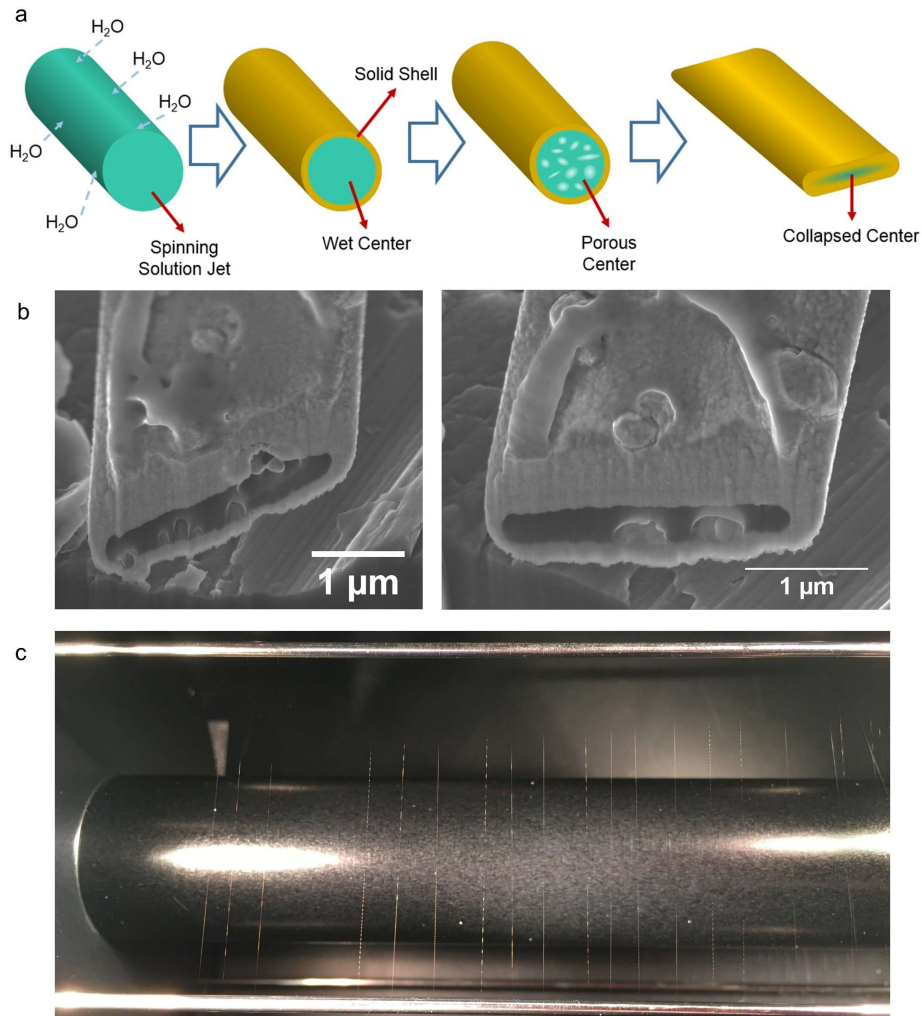
Figure 2.4. Ribbon shaped fiber formation and visual appearance. (a) Ribbon Shaped Fiber Formation Hypothesis: Water diffuses into the spinning jet, causing precipitation of the polymer on the periphery. Solidified shell fixes the outer diameter of the structure, and the still liquid solution within evaporates over time, leaving behind a porous structure. This porous structure gets crushed by ambient pressure to form the ribbon shape. (b) Some pores do not get crushed and are visible in the fiber cross sections. (c) Visual appearance of dashed lines that correlate with ribbon shaped fibers.

2.3 Humidity Dependent Morphology Evolution

After having initial success in controlling the fiber shape, we encountered a second morphological problem when the weather became warmer and more humid: We started observing increased roughness with protrusions or "bumps" on the fibers and their coated wire versions (Figure 2.5-a). While fibers are highly smooth just after electrospinning (Figure 2.5-b) when the chamber humidity is kept low, they quickly start forming protrusions when exposed to even mildly humid air at ~30% RH (Figure 2.5-c). We can roughly simulate longer term exposure to humid air by having a high flow rate of humid air go through a frame of suspended fibers (for shorter times), and this was done for Figure 2.5-d and e at relative humidity of 45% and 60%, respectively, which yields substantially porous crystallite growth out of the fibers. Fibers appear to remain smooth under 20% RH and start roughening when standing in air with RH somewhere between 20-25% at 24 °C.

a - typical fiber with protrusions

├── 10 μm ──┤

b - fiber preserved in vacuum

├─ 3 μm ─┤

c - exposed to ~30% r.h. air for 2 hours

├─ 3 μm ─┤

d - exposed to 45% r.h. air at high flow rate

├─ 3 μm ─┤

e - exposed to 60% r.h. air at high flow rate

├─ 30 μm ─┤
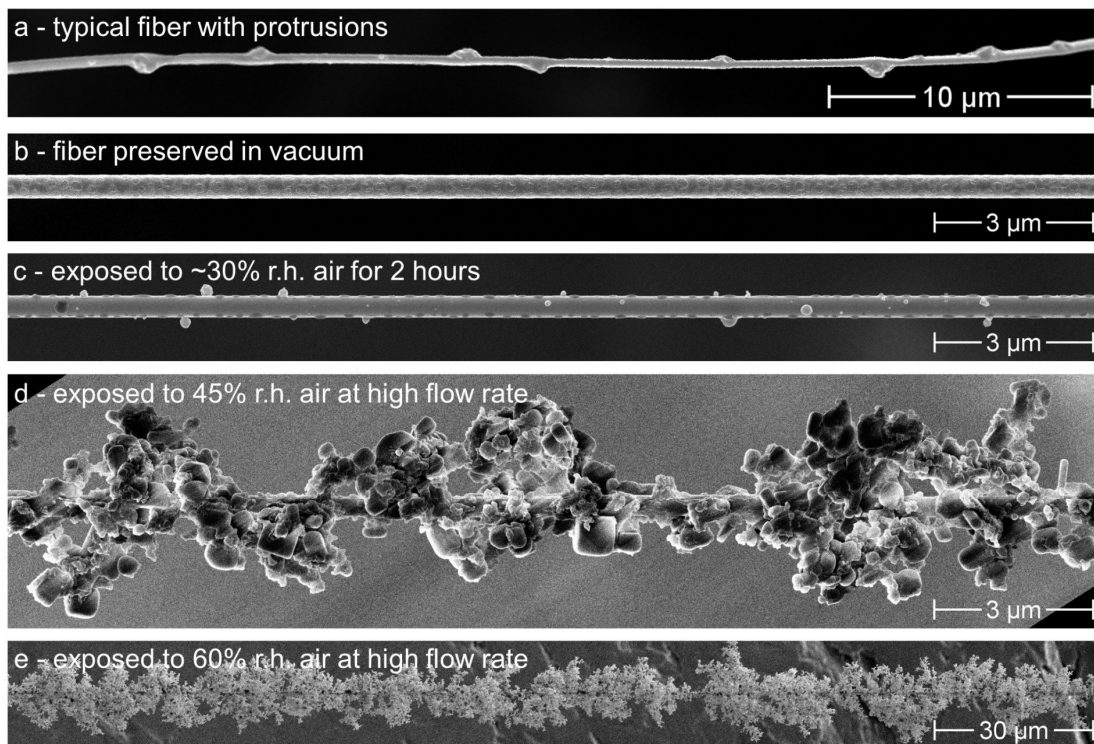
Figure 2.5. Humidity-dependent morphology evolution. (a) SEM image of a bumpy Pt/Pd alloy (80/20) coated PMIA fiber. (b) Fiber kept in vacuum for 2 hours before imaging. (c) Fiber exposed to ambient air at ~30% RH for 2 hours. (d) Fiber annealed with a high flow rate 45% RH air at room temperature. (e) Fiber annealed with a high flow rate 60% RH air at room temperature. (All fibers were coated with a thin layer of Pt/Pd alloy (80/20) to assist with imaging.)

The humidity-dependent formation of rough structures on the fibers is consistent with a mechanism based on deliquescence of $CaCl_2$: when air humidity is above the critical relative humidity of $CaCl_2$, it absorbs water to form a solution that beads up on the fibers (Figure 2.6). These droplets possibly form the porous protrusions on the fibers

when rapidly dried under vacuum during PVD. Slower evaporation under dry air seems to form crystallites shown in Figure 2.5-d and e, instead. Increased contrast is observed at the protrusions under TEM (Figure 2.6-b and c), which agrees with stronger electron scattering from heavier Ca and Cl atoms compared to PMIA. Cross-sections at the bumps reveal a darker core region with the same contrast as that of the core of smooth parts of the coated fibers, likely being that of PMIA, along with a porous brighter region around this core, likely being that of $CaCl_2$ (Figure 2.6-d and e).
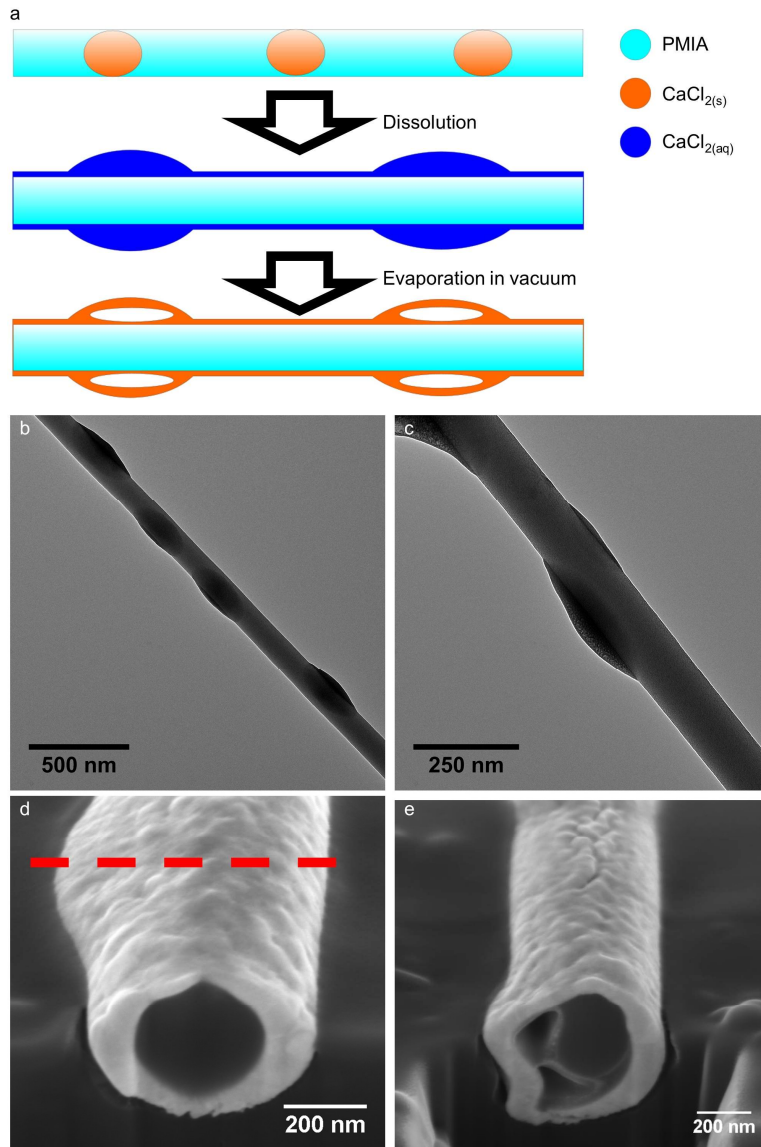
Figure 2.6. Morphology evolution mechanism. (a) Proposed mechanism for the formation

of the protrusions: $CaCl_2$ dissolves upon capturing air humidity, forming droplets along

the fibers. The droplets rapidly dry under vacuum to form porous beads. (b and c) TEM

images of PMIA fibers with protrusions. The protrusions appear darker, consistent with

the higher atomic mass of $CaCl_2$. (d) Cross section of a metal coated PMIA fiber at a

(Continued) round part. Also indicated with the red line is where the next cross section in part (e) was performed. (e) Cross section of the same fiber at a protrusion. The fiber core has different contrast than the porous structure.

Another evidence we had that suggested the protrusions are initially $CaCl_2$ solution droplets was obtained by placing fibers under humid conditions on carbon planchets. Inside the vacuum chamber of an SEM, the solution dries up, and we found what appeared to be solution droplets that wetted the carbon surface in circular regions around the fibers (Figure 2.7).
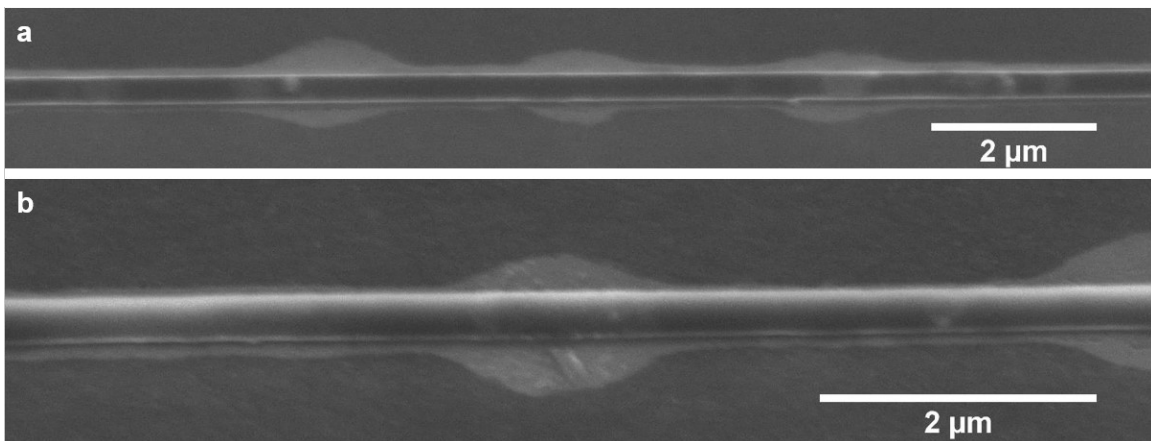
Figure 2.7. Uncoated fibers placed on a carbon surface under humid conditions. Droplets of $CaCl_2$ solution appear to have come off the fiber and wetted the surface.

For the most part, to keep wires from roughening for most of the experiments, the fibers were not washed, but simply kept in dry storage conditions (e.g., stored in vacuum, under nitrogen, or in dry air with silica gel packs). This includes any sample we prepared in since gaining this understanding for Draper, and all their samples were vacuum packed

with desiccant bags. We are interested in eliminating this humidity protection

requirement, and thus, the next section describes our efforts for removing the $CaCl_2$ from

the fibers.

2.4 Removing CaCl₂ from PMIA Nanofibers

We investigated various treatments for removing the $CaCl_2$ present in the fibers.

Directly exposing suspended fibers on a frame to a stream of water or trying to dip and

remove them from a container of water often breaks some of the fibers due to capillary

forces as the fibers pass the water-air interface. We tried lowering the surface tension of

water with surfactants or various alcohols with lower surface tension, but the fibers still

broke frequently.

One strategy that works is to support fibers temporarily with a smooth Si wafer

surface during direct washing by immersion in water, and then to remove the support.

This can be done in high yield and a clean Si surface does not seem to adhere to the

PMIA strongly, and once the support is removed, fibers can be left suspended. In fact,

under adequate ambient humidity, bringing the fibers in contact with the hydrophilic

surface of a thermal oxide coated Si wafer alone is enough to remove much of the salt.

The small salt solution droplets that coalesce on the nanofibers can wet the wafer surface

just as in Figure 2.7 and stay there as the fibers are then removed from the surface.

Results of this experiment are shown in Figure 2.8. While the fiber appeared to become

smoother, we were also able to locate dark regions arranged in long line patterns on the

wafer that likely correspond to the CaCl$_2$ salt left on the surface. This method is conceptually similar to wiping the salt solution off the fibers with paper towel.
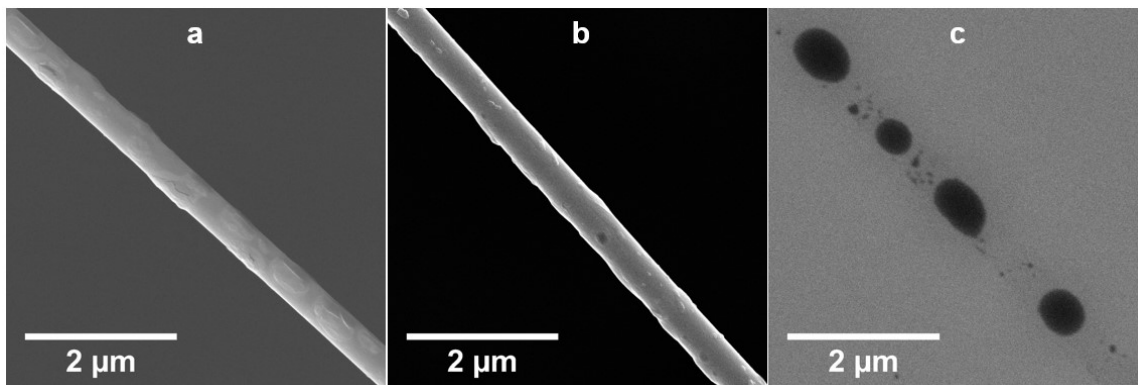
Figure 2.8. CaCl$_2$ removal by contact with a hydrophilic surface. (a) Surface structure of as spun fiber (with a thin layer of metal to assist with imaging). The small emblem shapes on the fiber are likely smaller droplets of CaCl$_2$. They are smaller than the previous examples since the weather became drier during these experiments and they were only left standing for one day. (b) Fibers from the same batch were brought into contact with a Si wafer and re-suspended. This procedure was repeated 3 times. The rough emblem shapes were not found on the fibers after this procedure when imaged under same conditions. (c) Impression of the fiber on the Si surface. The dark regions are likely residue of CaCl$_2$ that got transferred from the fibers.

We also considered methods of continuously putting small water droplets the nanofibers and letting them run down to provide a gentle wash. We investigated exposing fibers to a mist of steam in multiple conditions such that water droplets collect on the fibers and run down, washing away the salt. Hanging the fibers above a beaker full of

hot, steaming water seems to induce very large agglomerations of $CaCl_2$ along the fibers (Figure 2.9-a) as the droplets do not run down efficiently. Suspending a frame of fibers in front of a mist stream of water droplets generated from a sonicating humidifier does induce effective washing by movement of droplets along the fibers (Figure 2.10). This leads to relatively smooth fibers (Figure 2.9-b). We further exposed fibers washed with such a humidifier to a high flow rate of 60% RH air (akin to the conditions in Figure 2.5-e) and observed much less roughening as shown in Figure 2.9-c, which suggests that almost all of the salt is removed with the mist-based washing treatment. Coating fibers with the water diffusion barrier nanolaminate of Al_2O_3 and HfO_2 also dramatically reduced fiber roughening.

a - fiber treated with hot mist from water at 95°C for 6.5 hours
30 μm

b - washed fiber
3 μm

c - washed fiber → exposed to 60% r.h. air at high flow rate
3 μm
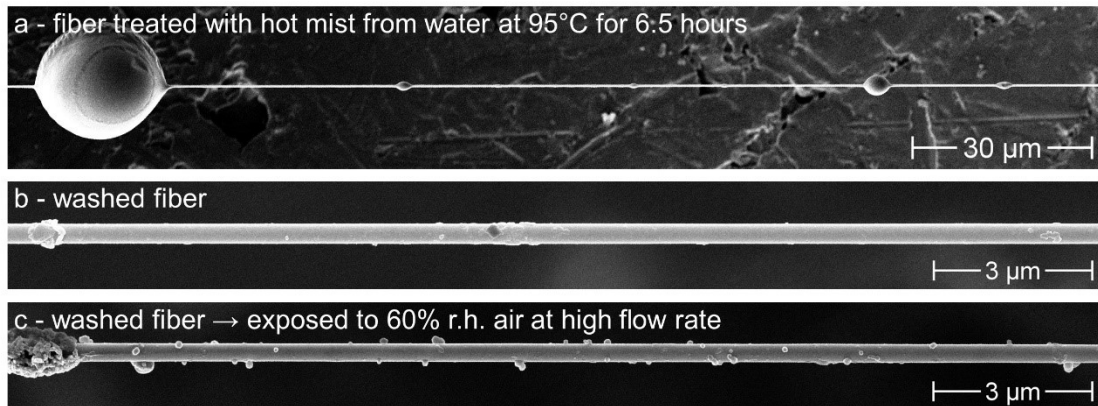
Figure 2.9. Gentle fiber washing experiments. (a) Fiber annealed over a beaker of hot water for 6.5 hours. (b) Fiber where $CaCl_2$ is mostly removed by treatment with an ultrasonic humidifier for 6 hours. (c) After $CaCl_2$ was removed with the previous treatment, fibers were exposed to a high flow rate of 60% RH air as in part d, but they did

(Continued) not roughen nearly as much. (All fibers were coated with a thin layer of Pt/Pd alloy (80/20) to assist with imaging.)
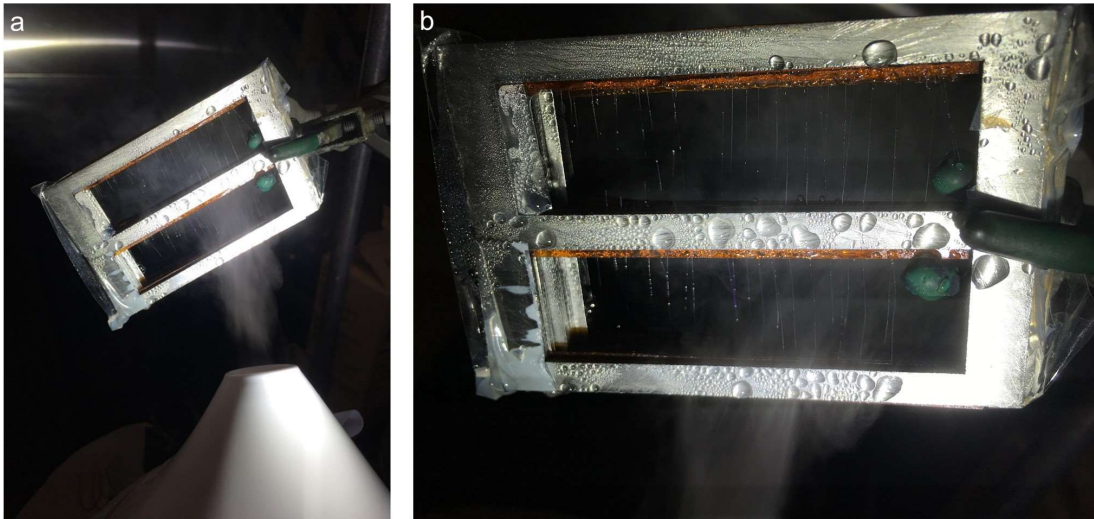
Figure 2.10. Water mist-based nanofiber washing for removing CaCl2. (a-b) Photographs of a stack of three holders with nanofibers being exposed to water mist from a sonicating humidifier. Small droplets accumulating on the fibers can be seen.

While we were able to demonstrate this water mist-based method for a few fibers, scaling it up to wash all the fibers we prepare for twisting experiments had proved infeasible. Our Draper colleagues suggested that supporting the fibers from the top side of the frame could be achieved much more reliably than what we had achieved with a Si wafer inserted from the bottom of the frame, and they identified anodized aluminum as a suitable and more convenient support substrate that the fibers do not stick to. Starting with fibers sitting on the double-sided tapes on two edges of a frame, we first covered the

exposed double-sided tapes with single sided Kapton tape, leaving the nanofibers sandwiched between two layers of tape at the edges. This was done so that the added support would not stick to the sample permanently. Then, we placed a matching sized anodized aluminum plate on top and fixed it using a binder clip. Once the fibers are supported, we lowered them into a washing bath. We kept them soaked for various numbers of hours, and then removed them. After this washing treatment and removing the support, fibers often look smooth or mostly smooth under an SEM (Figure 2.11), though they can pick up occasional dust particles in the water.
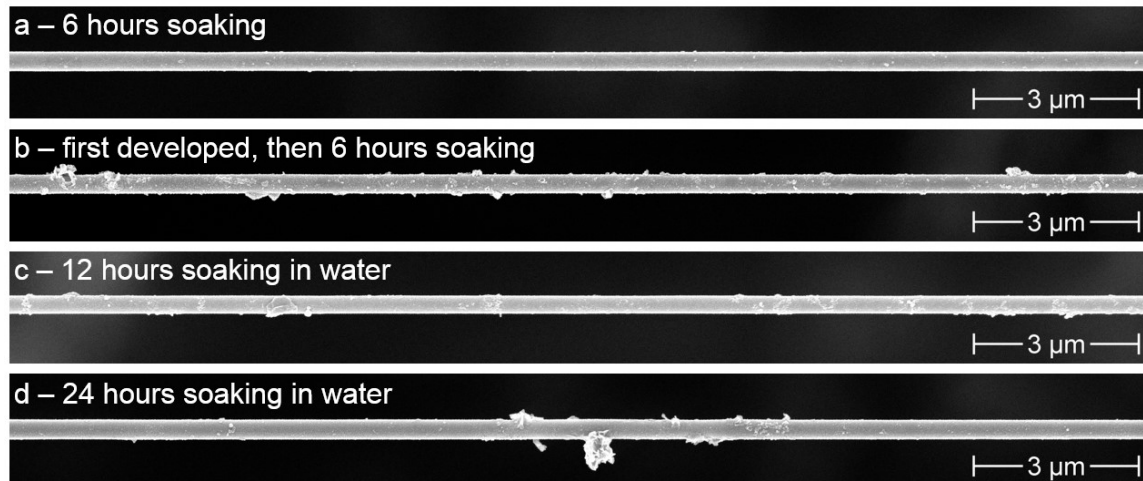
Figure 2.11. Fibers that were supported and soaked in water at room temperature for different lengths. In (b), fiber was first treated with high humidity air (akin to the conditions used to assess the salt removal, referred here as "developed"), and then soaked in water.

To better assess how well $CaCl_2$ is removed, we once again exposed the fibers to a high flow rate humid air for 2 hours and looked for morphological changes. If all the $CaCl_2$ salt were removed, the fibers should remain smooth after the humidity treatment, but depending on the conditions, they tend to grow some protrusions (Figure 2.12), though the protrusions remain much smaller than those unwashed fibers grow under the same extreme conditions (Figure 2.5-d). We also investigated whether the salt locked inside the fiber is getting better accessed when exposed to humid air compared to soaking underwater (Figure 2.11-b and Figure 2.12-b), but the difference seemed indistinguishable. Further soaking the samples up to 8 days did not improve the results.
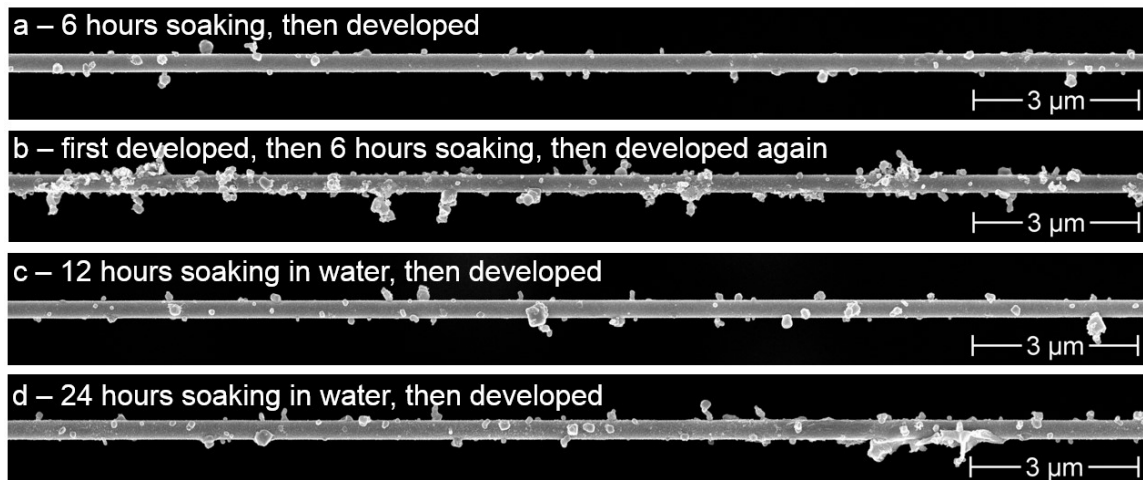
Figure 2.12. Fibers after soaking treatments with a support were treated to extreme humidity conditions to reveal any residual salt. The term developed is used to express this last treatment that reveals the remainder of the salt after washing. The fibers often tend to grow some crystallites after this treatment, even after the soaking, but the growths are much smaller compared to an unwashed fiber shown in Figure 2.5-e.

42

In terms of yield, breaking of fibers can be minimized by adequately drying the samples before removing the support at the end. This can be achieved by leaving the sample in a dry environment for more than an hour, otherwise the fibers tend to stick to the anodized aluminum surface. Also, we looked at stirring the water bath to improve mass transport but found that too high rate of stirring seem to press the fibers onto the support and break them at multiple points. There might still be potential gains from having some low rate stirring in washing speed.

The washing experiments were successful in significantly reducing the sensitivity of the PMIA nanofibers to humidity. This can be seen when comparing any of the washed fibers to the unwashed one shown in Figure 2.5-e with the much larger crystallites. With the supports reversibly attached using binder clips, we now have a substantially more scalable way of washing the fibers then before. We can start washing frames by the dozens in our regular workflow and use these less humidity-sensitive fibers in the coating and twisting experiments. Going forward, our goal in this part of the project is to eliminate the last bit of protrusions we can still detect after the extreme humidity testing, and we are continuing to test different conditions to that end. One issue might be related to the carbonic acid dissolved in water that can react with Ca^{2+} to make $CaCO_3$, which is sparingly soluble at ~10 mg/L. We could better avoid this by washing the fibers with a descaling agent or chelating the Ca^{2+} ions.

2.5 Routine Nanofiber Sample Preparation for NanoLitz Development

Once the PMIA nanofiber protocol was developed, fibers suspended on frames were routinely produced and transferred to Draper to support the NanoLitz twist making an electrical tests research.[33] After some iterations, frames of the type shown in Figure 2.13 became the standard holder for these samples. Routine samples had about 10-20 fibers / frame and a diameter of ~ 350 nm (from 8 cm distance and 10 kV length spinning conditions, see Figure 2.3-c). They were fixated within PS petri dishes with more double-sided tape.

Electrospun nanofibers are highly charged, and a static gun was applied to each sample and petri dish to minimize sagging from fibers getting attracted to the petri dish. If the static charges are not minimized, fibers sag significantly upon getting placed inside the dish, but immediately recover once lifted back out. However, if they are left in the sagging state where they are experience a continuous pulling force, they eventually become permanently sagging and cannot be conformally coated with PVD.
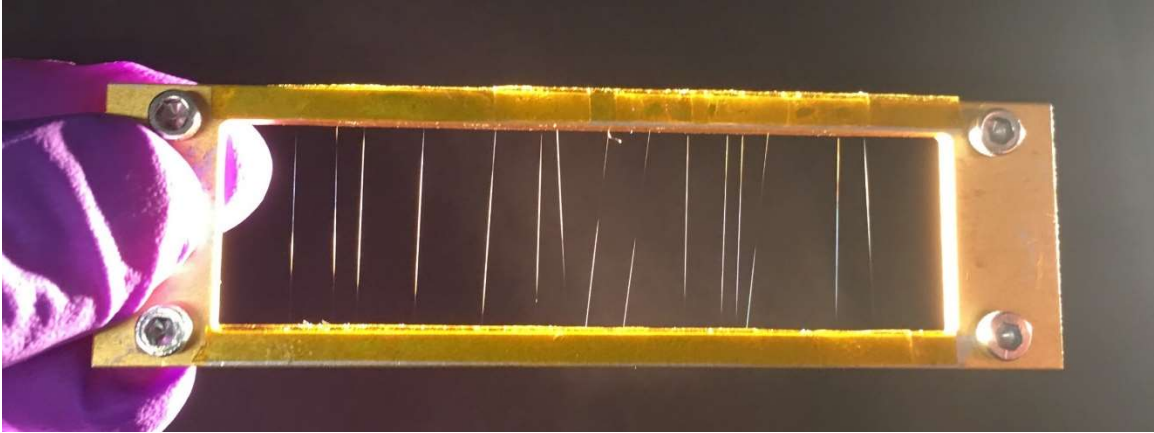
Figure 2.13. Photo of a typical PMIA nanofiber sample for Draper.

Well over a hundred such samples were prepared throughout this project, showcasing the reproducibility of these results. For the most part, these nanofibers were used without any washing at Draper. For the most recent ~ 150 samples, they were vacuum packed in groups of four along with a desiccant bag shortly after the spinning. Vacuum packing alone does not mitigate the roughening of unwashed fibers but adding in a desiccant bag seems to maintain smooth fibers.

2.6 Suspending Longer Fibers

To further scale up our process, we also practiced collecting and handling longer segments of these nanofibers. Nomex nanofibers can be unwound from the spoked drum collector and attached onto holders along their length. Nanofiber samples about 6 cm and 12 cm long were prepared in this way (Figure 2.14). In collaboration with Xian Gong, we also heated such long samples up to 200°C under nitrogen flow in conditions similar to what is used in the chemical vapor depositions of various metals we have available, and

we observed that the fibers remained intact upon such thermal treatments. Even longer

fiber segments can be handled using a spool of nanofibers. This is described in Chapter 5.
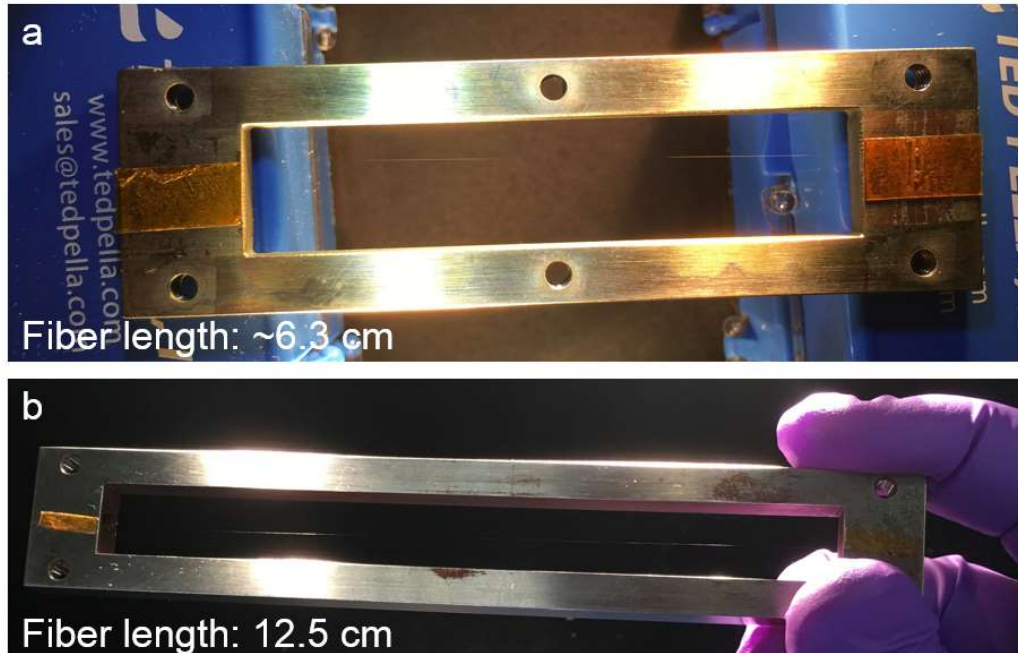
Figure 2.14. Longer Nomex nanofibers on holders. High temperature compatible Kapton

tape with adhesive on both sides was used for the attachment of the fibers.

2.7 Conclusions

PMIA nanofibers form the scaffold for the insulated nanocables for the Nano Litz

Project. Here, we described the electrospinning method for making single suspended

PMIA nanofibers on a frame, starting from earlier attempts to the final process we have

been using based on a spoked-drum setup. Description of fiber handling after the fibers

are prepared on the collector are described in Section 1.4 and Appendix D.

In Section 2.2, we reviewed the properties of the electrospun fibers, such as their thermal stability and diameter distribution, as well as the dependence of their morphology on the electrospinning chamber humidity. In Section 2.3, we described the observation of protrusions that form on the fibers depending on how dry their storage environment is. In Section 2.4, we listed some of the ways we have can minimize this humidity sensitivity by removing $CaCl_2$ from the nanofibers. Another strategy of minimizing humidity sensitivity, coating fibers with a water diffusion barrier, is described in Section 3.3. Section 2.5 describes our routine nanofiber manufacture process, which includes packaging of the fibers in desiccated vacuum bags – another way we minimize the protrusions that can otherwise form on the fibers. In Section 2.6, we demonstrate the handling of much longer segments of nanofibers.

In Chapter 3, these PMIA nanofibers form the base scaffold for all the metal or insulator coated wire deposition demonstrations. In Chapter 4, we explore the electrospinning of alternative polymers to replace PMIA which is inspired by the goal to eliminate the water sensitivity of the nanofiber scaffold described in Section 2.3. In Chapter 5, we describe the handling of meter-scale segments of the PMIA nanofibers using a reel-to-reel process.

2.8 References

1. Chen, K.; Zhang, S.; Liu, B.; Mao, X.; Sun, G.; Yu, J.; Al-Deyab, S. S.; Ding, B., Large-scale fabrication of highly aligned poly(m-phenylene isophthalamide) nanofibers with robust mechanical strength. *RSC Adv.* **2014,** *4* (86), 45760-45767.

2.   Zhang, S.; Liu, H.; Yin, X.; Li, Z.; Yu, J.; Ding, B., Tailoring Mechanically Robust Poly(*m*-phenylene isophthalamide) Nanofiber/nets for Ultrathin High-Efficiency Air Filter. *Scientific Reports* **2017,** *7*, 40550.

3.   Liu, W.; Graham, M.; Evans, E. A.; Reneker, D. H., Poly(*meta*-phenylene isophthalamide) nanofibers: Coating and post processing. *Journal of Materials Research* **2002,** *17* (12), 3206-3212.

4.   Wen, Y.; Hao, Y.; Meifang, Z.; Hongwei, B.; Yanmo, C., Poly(*m*‐Phenylene Isophthalamide) Ultrafine Fibers from an Ionic Liquid Solution by Dry‐Jet‐Wet‐Electrospinning. *Journal of Macromolecular Science: Physics* **2006,** *45* (4), 573-579.

5.   Zhao, T.; Wang, H.; Zhang, Y.; Wang, B.; Jiang, J., The Preparation and Characterization of Poly(*m*-phenylene isophthalamide) Fibers Using Ionic Liquids. *International Journal of Molecular Sciences* **2007,** *8* (7), 680-685.

6.   Yao, L.; Lee, C.; Kim, J., Fabrication of electrospun meta-aramid nanofibers in different solvent systems. *Fibers and Polymers* **2010,** *11* (7), 1032-1040.

7.   Oh, H. J.; Pant, H. R.; Kang, Y. S.; Jeon, K. S.; Pant, B.; Kim, C. S.; Kim, H. Y., Synthesis and characterization of spider-web-like electrospun mats of meta-aramid. *Polym. Int.* **2012,** *61* (11), 1675-1682.

8.   Oh, H. J.; Han, S. H.; Kim, S. S., A novel method for a high-strength electrospun meta-aramid nanofiber by microwave treatment. *Journal of Polymer Science Part B: Polymer Physics* **2014,** *52* (12), 807-814.

9.   Park, Y. S.; Lee, J. W.; Nam, Y. S.; Park, W. H., Breathable properties of *m*-Aramid nanofibrous membrane with high thermal resistance. *Journal of Applied Polymer Science* **2015,** *132* (8), 41545.

10.   Chen, W.; Weng, W., Ultrafine lauric–myristic acid eutectic/poly (*meta*-phenylene isophthalamide) form-stable phase change fibers for thermal energy storage by electrospinning. *Applied Energy* **2016,** *173*, 168-176.

11.   Chen, W.; Weng, W., Continuous aligned poly(*meta*-phenylene isophthalamide) fibers via stable jet electrospinning. *Journal of Applied Polymer Science* **2016,** *133* (29), 43690.

12.   Heikkila, P.; Harlin, A., Electrospinning of polyacrylonitrile (PAN) solution: Effect of conductive additive and filler on the process. *Express Polymer Letters* **2009,** *3* (7), 437-445.

13.   Paneva, D.; Manolova, N.; Rashkov, I.; Penchev, H.; Mihai, M.; Dragan, E. S., Self-organization of fibers into yarns during electrospinning of polycation/polyanion polyelectrolyte pairs. *Digest Journal of Nanomaterials and Biostructures* **2010,** *5*, 811-819.

14.   Yousefzadeh, M.; Latifi, M.; Amani-Tehran, M.; Teo, W.-E.; Ramakrishna, S., A Note on the 3D Structural Design of Electrospun Nanofibers. *Journal of Engineered Fabrics & Fibers (JEFF)* **2012,** *7* (2), 17-23.

15.   Sun, B.; Long, Y.-Z.; Yu, F.; Li, M.-M.; Zhang, H.-D.; Li, W.-J.; Xu, T.-X., Self-assembly of a three-dimensional fibrous polymer sponge by electrospinning. *Nanoscale* **2012,** *4* (6), 2134-2137.

16.   Shah, H. V.; Sandy, J. R.; Ireland, A. J.; Su, B., Electrospinning of 2D and 3D Silica Nanofibres from a Colloidal Solution. *Ceramics - Silikaty* **2012**, 112-116.

17.   Bonino, C. A.; Efimenko, K.; Jeong, S. I.; Krebs, M. D.; Alsberg, E.; Khan, S. A., Three-Dimensional Electrospun Alginate Nanofiber Mats via Tailored Charge Repulsions. *Small* **2012,** *8* (12), 1928-1936.

18.   Cai, S.; Xu, H.; Jiang, Q.; Yang, Y., Novel 3D Electrospun Scaffolds with Fibers Oriented Randomly and Evenly in Three Dimensions to Closely Mimic the Unique Architectures of Extracellular Matrices in Soft Tissues: Fabrication and Mechanism Study. *Langmuir* **2013,** *29* (7), 2311-2318.

19.   Poologasundarampillai, G.; Wang, D.; Li, S.; Nakamura, J.; Bradley, R.; Lee, P. D.; Stevens, M. M.; McPhail, D. S.; Kasuga, T.; Jones, J. R., Cotton-wool-like bioactive glasses for bone regeneration. *Acta Biomaterialia* **2014,** *10* (8), 3733-3746.

20.	Yoon, J. W.; Park, Y.; Kim, J.; Park, C. H., Multi-jet electrospinning of polystyrene/polyamide 6 blend: thermal and mechanical properties. *Fashion and Textiles* **2017,** *4* (1), 9.

21.	Kim, S.-S.; Park, J.-E.; Jung, D.-U.; Seo, B.-J.; Huh, M.-W.; Lee, J.-W., Improved Antimicrobial Efficacy of *m*-Aramid. *Textile Coloration and Finishing* **2009,** *21* (5), 58-62.

22.	Koombhongse, S.; Liu, W.; Reneker, D. H., Flat polymer ribbons and other shapes by electrospinning. *Journal of Polymer Science Part B: Polymer Physics* **2001,** *39* (21), 2598-2606.

23.	Yarin, A. L.; Kataphinan, W.; Reneker, D. H., Branching in electrospinning of nanofibers. *Journal of Applied Physics* **2005,** *98* (6), 064501.

24.	Paruchuri, S.; Brenner, M. P., Splitting of a Liquid Jet. *Phys. Rev. Lett.* **2007,** *98* (13), 134502.

25.	Amiraliyan, N.; Nouri, M.; Kish, M. H., Effects of some electrospinning parameters on morphology of natural silk‐based nanofibers. *Journal of Applied Polymer Science* **2009,** *113* (1), 226-234.

26.	Reneker, D. H.; Yarin, A. L., Electrospinning jets and polymer nanofibers. *Polymer* **2008,** *49* (10), 2387-2425.

27.	Katta, P.; Alessandro, M.; Ramsier, R. D.; Chase, G. G., Continuous Electrospinning of Aligned Polymer Nanofibers onto a Wire Drum Collector. *Nano Letters* **2004,** *4* (11), 2215-2218.

28.	Pai, C.-L.; Boyce, M. C.; Rutledge, G. C., Morphology of Porous and Wrinkled Fibers of Polystyrene Electrospun from Dimethylformamide. *Macromolecules* **2009,** *42* (6), 2102-2114.

29.	Wang, L.; Pai, C.-L.; Boyce, M. C.; Rutledge, G. C., Wrinkled surface topographies of electrospun polymer fibers. *Applied Physics Letters* **2009,** *94* (15), 151916.

30.   Lin, J.; Ding, B.; Yu, J., Direct Fabrication of Highly Nanoporous Polystyrene Fibers via Electrospinning. *ACS Applied Materials & Interfaces* **2010,** *2* (2), 521-528.

31.   Fashandi, H.; Karimi, M., Pore formation in polystyrene fiber by superimposing temperature and relative humidity of electrospinning atmosphere. *Polymer* **2012,** *53* (25), 5832-5849.

32.   Li, L.; Jiang, Z.; Li, M.; Li, R.; Fang, T., Hierarchically structured PMMA fibers fabricated by electrospinning. *RSC Advances* **2014,** *4* (95), 52973-52985.

33.   Russell, K. J.; Aydin, A.; Carter, D. J. D.; Kim, E.; Lewis, P. H.; Sun, L.; Gong, X.; Chang, C.; Gordon, R.; Duwel, A., Fabrication of sub-micron metal wires for high-frequency litz wire. In *Hilton Head Workshop 2018*, 2018.

Chapter 3   Vapor phase depositions on PMIA Nanofibers

3.1 Introduction

In this chapter, we describe the methods with which we applied metal and insulator coatings onto our polymer nanofiber scaffolds and their results. Depositions of various coatings have previously been applied onto non-woven networks of PMIA nanofibers.[1] Electrospinning and physical vapor deposition (PVD) methods have also been previously combined to make transparent electrodes: Wu and coworkers used electrospun fibers as temporary templates, which they coated using PVD and then dissolved away the polymer fibers to make a network of trough-shaped structures.[2] He and coworkers later used electrospun fibers as a positive mask during etching of a copper film, leaving behind a network of undissolved line-shaped areas of copper wire.[3] What has not yet been demonstrated is the ability to leverage the strength of PMIA or other high-strength polymer nanofibers. In this chapter, we demonstrate that our improved control over PMIA nanofiber morphology and being able to make suspended single nanofibers enables the fabrication of centimeter-scale long individual nanowires with functional layers.

3.2 Coating of PMIA Fibers with Physical Vapor Deposition

We applied metal coatings on suspended PMIA fibers using sputter coating or thermal evaporation to make conductive wires with sub-micron diameters. Since both these methods use line-of-sight deposition with respect to the source materials,

depositions were performed from two different sides of the holders with PMIA

nanofibers (Figure 1-d).
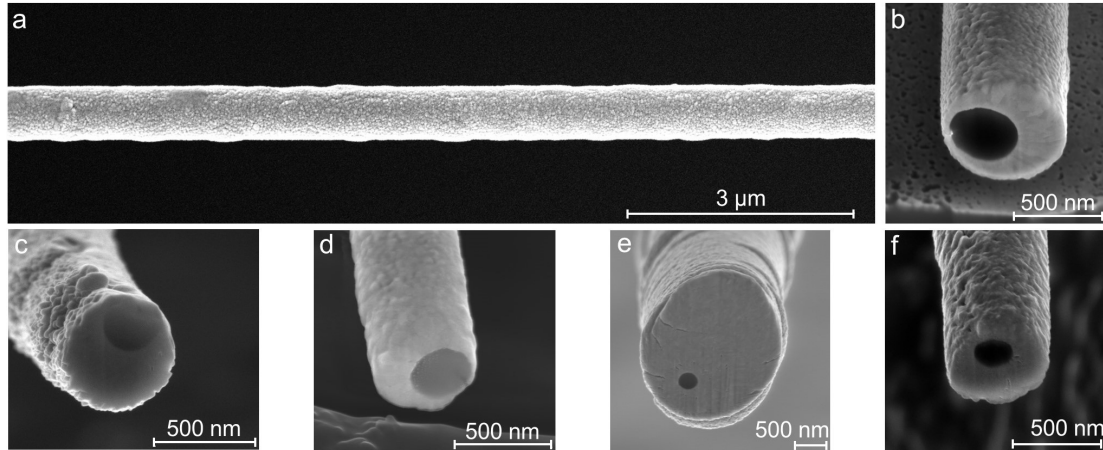
Figure 3.1. Examples of non-conformal PVD coating results. (a) Platinum sputter coated

fiber and (b) its cross-section. (c) Cross-section of a fiber sputter coated with titanium

from one side only. Cross-sections of (d) gold, (e) copper, and (f) cobalt coated fibers

sputtered from both sides.

PVD often provides non-conformal coatings around the fibers (Figure 3.1). For

sputtering, conformality seems to be somewhat improved with certain metal targets, such

as Ag (Figure 3.2-a-b), while Au sputtering consistently gives off-centered coatings.

Sputtered fibers occasionally become slack within their frame fixtures, which confounds

the problem. We have also observed that sputtering of Cu under our conditions often

leads to samples becoming more brittle, and wires tend to break off from their frames

after metal deposition. More stable Cu coated wires can be prepared with thermal

evaporation of copper, and the slacking behavior is much less apparent. As the fibers

remain tightly held within their fixtures, evaporation of a thin layer of Cu (75 nm onto two sides of the fibers) seems to yield a conformal coating, but a thicker deposition yields the wire cross-section with two crescent shaped coatings on two opposite sides of the wire (Figure 3.2-c and d).

We then evaluated the DC electrical conductivity of the metal coated wires. Wires are placed on a Si wafer with a thermal oxide layer using double-sided tape, and Ag paste droplets were added at the two ends to serve as connection pads. A probe station was used to obtain the current vs. voltage values for different wires. Lengths of the wires between the Ag connections were varied between ~1 and 9 mm in these samples. A few of the wires showed a non-Ohmic response likely due to Ag contact irreproducibility and were excluded as outliers. Results were normalized with respect to 5 mm wire length, 400 nm inner fiber diameter, and 500 nm outer wire diameter for better comparison in Figure 3.2-e. Silver coated wires show the lowest resistivity within our samples. When high voltages are applied, wires typically break in the 10-20 V range, acting as sub-micron thick fuses. In these tests, only a few of the Ag or Au coated wires survived 20 V applied voltage applied across them. If higher voltage applications are desired, thicker metal layers would be needed.
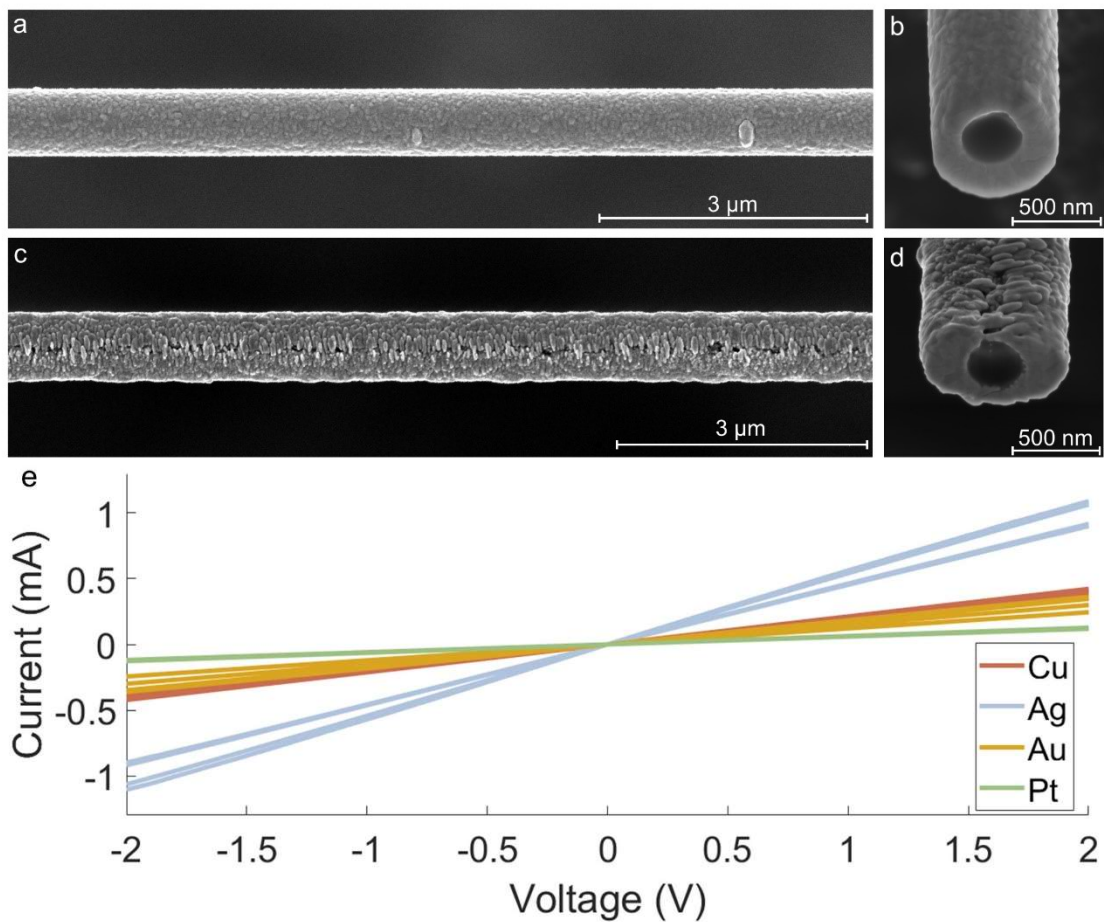
Figure 3.2. PVD-coated fibers and electrical testing. (a) Fiber sputter-coated with Ag from both sides and (b) its cross-section. (c) Fiber coated with Cu by thermal evaporation from both sides and (d) its cross-section. (e) Current vs. voltage curves of PMIA nanofibers coated with various materials using PVD. (Current values were normalized for 5 mm wire length, 400 nm inner fiber diameter, and 500 nm outer diameter of coated wire for better comparison.)

3.3 Coating of PMIA Fibers with ALD and CVD

PMIA nanofibers were also coated using CVD and ALD. These methods yield conformal coatings and do not require the sample to be coated twice from different sides. Figure 3.3-a and b show SEM images of a nanofiber that was coated with an Al_2O_3 and HfO_2 nanolaminate layer using ALD. The nanolaminate layer is the gray region between the dark polymer core and the bright gold shell. This layer can serve as a water barrier layer that reduces roughening which the salt-containing fibers undergo upon exposure to humid environments (Figure 3.4).

Figure 3.3 - c-e show images of fibers coated with cobalt using direct-liquid-evaporation (DLE) CVD in collaboration with Xian Gong.[4-5] Once again, the deposition conformality can be seen from the cross-sectional SEM images. Figure 5-f shows the cross-section of a wire that was first coated with Co using CVD, and then with an insulating layer of $MnSi_xO_y$ in collaboration with Dr. Lu Sun,[6] making a full micron scale conductive wire with an insulating shell.
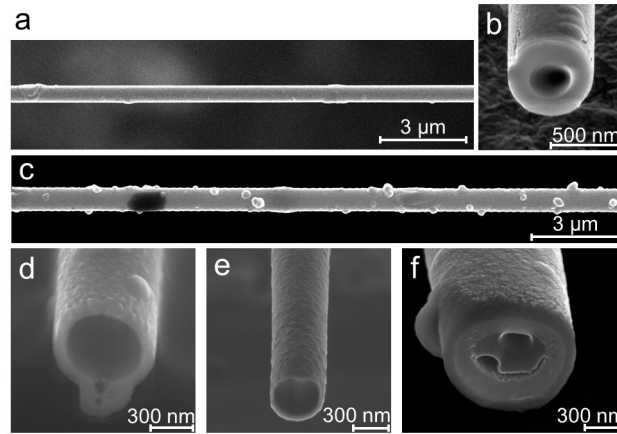
Figure 3.3. ALD and CVD onto PMIA nanofibers. (a) PMIA fiber coated with a ~ 150 nm Al_2O_3 and HfO_2 nanolaminate layer by ALD, and its cross-section (b). Deposition temperature was 200°C. (A thin layer of Pt/Pd (80/20) alloy was sputtered from the top to assist with imaging.) (c) Image of a fiber coated with cobalt using DLE-CVD and its cross-section (d). (Roughening of this fiber was likely caused by exposure to humid air as described in the text.) (e) Cross-section of a DLE-CVD cobalt coated fiber that was not as roughened. (f) Co-coated fibers from c & d were then coated with an insulating layer of $MnSi_xO_y$. (A final thin layer of Pt/Pd (80/20) was applied on the top to assist with imaging.)

a) Bare PMIA fiber with salt:
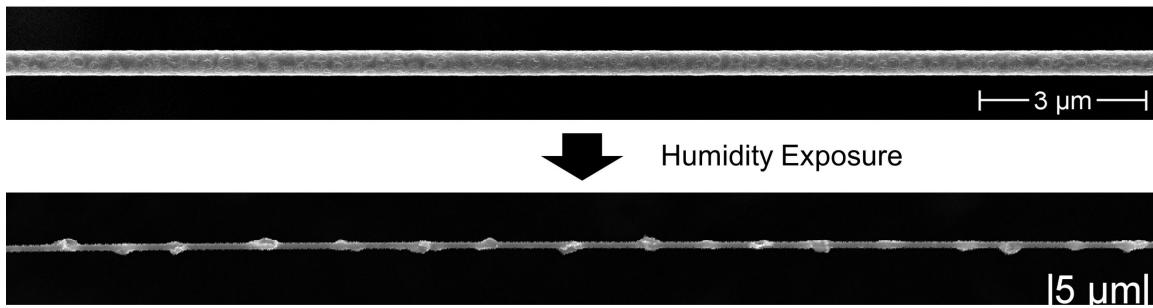
Humidity Exposure

b) Al$_2$O$_3$ + HfO$_2$ coated PMIA fiber with salt:
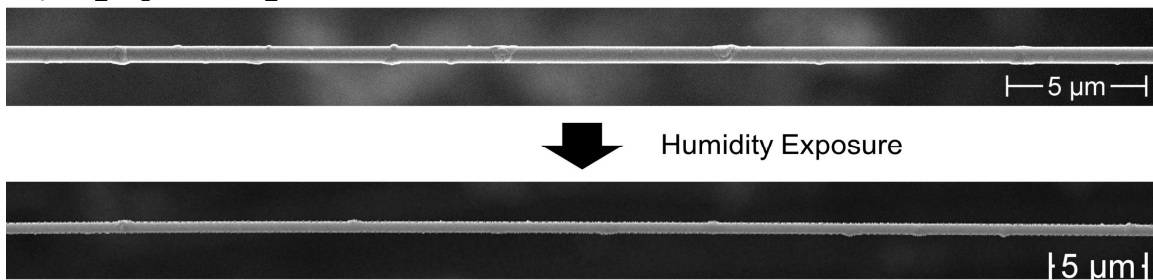
Humidity Exposure

Figure 3.4. Water diffusion barrier reduces fiber roughening due to humidity exposure. Uncoated and Al$_2$O$_3$/HfO$_2$ nanolaminate coated nanowires were exposed to ambient humidity conditions. In (a), the uncoated fiber developed large protrusions (contrasted with the image of a nanofiber image from a different experiment that was kept in vacuum). In (b), the nanolaminate coated nanofiber is shown to not change in smoothness over such ambient humidity exposure.

3.4 Combining Different Methods for Core-Multishell Structures

In this section, we describe samples with multiple layers of coating prepared by mixing PVD and ALD methods. One purpose for doing so is to prepare core-multishell structures with alternating metal and insulator layers. Multilayer nanowires with similar

or more elaborate structures have been described in literature as having potential in nanophotonic[7] or X-ray microscopy applications.[8-15]

Figure 3.5, we combined sputtering coating of conductive Pt/Pd alloy (80/20) with ALD deposition of $MnSi_xO_y$ to get multilayered structures. First, we deposited a layer of Pt/Pd alloy (80/20) by sputtering from both sides onto suspended nanofibers. Then, we carried the ALD deposition of MnSixOy at 350°C, yielding an insulated conductive wire (Figure 3.5-a). This insulated wire was coated with a thin layer of Pt/Pd to assist with imaging. We repeated these two consecutive depositions two more times to create first a coaxial and then a triaxial wire (Figure 3.5-b and c, respectively). This experiment showed that the PMIA fiber-based structure could withstand multiple rounds of metal and insulator depositions since we had minimal unintended nanofiber loss throughout these multiple depositions.
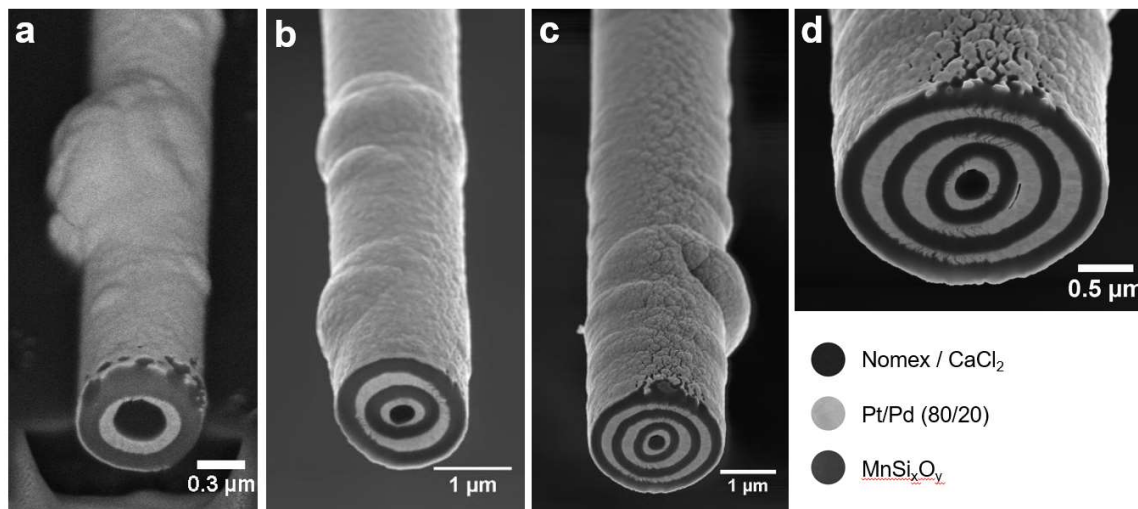
Figure 3.5. Core-multishell wire with conductor and insulator layers. (a) An insulated nanowire, where the polymer core (black), conductive metal layer (bright gray), and insulating oxide layer (dark gray) can be seen. (b) Coaxial wire with two layers of conductive metal and two layers of insulator. (c) Triaxial wire with three layers of metal and insulator stacked. (d) Higher magnification image of the cross section of the triaxial wire. (A final capping layer of Pt/Pd was added for each nanowire to assist with the FIB cross sectioning for each step.)

The first core-multishell structure we presented above had two defects that could limit their potential use: They were prepared before we developed protocols to minimize humidity exposure related protrusions, and the Pt/Pd alloy layers were non-uniform. To improve these results, protrusions were minimized by keeping the fibers desiccated between experiments. Then, as noted above, we chose to use Ag for the sputtered metal layers since that often gives the most conformal sputtered layers within the metals we have tried sputtering. The ALD deposited oxides already show great conformality in

general, but the Pt/Pd alloy we sputter coated before was not fully conformal. We wanted to improve the conformality of metal layers in our results by sputtering silver instead, which we noticed often yields more conformal layers when coated from two opposite sides of the fibers compared to other metals we have tested. For the insulator layer, we switched to an Al_2O_3/HfO_2 nanolaminate structure with alternating atomic layer depositions of the two oxides. This structure seems to act well as a water barrier layer that minimizes fiber roughening due to humidity exposure as we have described earlier.

In an earlier attempt, while the silver layer seems to start conformally, we observed what seemed to be silver agglomerating on one side of the fiber after to 200°C ALD process that takes about 5 hours. This dewetting is likely enhanced by the high diffusion rate of silver. The silver layer did not seem to be dewetting the subsequent oxide layers, however, as indicated by the focused ion beam (FIB) cross-section of this sample shown in Figure 3.6.
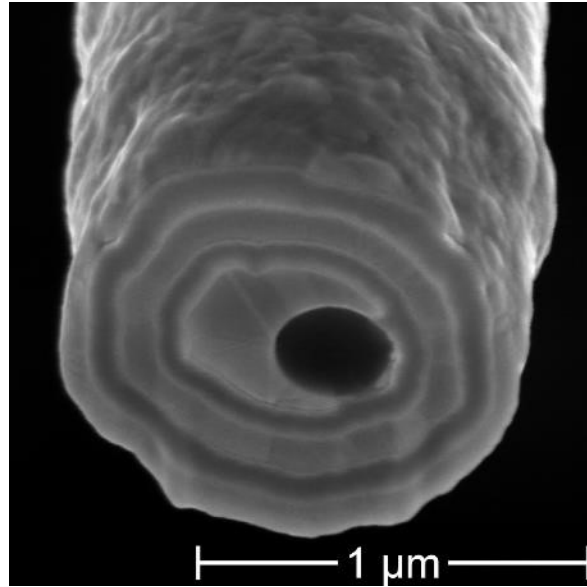
Figure 3.6. Core-multishell wire structure with Nomex fiber at the center, followed by alternating layers of Ag and Al_2O_3/HfO_2. Bright regions are Ag. The centermost Ag layer is not conformal.

We then prepared two samples in parallel where on sample was a bare Nomex fiber and the other was first coated with Al_2O_3/HfO_2. When both samples were coated with silver, we observed that while the bare fibers became slacked and loose upon sputtering, the initially oxide coated fibers did not become slacked upon sputter coating (Figure 3.7). Both samples were then coated with a layer of Al_2O_3/HfO_2 after the silver deposition. While the tight fibers of the initially ALD coated sample survived the second ALD deposition fully, many fibers broke in the first sample that was initially directly Ag coated with the oxide layer. To the fibers that were initially oxide coated, we added an additional Ag layer to make a coaxial wire (Figure 3.7-b) and two more alternating layers to make a triaxial wire (Figure 3.7-d). Compared to the previous multilayered structure

described above, these multilayered structures have more conformal layers (as well as fewer and much smaller humidity caused protrusions since we were keeping these samples desiccated).
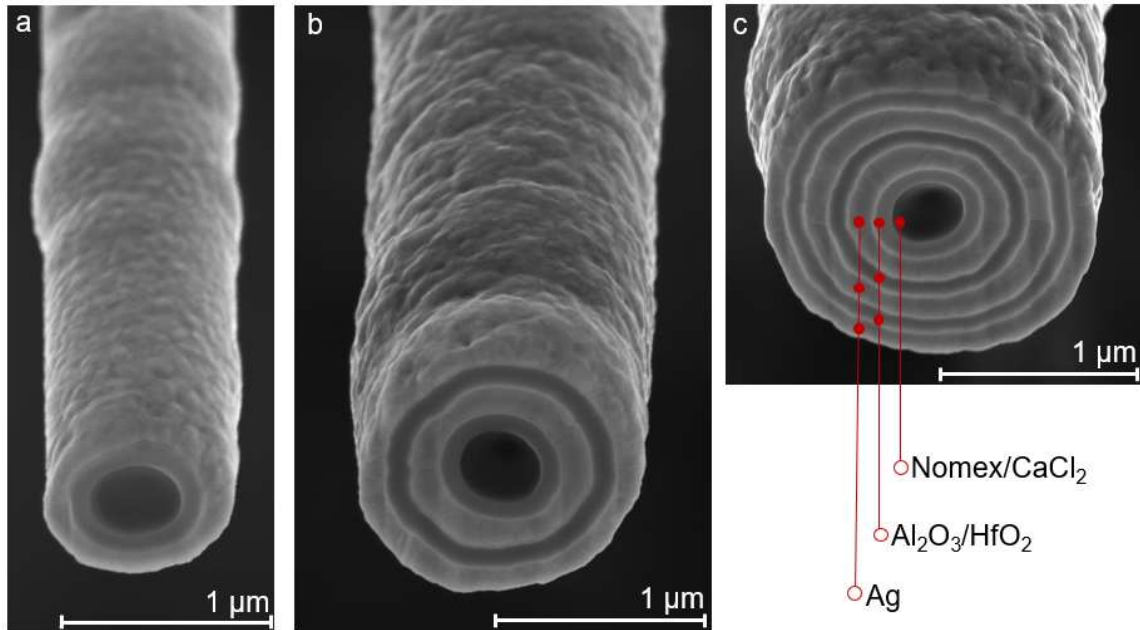
Figure 3.7. Multilayered depositions with improved conformality. (a) Nomex fiber first coated with Al_2O_3/HfO_2 and then with silver. These fibers remained intact and did not become slacked after sputtering. (b) Coaxial wire. Nomex fiber was first coated with Al_2O_3/HfO_2, and then with alternating layers of silver, Al_2O_3/HfO_2, and silver again. (c) Triaxial wire. The rest of the fibers from part (b) (after removing some for cross-sectioning and imaging) were coated with an additional layer of Al_2O_3/HfO_2 and silver.

The wires shown in Figure 3.7 closely resemble ones hypothesis in literature to have potential applications in photonics.[7] Greatly increasing the number of coatings and

have the thickness of each subsequent layer be slightly lower could be used in making an X-ray focusing lens (where the final lens is couple-micron thick slice cut from the wire with FIB).[8-15] The field typically uses glass fibers for this purpose and coat that section with a metal block layer, throwing away a portion of the X-ray intensity. A thinner fiber scaffold at the center would require more layers (and longer coating times) to make a lens, but the result could allow notably higher intensity X-ray to be focused.

By now, we have shown two different advantages of having a Al_2O_3 and HfO_2 coating on the PMIA nanofibers: (1) It can act as a water diffusion barrier, minimizing morphology changes when the fibers are not washed, and (2) it can minimize dewetting of silver from PMIA when the sample is heated. We found a third application for this coating around improving sputter layer conformality for other metals that technically falls under core-multishell structures. When the initial taut fibers are sputter coated, they often sag and break more easily during handling. Using a silver sputtering target minimized this effect, but most other sputtering targets, including gold that most of the NanoLitz development focuses on, had this effect which lead to non-conformal metal layers (Figure 3.1). Hypothesizing that the polymer core might be getting damaged by ion bombardment or UV exposure within the sputtering system, we decided to first add an oxide layer that would potentially block both. Al_2O_3/HfO_2 is adequately absorbing in the UV-region, and a thick enough layer of it would block any ion damage.

We first employed the Al_2O_3/HfO_2 protection layer with gold sputtering. We knew from many repeats of gold sputtering both in our group and at Draper that gold

sputtering tends to cause the fibers to become slack and forms highly non-conformal

coatings as the fibers are sputter coated twice from opposite sides. When fibers were first

coated with the ALD nanolaminate layer and then sputter coated with gold from two

sides, we got our first conformally gold sputter coated nanocables. These results are

shown in Figure 3.8.
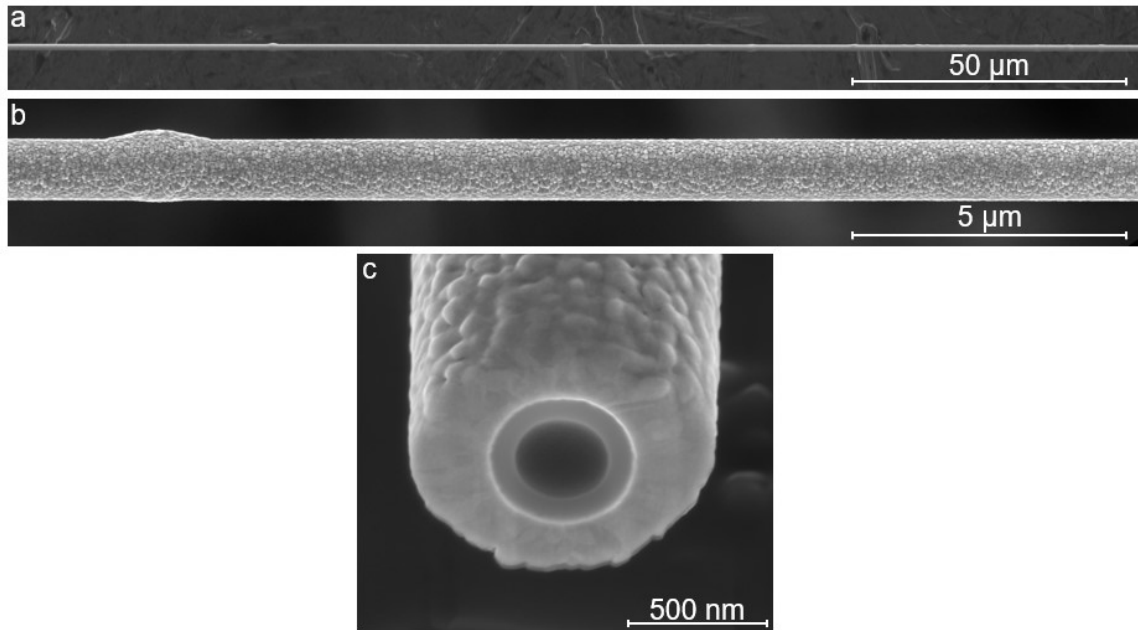
Figure 3.8. Conformal gold sputtered onto Al_2O_3/HfO_2 coated PMIA nanofibers. (a and

b) Side view of the gold coated cable at two different magnifications. (c) FIB cross

section showing a conformal coating (imaged at a 52° tilt angle).

Going beyond improving conformality, the nanolaminate protection layer

markedly improves fiber handling. We observed the biggest effect of this with copper

sputtering. Copper sputtering on PMIA nanofibers was repeated many times on multiple

systems and always yielded highly fragile nanowires. While these could be transferred onto SEM stubs and studied immediately after deposition, ones that were left suspended on the frames would break off within minutes. Using the nanolaminate protection layer yielded the first copper sputter coated wires that did not break so readily. In this experiment, we employed another strategy that was suggested by Mac Hathaway: Instead of doing one deposition, taking out the sample, flipping it, and depositing on the second side, Mac suggested placing the sample vertically at the center of the stage and relying on the stage rotation to attain conformality. Importantly, the sputtering target is to the side of the sample and views the fibers directly as they are being rotating. This arrangement is shown in Figure 3.9.

Figure 3.9. One step conformal sputter coating of copper experiment. (a) Scheme of one step conformal coating: Sample is rotating in front of the copper target. (b) Photo of the sputter coater with the sample loaded perpendicularly.

The one step conformal Cu sputtering experiment worked well once the nanolaminate protection layer was in place, and conformally copper coated nanocables were obtained. Cross sections of this are shown in Figure 3.10. One caveat of this method is that there is a slight thickness gradient in these samples due to the varied deposition heights fibers experience along the height of the frame.
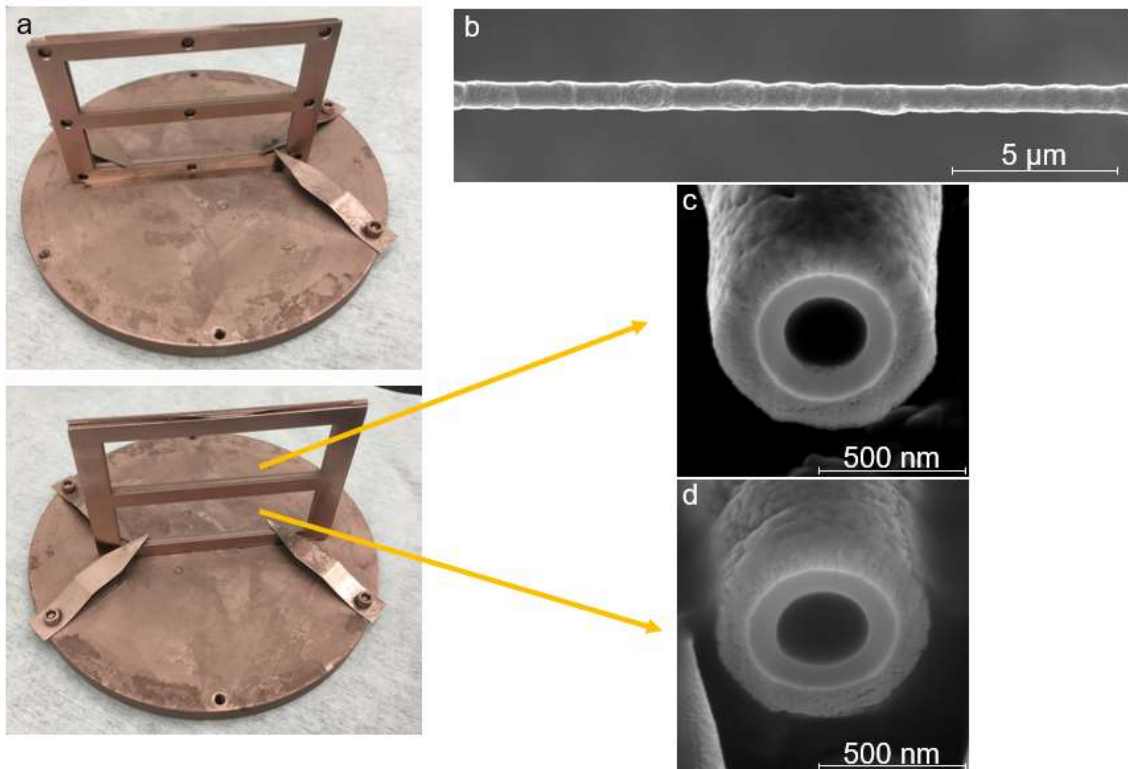
Figure 3.10. Results of one step conformal Cu sputtering coating. (a) Photos of the nanowire frames after sputter coating. (These frames with two windows are used to increase the number of fiber samples. Outer width of the frame corresponds to the spoke-to-spoke distance of our collector, or roughly the maximum fiber length we attain without needing to unravel the fiber. Cutting them in two this way essentially doubles the number

(Continued) of fibers we can remove and image while keeping the rest suspended.) (b) SEM side image of the resulting Cu coated nanocable. (c and d) Cross sections of the nanocable, showing the PMIA core, Al_2O_3/HfO_2 nanolaminate middle layer, and copper outer layer.

3.5 Polymer Insulator Coatings with iCVD

We and our collaborators considered various polymer deposition methods to apply outer dielectric layers for the insulated nanocables NanoLitz project requires. This section describes the depositions performed with Prof. Karen Gleason and Dr. Junjie Zhao at Massachusetts Institute of Technology.

Professor Gleason's group has developed initiated chemical vapor deposition (iCVD) methods to deposit polymer films from the gas phase.[16-17] In particular, poly(1,3,5-trimethyl-1,3,5-trivinyl cyclotrisiloxane) (pV3D3) presents a promising insulator layer that can be coated with precise thickness control.[18] Depositions of pV3D3 were performed on PMIA nanofibers metalized with Cu, Au, and Pt/Pd alloy (Figure 3.11). (Note that these metalized samples suffered from the humidity related protrusions as they were prepared early on in the project before we developed measures against that.) Results show a conformal insulator coated around the nanowires. Dr. Lu Sun validated the insulating performance of these films.
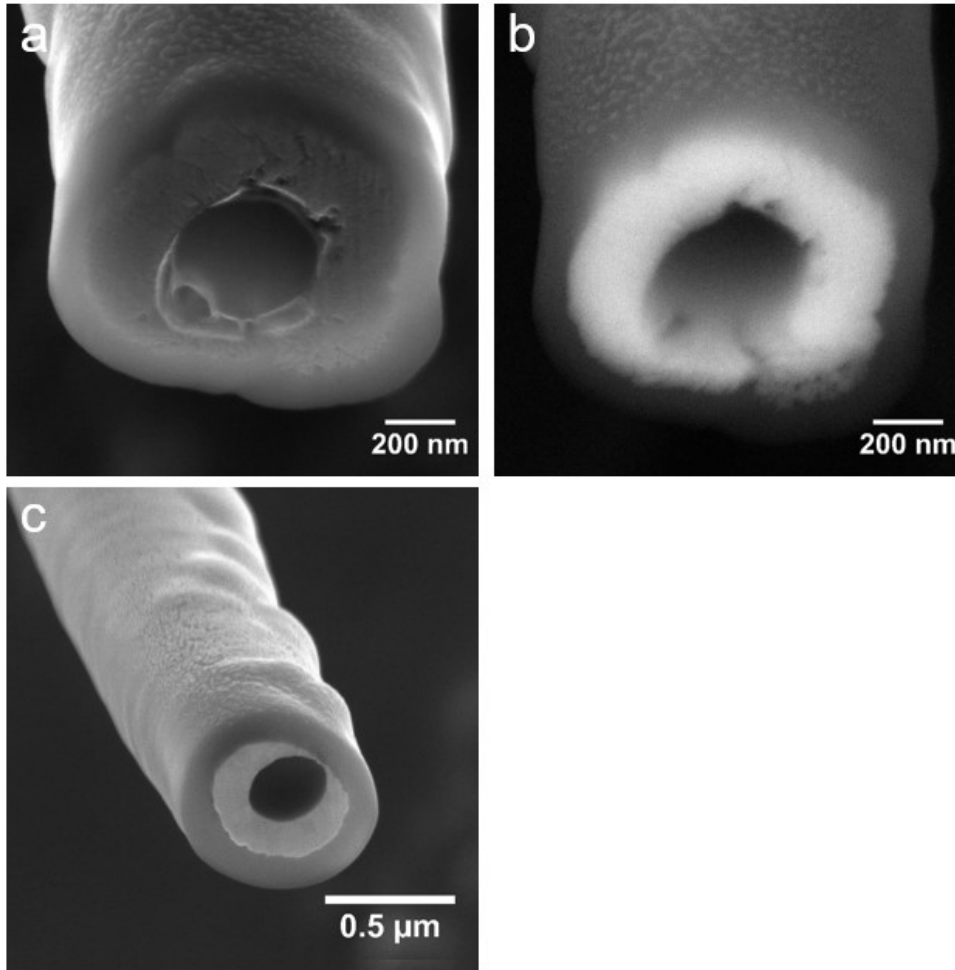
Figure 3.11. Nanowires insulated with pV3D3. (a) SE2 image of a PMIA nanofiber cross section with a Cu layer and outer pV3D3 coating. (b) Backscattered electron image of the same region in (a), providing better contrast between the outer polymer layer and the metal in the middle. (c) Cross section of a nanofiber coated first with gold and then with pV3D3.

In the case of a particularly roughened Cu nanowire, the pV3D3 layered seems to flow over the bumps and somewhat reduce the roughness. This is shown in Figure 3.12.

Without pV3D3:
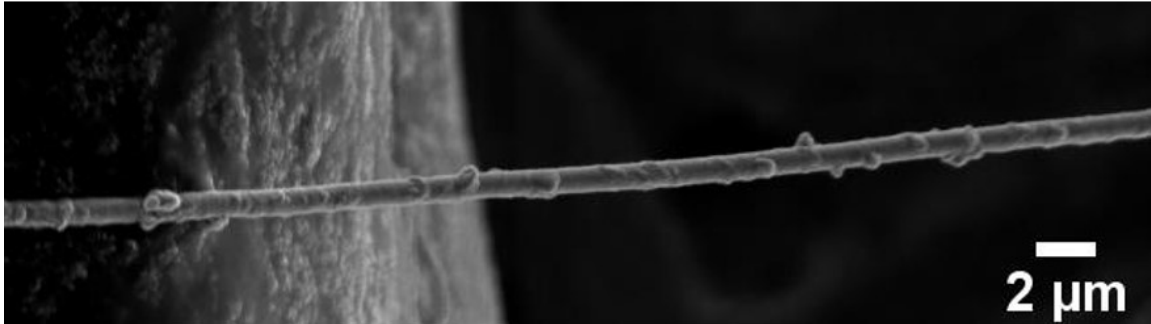
With pV3D3:
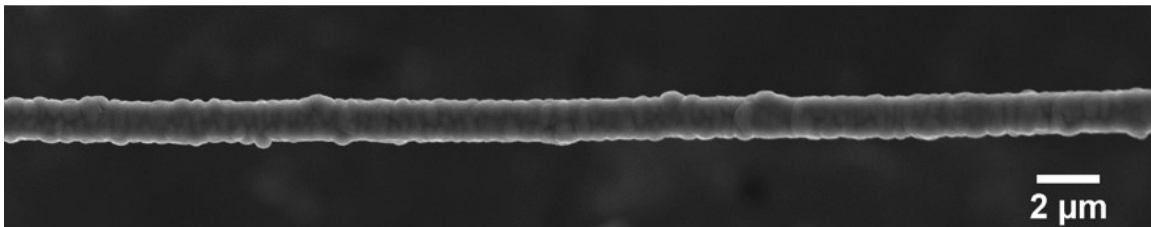
Figure 3.12. Copper coated nanowire before and after pV3D3 deposition.

3.6 Conclusions

In this chapter, we have listed our findings on depositions onto the PMIA nanofiber scaffolds. These coatings are used to make the nanowires conductive and to add an outer insulating layer.

In Chapter 3.2, we described some of our findings from depositing metals around the PMIA nanofibers using sputtering. In these experiments, fibers were coated twice from opposite sides to improve coating conformality. While most metals when sputtered cause the fibers to sag and move around, leading to a nonconformal coating, Ag tends to

give a more conformal coating consistently. Based on some of our early results, our collaborators at Draper adapted gold sputtering as the main method they have been using for metalizing the nanofibers in the Nano Litz development, but we have continued to showcase the materials generality of our nanofiber scaffolds with various metals and insulators.

In Section 3.3, we showed some of our results on ALD and CVD growth on our nanofibers. These depositions yield the best coating conformality around our fibers. For vapor chemistries that are sensitive to the presence of tape in the chamber (which can e.g. volatilize and interfere with precursor adsorption), we used a mechanically clamped fiber holder instead that was described in Section 1.4 and Figure 1.6-c. In this holder, the fibers are sandwiched between two frames that are pressed against each other with screws, and a thin polymer film is placed also in between the frames to serve as a gasket. More details on sample preparation for this is given in Appendix D.

We showed the ALD deposition of Al_2O_3/HfO_2, which is a water diffusion barrier layer that can mitigate fiber morphology from degrading when stored in humid environment as described in Section 2.3. We also showed films deposited in custom reactors in our group (in collaboration with Xian Gong and Dr. Lu Sun) to afford a conductive Co layer and an insulating $MnSi_xO_y$ layer. In section 3.4, we combined different coatings using PVD and ALD to make core-multishell structures. Such structures have potential applications beyond the Nano Litz project. In particular, we

demonstrated that a Al_2O_3/HfO_2 coating can mitigate the sputtering damage and sagging behavior and can allow conformal metal layers to be deposited for metals other than Ag.

Finally, in Section 3.5, we described our findings from a collaboration with Prof. Karen Gleason's group on depositing an insulating polysiloxane coating onto the nanofibers. This collaboration eventually led our current routine insulation process by employing the services of GVD Corporation, which was co-founded by Prof. Gleason and can perform large scale PTFE coatings. Research on better performing (lower leak rate) insulating layer depositions are actively ongoing within our group where we have been looking at vapor deposition chemistries for various polyimides.

3.7 References

1.   Liu, W.; Graham, M.; Evans, E. A.; Reneker, D. H., Poly(*meta*-phenylene isophthalamide) nanofibers: Coating and post processing. *Journal of Materials Research* **2002,** *17* (12), 3206-3212.

2.   Wu, H.; Kong, D.; Ruan, Z.; Hsu, P.-C.; Wang, S.; Yu, Z.; Carney, T. J.; Hu, L.; Fan, S.; Cui, Y., A transparent electrode based on a metal nanotrough network. *Nature Nanotechnology* **2013,** *8* (6), 421-425.

3.   He, T.; Xie, A.; Reneker, D. H.; Zhu, Y., A Tough and High-Performance Transparent Electrode from a Scalable and Transfer-Free Method. *ACS Nano* **2014,** *8* (5), 4782-4789.

4.   Yang, J.; Li, K.; Feng, J.; Gordon, R. G., Direct-liquid-evaporation chemical vapor deposition of smooth, highly conformal cobalt and cobalt nitride thin films. *J. Mater. Chem. C* **2015,** *3* (46), 12098-12106.

5.   Feng, J.; Gong, X.; Lou, X.; Gordon, R. G., Direct-Liquid-Evaporation Chemical Vapor Deposition of Nanocrystalline Cobalt Metal for Nanoscale Copper Interconnect Encapsulation. *ACS Applied Materials & Interfaces* **2017,** *9* (12), 10914-10920.

6.   Gordon, R.; Sun, L.; Chen, Q.; Park, J.-S.; Kim, S. In *ALD of Manganese Silicate*, 2015; 2015; pp 1-20.

7.   Kim, K.-H.; No, Y.-S.; Chang, S.; Choi, J.-H.; Park, H.-G., Invisible Hyperbolic Metamaterial Nanotube at Visible Frequency. *Scientific Reports* **2015,** *5*, 16027.

8.   Saitoh, K.; Inagawa, K.; Kohra, K.; Hayashi, C.; Iida, A.; Kato, N., Fabrication and Characterization of Multilayer Zone Plate for Hard X-Rays. *Jpn. J. Appl. Phys.* **1988,** *27* (11A), L2131.

9.   Kamijo, N.; Tamura, S.; Suzuki, Y.; Handa, K.; Takeuchi, A.; Yamamoto, S.; Ando, M.; Ohsumi, K.; Kihara, H., Fabrication of a hard x-ray sputtered-sliced Fresnel phase zone plate. *Review of Scientific Instruments* **1997,** *68* (1), 14-16.

10.   Tamura, S., High-Energy X-ray Microprobe by Multilayer Zone Plate and Microscopy at SPring-8. **2004,** *716*, 144-147.

11.   Koyama, T.; Takano, H.; Konishi, S.; Tsuji, T.; Takenaka, H.; Ichimaru, S.; Ohchi, T.; Kagoshima, Y., Circular multilayer zone plate for high-energy x-ray nano-imaging. *Review of Scientific Instruments* **2012,** *83* (1), 013705.

12.   Mayer, M.; Grévent, C.; Szeghalmi, A.; Knez, M.; Weigand, M.; Rehbein, S.; Schneider, G.; Baretzky, B.; Schütz, G., Multilayer Fresnel zone plate for soft X-ray microscopy resolves sub-39 nm structures. *Ultramicroscopy* **2011,** *111* (12), 1706-1711.

13.   Mayer, M.; Keskinbora, K.; Grévent, C.; Szeghalmi, A.; Knez, M.; Weigand, M.; Snigirev, A.; Snigireva, I.; Schütz, G., Efficient focusing of 8 keV X-rays with multilayer Fresnel zone plates fabricated by atomic layer deposition and focused ion beam milling. *J Synchrotron Radiat* **2013,** *20* (Pt 3), 433-440.

14.   Keskinbora, K.; Robisch, A.-L.; Mayer, M.; Sanli, U. T.; Grévent, C.; Wolter, C.; Weigand, M.; Szeghalmi, A.; Knez, M.; Salditt, T.; Schütz, G., Multilayer Fresnel zone

plates for high energy radiation resolve 21 nm features at 1.2 keV. *Opt. Express* **2014,** *22* (15), 18440-18453.

15.   Sanli, U. T.; Keskinbora, K.; Grevent, C.; Szeghalmi, A.; Knez, M.; Schiitz, G., Multilayer Fresnel Zone Plates for X-ray Microscopy. *Microscopy and Microanalysis* **2015,** *21* (S3), 1987-1988.

16.   Tenhaeff, W. E.; Gleason, K. K., Initiated and Oxidative Chemical Vapor Deposition of Polymeric Thin Films: iCVD and oCVD. *Advanced Functional Materials* **2008,** *18* (7), 979-992.

17.   Chen, N.; Reeja-Jayan, B.; Liu, A.; Lau, J.; Dunn, B.; Gleason, K. K., iCVD Cyclic Polysiloxane and Polysilazane as Nanoscale Thin-Film Electrolyte: Synthesis and Properties. *Macromolecular Rapid Communications* **2016,** *37* (5), 446-452.

18.   Moon, H.; Seong, H.; Shin, W. C.; Park, W.-T.; Kim, M.; Lee, S.; Bong, J. H.; Noh, Y.-Y.; Cho, B. J.; Yoo, S.; Im, S. G., Synthesis of ultrathin polymer insulating layers by initiated chemical vapour deposition for low-power soft electronics. *Nature Materials* **2015,** *14* (6), 628-635.

Chapter 4   Electrospinning Studies into Other High Temperature Stable Polymers

4.1 Overview

Throughout this project, we have studied the possibility of electrospinning various high temperature stable polymers for making single nanofibers. Early in the project, this was done simultaneously with PMIA electrospinning development because of the challenges spinning that were presenting as described in Chapter 2. After the PMIA protocol was mature, we eventually discovered the $CaCl_2$ required to dissolve the polymer leads to humidity sensitivity and potential morphological defects in the form of protrusions. While we could minimize those challenges by (a) keeping the fibers desiccated, (b) washing out the salt, or (c) coating them with a water diffusion barrier, it would be ideal to remove such an extra step. That is why we went back to looking at alternative polymers that could be solubilized and spun without the addition of a hygroscopic salt. This chapter provides an overview of these efforts.

Most notably, we have identified and tested a number of polyimides with high thermal stability, and this class of polymers seem to provide a promising alternative to PMIA in making salt-free polymer fibers. Polyetherimide (PEI, ULTEM 1000) was among the list of potential candidates we initially generated as we scanned literature for high-temperature stable polymer candidates to try spinning. Encouraged by its high decomposition temperature, we developed a protocol for electrospinning uniform

nanofibers of PEI, but eventually realized its low glass transition temperature and melting point would likely not allow PEI to be used in our ALD and CVD depositions. Later, we encountered other promising polyimides that showed promising properties for our purposes. There are many different polyimides with relatively high mechanical strength and thermal stability that warrants attention. In Sections 4.4 – 4.6, we describe some of them that we tried electrospinning and our findings.

4.2 Polyacrylonitrile (PAN)

Our collaborators at IME Technologies gave us initial guidance for the spinning protocol and appropriate molecular weight of PAN to use for making nanofibers. Working based on their protocol produced nanofibers with diameters in the range of 1.4 - 2.5 µm depending on the exact spinning conditions. Lowering the polymer concentration and optimizing conditions achieved nanofibers with diameters around 330 nm or 670 nm. These were perceived to be appropriate for the desired target; however, PAN is not suitable for making nanowire scaffolds because of literature thermogravimetry (TGA) data showing onset of mass loss just around 200°C, which make it unsuitable for most of our metal CVD processes. Nevertheless, PAN nanofibers enabled us to develop some fiber transfer and handling strategies and served as model wires for our collaborators before the PMIA protocol was developed.
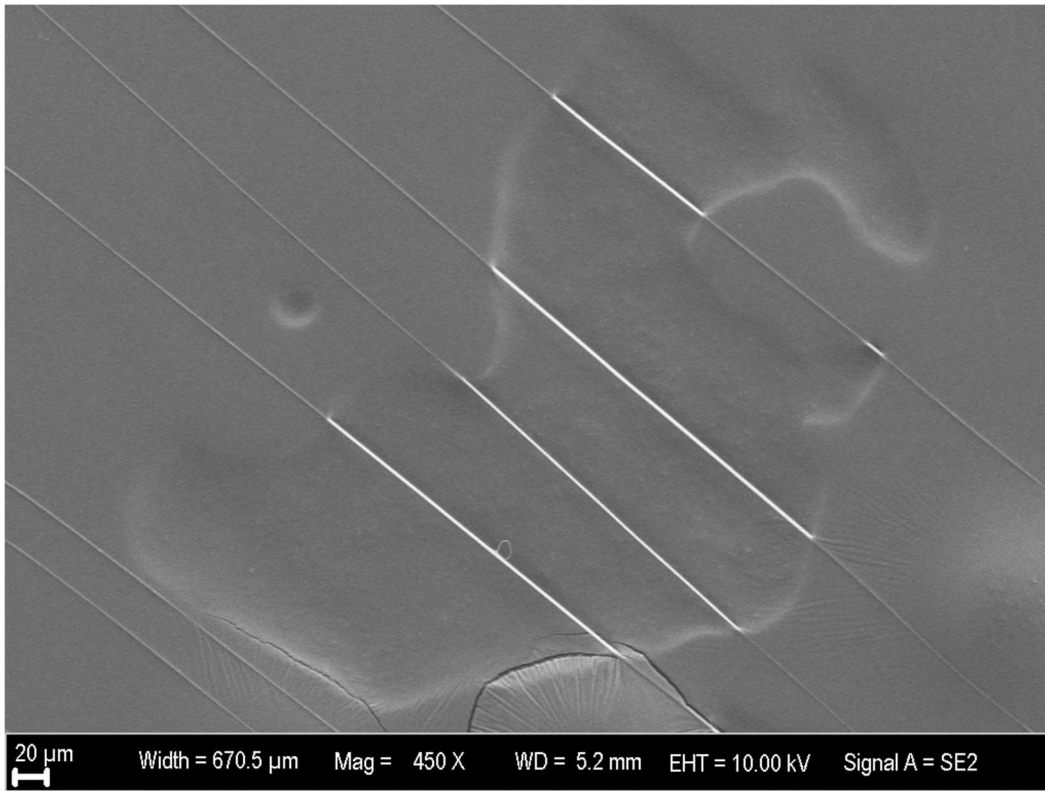
Figure 4.1. SEM image of aligned PAN nanofibers.

We optimized electrospinning conditions for our system early on when the PMIA development was lagging and our collaborators in the self-assembly group requested well-aligned polymer nanofibers to use without coating as model systems. Initially we had trouble with solution mixing as heating to reduce viscosity instigated a color change which we interpreted to be some degradation. Heating at this stage turned out to be crucial for proper mixing, and without it, the polymer forms a clear solution, but it does not appear homogenous when flowing and produces ribbon shaped nanofibers when electrospun. Upon overcoming this, alignment of the nanofibers was optimized to make them adequate for the ensuing experiments (Figure 4.1). The main insight we gained at

this stage was that achieving electrospinning at lower voltage was significantly more effective at aligning nanofibers than trying to increase the drum collector rotation speed. PAN solutions we tested start spinning at much lower voltages than what is typical for PMIA ones (at least for the jet initiation step).

PAN was dissolved in DMF and tested concentrations were in the range of 10-15 wt. %. Fibers with diameters down to 329 ± 39 nm and up to 2.46 ± 0.42 μm were obtained by adjusting the spinning parameters. In addition to voltage and concentration, solution flow rate is a key parameter in diameter control for PAN, as all the solution that reaches the edge of the nozzle gets ejected with the applied voltage. This is quite different from PMIA, which tends to form a very small Taylor cone at the edge of a droplet, seemingly regardless of the solution flow rate. For PMIA, the effect of increased flow rate is to simply grow the solution droplet at the nozzle, which can then fall with gravity if it grows too much, causing interruptions in the jet.

PAN fibers are readily aligned on the rotating-drum collector and can be transferred and suspended over some gaps using double sided tape. Gap size in the frame needs to be very narrow (a couple mm), lest these fibers start breaking. PAN nanofibers are much weaker than PMIA ones, and they cannot be suspended over centimeter-scale gapped frames as readily as PMIA.

4.3 Poly(*p*-phenylene-2,6-benzobisoxazole) (Zylon)

We investigated the making poly(*p*-phenylene-2,6-benzobisoxazole) of polybenzoxazole (PBO) nanofibers. This polymer is commercially known as Zylon, and it is about twice as strong as Kevlar while being stable up to 650 °C.[1] We were provided with some of this polymer by Toyobo CO., LTD. for our research. PBO is soluble in a number of volatile organic acids that are suitable for electrospinning, such as methanesulfonic acid (boiling point: 167 °C).[2] A limited fraction of trifluoroacetic acid (boiling point: 72.4 °C) can be mixed into the PBO solution to make the solvent system more volatile.[3] Electrospinning PBO was challenged by too high molecular weight of the solution and some self-bundling problems: PBO solution attains very high viscosity in a low concentration range of ~1 – 1.5 wt. % solution. Though such solutions can work well in electrospinning, especially with lower boiling solvents, this solution stops spinning when the viscosity gets too high and instead shoots large droplets at the substrate.

4.4 Polyamic Acid Electrospinning for Kapton Nanofibers

As the classical example of polyimides, poly(*4,4′*-oxydiphenylene-pyromellitimide), commercially known as Kapton, was first suggested for our project by Dr. Luke Davis. Kapton is typically synthesized in two steps (Scheme 4.1): (1) First, pyromellitic dianhydride and 4,4'-oxydiphenylamine are coupled in a condensation reaction to form an intermediate polymer, known as "polyamic acid" (PAA), and (2) second, this intermediate polymer is treated with heat (and in some cases, UV light) to drive the imidization to completion. While Kapton itself is not soluble in common

solvents, polyamic acid is. Dr. Davis suggested we could spin polyamic acid first and then complete the imidization to get thermally stable nanofibers. To test this approach, we tried using both commercially available polyamic acid solutions and synthesizing our own polyamic acid.
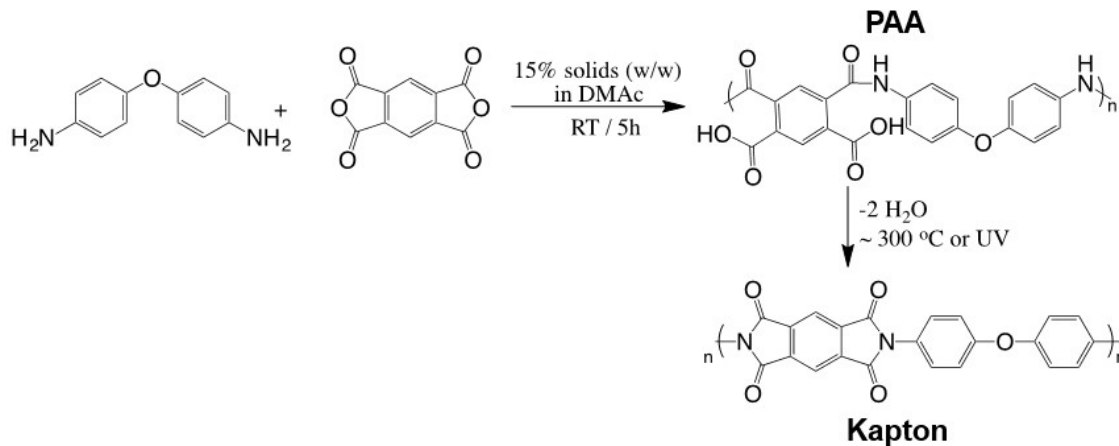
Scheme 4.1. Synthesis of PAA and Kapton.

We considered both commercially available PAA solutions (from Sigma-Aldrich) with various concentrations and solvent systems, and we also synthesized PAA in our group (Scheme 4.1). Commercial PAA solutions were too low in viscosity and seemingly resulted in electrospraying behavior with no discernable fibers getting deposited, forming some occasional particles and polymer film patches instead. PAA we synthesized was much higher in viscosity for the same concentration as the commercial sample (15 wt. %), and we were also able to make even more concentrated solutions (20 wt. %). These solutions yielded beaded nanofibers, indicating an even higher solution viscosity is

needed to make uniform fibers (Figure 4.2). We could potentially improve on these

results in the future by using a more concentrated PAA solution or deploying strategies

towards making higher molecular weight PAA. Since it is a step-growth polymerization,

the molecular weight is highly sensitive on completion of the reaction. This could

potentially be improved by better drying the particularly hygroscopic pyromellitic

dianhydride. A downside of this strategy is that the polymer fibers are formed from the

mechanically weak PAA instead of the strong imidized form which makes them more

susceptible to breakage on the collector during spinning, and they would be harder to

handle prior to the heat treatment step.
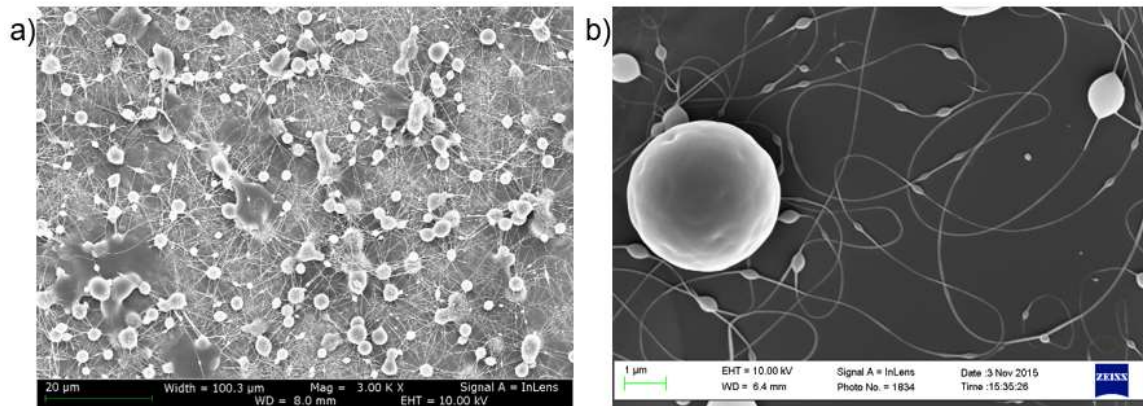
Figure 4.2. PAA electrospinning results. (a) 15 wt. % and (b) 20 wt. % PAA in DMAc

was used for the electrospinning. Fibers with beads indicate a higher solution viscosity is

needed in this case. In comparison, the commercially available PAA solutions (up to 15

wt. %) produced no fibers.

4.5 Nova Clear and CP1

We initially investigated two fluorinated polyimides that are commercially available from NeXolve Materials (AL, USA): Nova Clear and CP1. We could only spin nonwoven mats with Nova Clear, and fibers showed high variability in diameter and frequent branching (Figure 4.3) due to jet splitting (see Section 2.2).
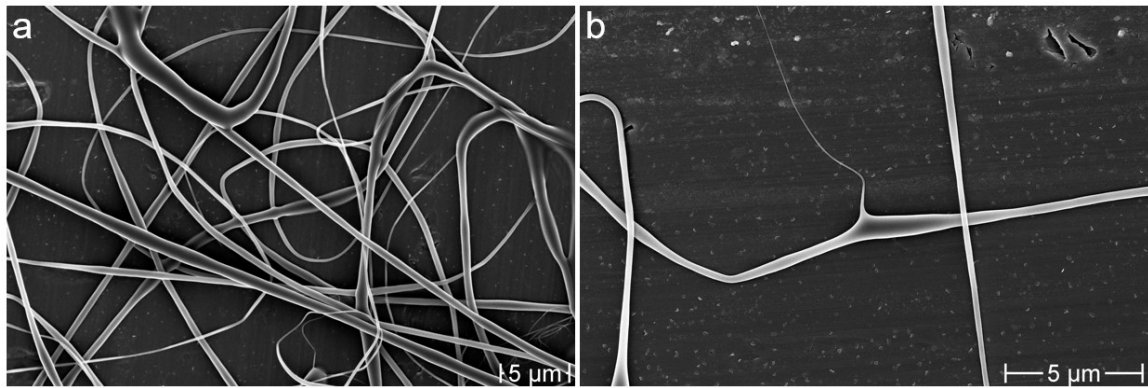
Figure 4.3. Nova Clear electrospinning results. These show high variability in fiber diameter, mat network structures, and branched fibers.

With CP1, we were able to spin single fibers on the spoked drum collector. The fiber microstructure depends strongly on the humidity within the electrospinning chamber (Figure 4.4), probably because water is a non-solvent for this polymer.[4] We obtained rough and porous fibers at high humidity, likely due to water induced polymer precipitation, and smooth fibers only at low humidity. The polymer solution also becomes cloudy when exposed to air above a certain humidity level. While the fiber

morphology of the fibers was promising at low humidity, there were problems with their stability. We observed that when single centimeter scale CP1 fibers are suspended using the previously developed frame shaped fixtures, they often break over time. When we attempted to sputter coat suspended CP1 nanofibers from alternating sides with a very thin layer of gold, we also observed that almost all the fibers failed. Overall, CP1 appears to be not strong enough to go through our deposition and handling steps.
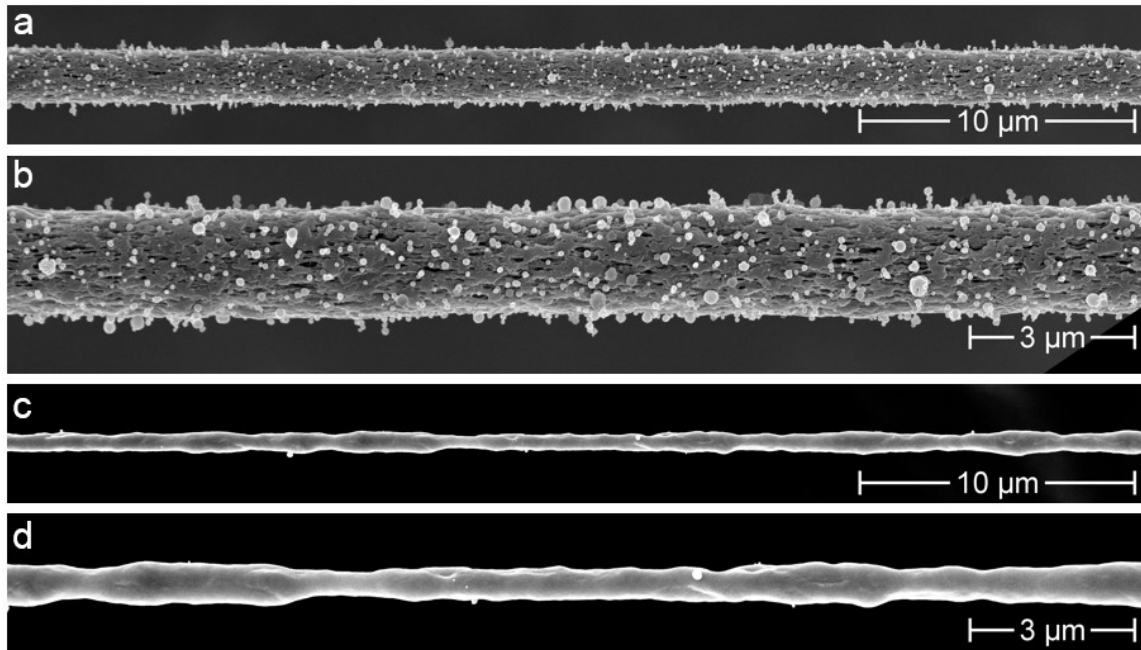
Figure 4.4. CP1 electrospinning results. (a) and (b) SEM images of a fiber spun at relatively high humidity (30% r.h., 24°C) at two different magnifications. (c) and (e) SEM images of a fiber spun at low humidity (10% r.h., 24°C) at two different magnifications.

4.6 P84

A commercially available solubilized polyimide, P84, is studied in this section. We obtained a sample of this polymer from HP Polymer Inc. (Austria). The manufacturer reports that this polymer has comparable strength with PMIA.[5] Initially, P84 was dissolved in N-methyl-2-pyrrolidone (NMP), producing a clear orange-brown solution at concentrations up to 40 wt. % without any added salt. Unlike PMIA, dissolution of P84 cannot be accelerated at high temperature without causing some degradation to the polymer that dramatically reduces viscosity. Electrospinning of this polymer has previously been reported at below 20 wt. % polymer solution concentrations.[6] Compared to the conditions in this report, we needed to increase polymer concentration much higher to get thicker fibers and slow down the spinning jet enough to collect single fibers (Figure 4.5). Similarly to CP1, P84 fibers spun at high humidity (40% RH) have rough surface morphology with protrusions, while fibers spun below 20% RH came out smoother (Figure 4.6). Latter fibers still have nonuniform diameter (Figure 4.6-c), and the solution jet is too fast to obtain single aligned fibers at low humidity under these conditions. Fiber generation rate at lower humidity is also much faster, making it harder to control the alignment to get single fibers as the one shown in Figure 4.5-c. The exact humidity that caused the switch in morphology from rough to smoother fibers decreased with increasing solution concentration.
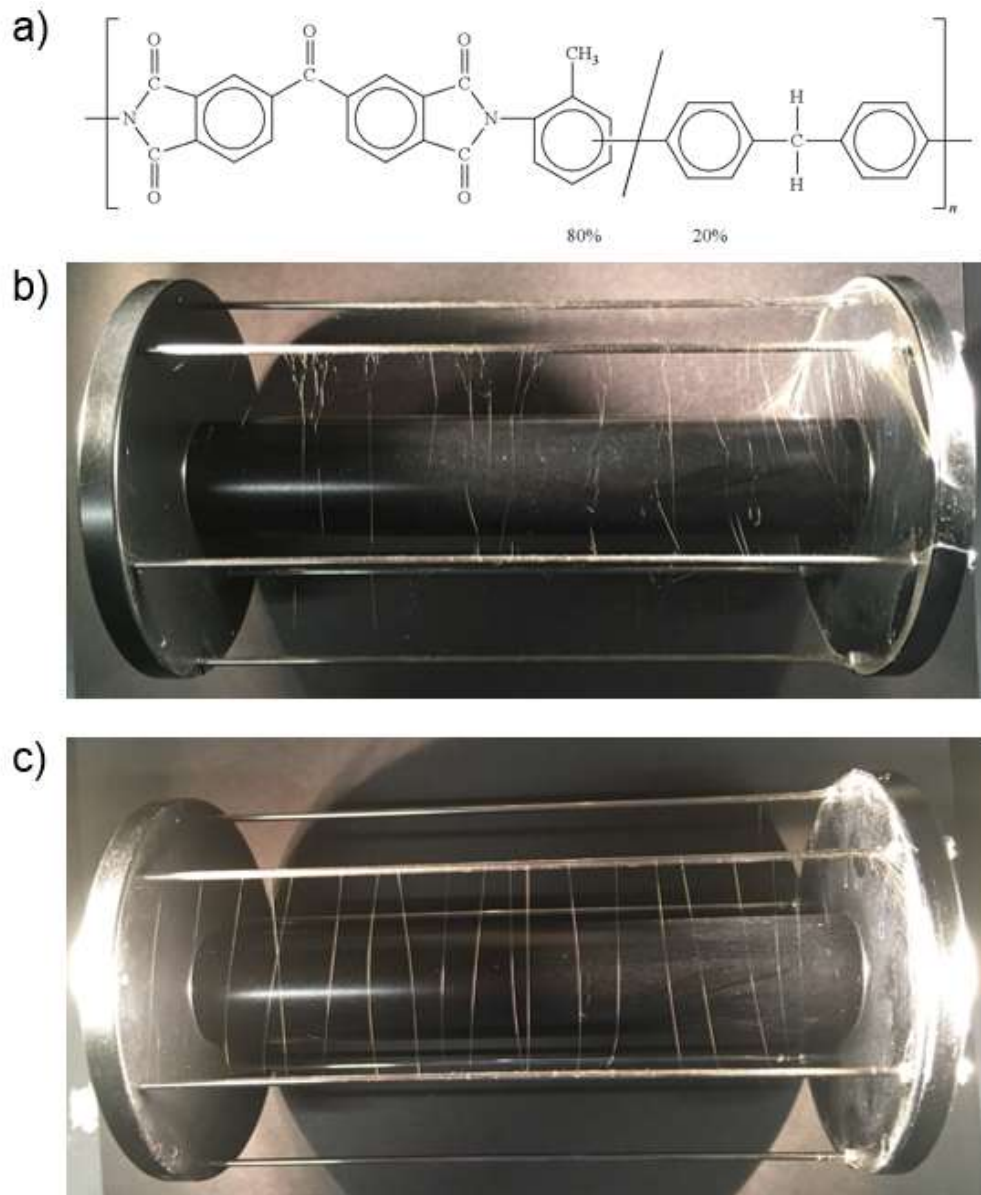
Figure 4.5. P84 structure and fiber alignment. (a) Structure of P84. (b) Fibers spun with 20 wt. % solution following literature protocol (55% RH). (c) P84 aligned fibers spun with 25 wt. % solution (30% RH).
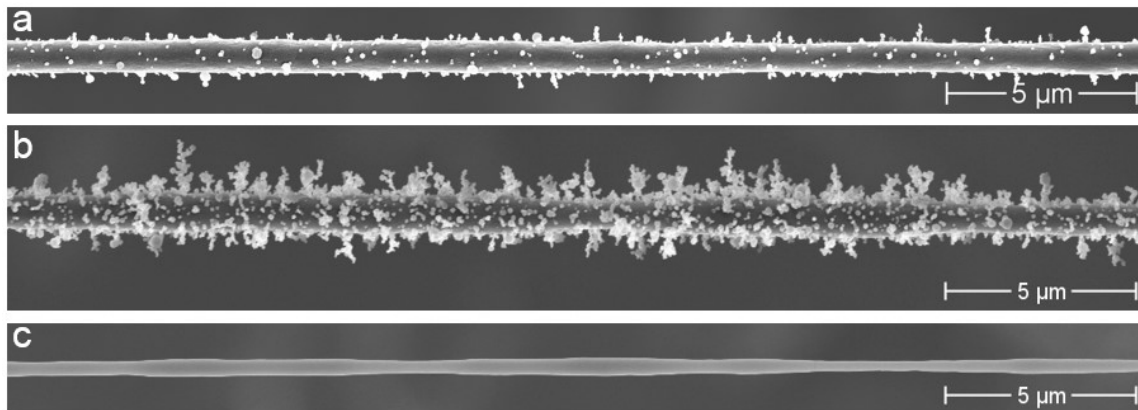
Figure 4.6. P84 electrospinning results. Fibers were spun from (a) 25 wt. % and (b-c) 30 wt. % P84 solutions in NMP under (a-b) 40% and (c) 15% RH at 24°C.The observation that low humidity yields smoother fibers remained consistent with different solvents and polymer concentrations. Non-uniform fiber diameter is indicative of a not adequately conductive spinning solution, and we were able to improve fiber diameter uniformity by adding a small amount of NH_4SCN into the solution (Figure 4.7) to increase its conductivity. However, the addition of the salt greatly increased fiber diameter as can be expected because of the higher concentration of charge carriers in the solution that lead to an increase in the force pulling on the jet. We chose NH_4SCN because it would be easily removable by decomposition into two gases upon heating the samples above 170°C later and it seems adequately soluble in these polymer solutions.

a) 35 wt. % P84 in DMAc | 23.9°C | 11 % r.h. (2.4 g H_2O / m^3)
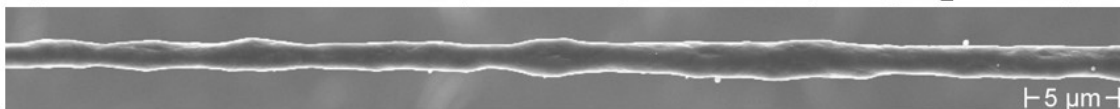
b) 30 wt. % P84 in DMAc + 1 wt. % NH_4SCN | 24°C | 13 % r.h.
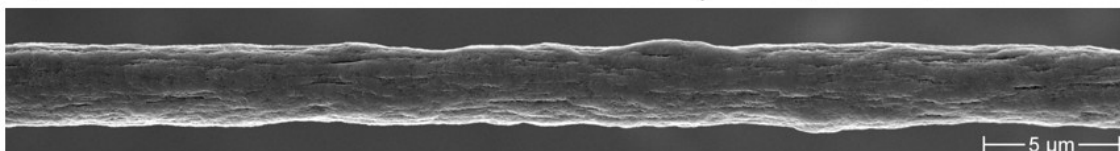
c) 25 wt. % P84 in DMAc + 1 wt. % NH_4SCN | 24°C | 7 % r.h.
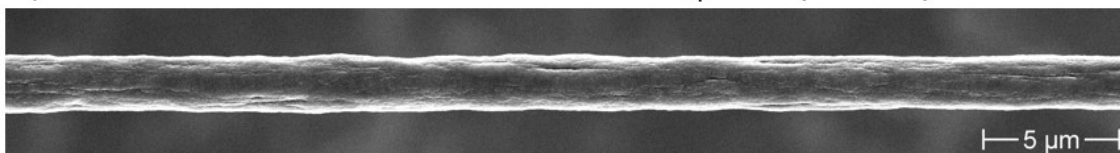
Figure 4.7. P84 Electrospinning in DMAc. (a) Even at 35 wt. % P84 concentration, the fibers have non-uniform diameter (usually associated with inadequate viscosity). (b-c) Fibers with improved diameter uniformity (and larger diameter) after some salt was added to improve solution conductivity.

Having the microstructure information explained above, we then focused on developing a process to yield aligned single P84 nanofibers. We have tested electrospinning multiple combinations of P84 concentration and NH_4SCN concentration mostly with DMAc as the solvent, but we have not yet been able to find conditions that reliably give single P84 nanofibers. We found that for most tested solution conditions, the chamber relative humidity needs to be below 5% at room temperature to allow a continuous spinning jet. Otherwise, the droplet at the nozzle can quickly solidify or give intermittent jets.

As with PMIA, we use a rotating spoked-drum collector where we initialize the jet on one end of the collector, and once the jet seems running and stable, we translate the nozzle along the collector and shut down the voltage when the nozzle reaches the other end. While a messy fibrous deposit almost always forms around the initiation region, we rarely observed any fibers depositing beyond that part.

For PMIA, while we found well aligned samples only form in a narrow set of conditions, in many conditions that were not optimal, we would still get some single fibers, albeit they would be loose, bundled or partly broken. With P84, it seems a significant amount of the fibers deposit directly on the spokes, and the ones that do span between spokes often have discontinuities. They tend not to continuously coil around the collector as a large spiral. We also occasionally observe fibers connecting from one spoke to the center (black rod in the middle). Experiments that did yield some single P84 fibers were often not reproducible such that we could not repeat the conditions that yielded a sample repeatedly to make more. Nevertheless, we were able to transfer some single fibers (and clean up any overlapping fibers using tweezers) to prepare suspended single fibers on a frame (Figure 4.8). Such frames could potentially support all aspects of the polymer fiber scaffold for making nanocables described in this work except the continuous spool processes in Chapter 5.
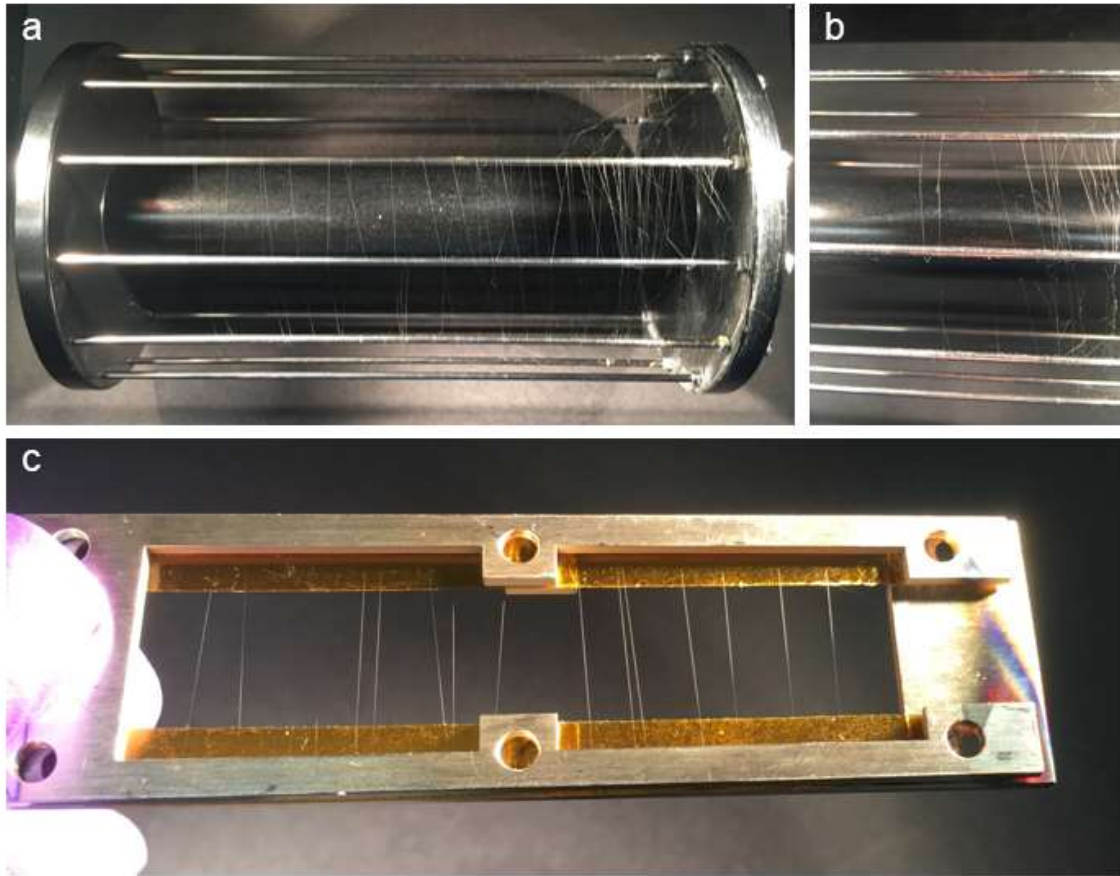
Figure 4.8. Electrospun NH$_4$SCN doped fibers. (a-b) Photos of the nanofibers on the spoked-drum collector. (c) Single P84 fibers suspended over a frame (with double-sided Kapton tape).

In a way, these broken fiber results with P84 were harder to draw conclusions from compared to our experience with PMIA, since it is easier to recover from a negative result that at least gives some fibers reproducibly. What certainly complicates the process is a requirement for higher voltages to get this solution to spin and the rapid precipitation of the solution beyond some very low humidity values. Also, the polymer molecular

weight seems to be low, requiring higher polymer concentration to compensate and leading to this low humidity clouding point. We continue to work on getting the electrospinner run at or near 0% RH which might improve the results. We previously had to test many conditions for PMIA to arrive at the vicinity of the conditions which reliably gave fibers, and with some good fortune, we might get to a similar point with P84 where most experiments start to give fibers in some form. It would be a lot more straightforward to optimize the process once we find such conditions. The alternative explanation might be that these nanofibers are too weak to remain intact when collected between spokes, despite having similar bulk strength values with PMIA, possibly due to excess solvent residue. Heating the chamber to ~40 °C lead to slightly oval-shaped fibers. Further experiments with *N,N*-dimethylformamide as a more volatile solvent are in progress.

a) 23.9°C | 11 % r.h. (2.4 g H_2O / m^3)
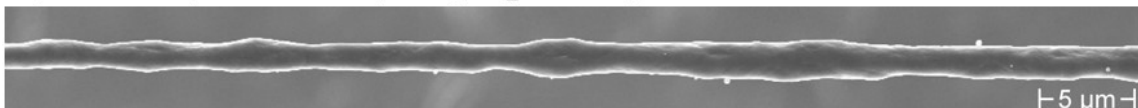
b) 41.3°C | 13 % r.h. (7.0 g H_2O / m^3)
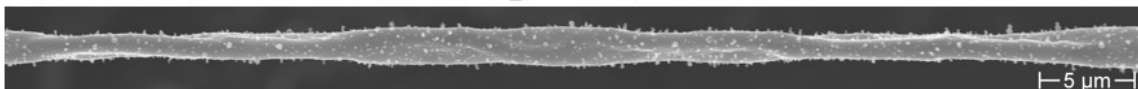
Figure 4.9. Electrospinning P84 at higher temperature. 35 wt. % P84 in DMAc was electrospun under two conditions with different temperature and absolute humidity. High temperature experiment was used to see if fibers were breaking because of solvent residue. (a) RT electrospinning result. (b) Ribbon-like P84 fibers spun at 41.3 °C.

Using fibers suspended on frames (Figure 4.8-c), we were able to sputter coated P84 fibers with Ag successfully (Figure 4.10). Unlike CP1, P84 turned out to be strong enough to handle the sputtering process, at least when spun with a couple-micron diameter. This is a quite promising result that invites further optimization of the P84 electrospinning process.
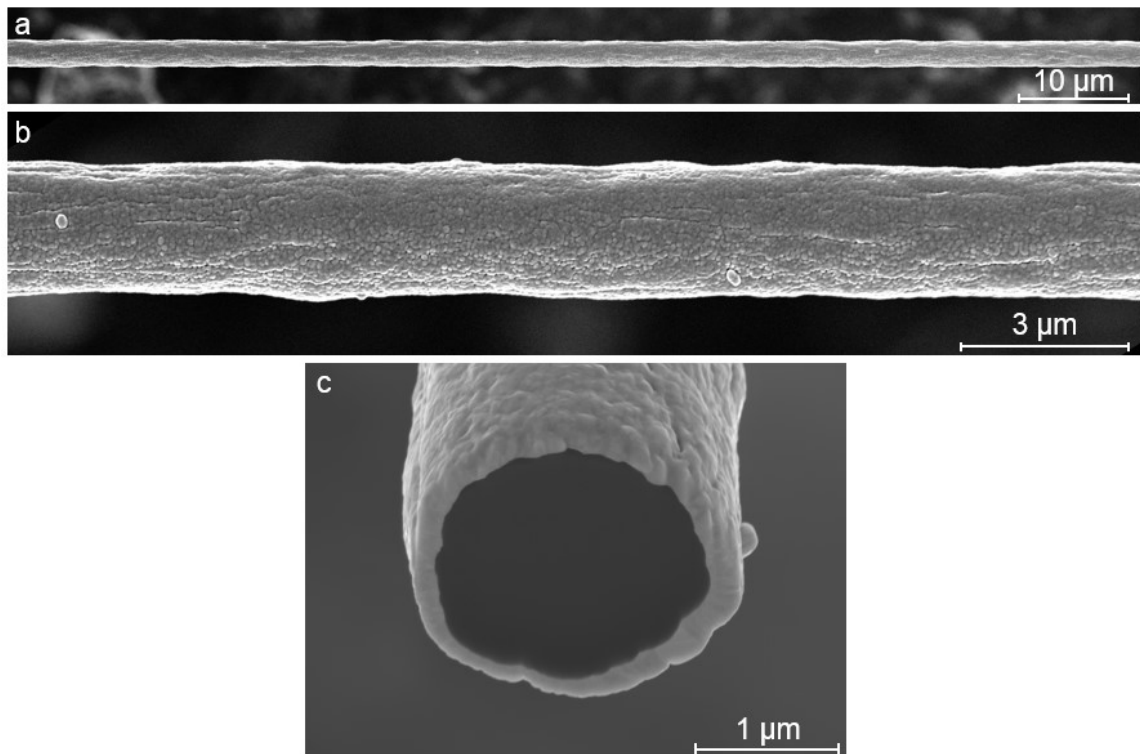
Figure 4.10. Ag sputter coated P84 fibers. (a-b) SEM image of a coated P84 fiber and (c) its cross section.

4.7 Conclusions

In this Chapter, we described our results from electrospinning polymers other than PMIA. More recently, we have redoubled our efforts towards looking for alternative polymers to replace PMIA and make salt-free nanofibers. This would have the potential advantage of eliminating extra storage requirements (desiccants and vacuum bags) or an extra nanofiber washing step. While these solutions are fairly simple to execute in the lab scale, they could complicate a larger scale production process should this technology be commercialized.

In Section 4.2, we discuss our results from electrospinning PAN, which is generally an easy polymer to electrospin. We used PAN nanofibers as nanocable models to practice wire handling before the PMIA method matured. In Section 4.3, we discuss our results from electrospinning Zylon (PBO), which turned out to be not suitable for making single nanofibers. In Section 4.4, we describe our results from electrospinning PAA, which would eventually be cured into Kapton nanofibers. Commercially available solutions of PAA were too low in molecular weight and viscosity, and they lead to heavily beaded fibers, and PAA solutions we synthesized at Harvard were higher viscosity for the same concentration range, but they still afforded some beads on fibers.

In Section 4.5, we discuss to similar fluorinated fully imidized soluble polyimides that have been developed for space applications. Nova Clear showed frequent jet splitting and poor fiber morphology, while with CP1, we were eventually able to make single aligned nanofibers with decent morphology. However, when we tried sputter coating

these nanofibers, they turned out to be too fragile and break off. In Section 4.6, we tested

another soluble polyimide that we acquired commercially, P84. P84 nanofiber

morphology was poorer initially, but adjusting its solution conductivity eventually lead to

uniform, albeit rather large diameter nanofibers. These can survive sputter coating.

Further optimization is underway for P84 as of this writing.

4.8 References

1.	Properties | ZYLON is a new high-performance fiber developed by TOYOBO. https://www.toyobo-global.com/seihin/kc/pbo/zylon_bussei.html#sds (accessed 4/4/2019).

2.	Duan, G.; Jiang, S.; Chen, S.; Hou, H., Heat and Solvent Resistant Electrospun Polybenzoxazole Nanofibers from Methoxy-Containing Polyaramide. *Journal of Nanomaterials* **2010,** *2010*, e219562.

3.	Kakzau, A. Aromatic polyamide nanofiber and fiber structure containing the same. US20100288692 A1, 2010/11/18/, 2010.

4.	Pai, C.-L.; Boyce, M. C.; Rutledge, G. C., Morphology of Porous and Wrinkled Fibers of Polystyrene Electrospun from Dimethylformamide. *Macromolecules* **2009,** *42* (6), 2102-2114.

5.	Inc., H. P. P84 Fibre Technical Brochure. https://www.p84.com/product/peek-industrial/downloads/p84-fibre-technical-brochure.pdf (accessed 4/8/2019).

6.	Lasprilla-Botero, J.; Álvarez-Láinez, M.; Lagaron, J. M., The influence of electrospinning parameters and solvent selection on the morphology and diameter of polyimide nanofibers. *Materials Today Communications* **2018,** *14*, 1-9.

Chapter 5 Reel-to-Reel Manufacture of Polymer Fiber Supported Microwires

5.1 Project Overview

While our initial goal has been to develop nanowires up to 10 centimeters in length, introduction of the spoked-drum collector lead to PMIA nanofibers continuously looping around the collector for multiple meters. Yet all the coating work described above as well as the hundreds of fiber samples coated at Draper all used chopped bits of these fibers, typically a few centimeters in length. Even with the partially unraveled longer fibers described in Section 2.6, it became clear that we are underutilizing the full potential of our findings. Our vision for the next stage of this project is to develop a semi-continuous process where we start with a spool of nanofibers and coat them in a reel-to-reel setup. For example, the fiber could be connected to a second spool, and as it unwinds from the first and gets wound on the second, it could pass through a deposition region. While we envisioned potentially building such systems for the metal CVD or PVD depositions, electrolytic copper plating would likely provide the fastest growth rate for metalizing the fibers. There could be more deposition streams for the metalized wire to go through to add electrical insulation or other functionalization.

Draper proposed and built a prototype to use the reel-to-reel setup in combination would liquid bridges to achieve electroplating on the wires in a continuous setup. Scheme shown in Figure 5.1 describes this prototype. We would start with a spool, the

preparation of which is detailed in the following section. One end of the fiber would get connected to the second spool using some tape. In between, the fiber passes through two liquid bridges where a solution comes from one tube at the top and flows into one below. They chose to use a gold deposition path for one of the solutions, though it could be any kind of electroplating solution, and the second tube contains a solution of KCl electrolyte to complete the circuit. There are electrodes immersed in the tubes connecting the solution to a power source, and the solutions are constantly pumped to provide mass transport.
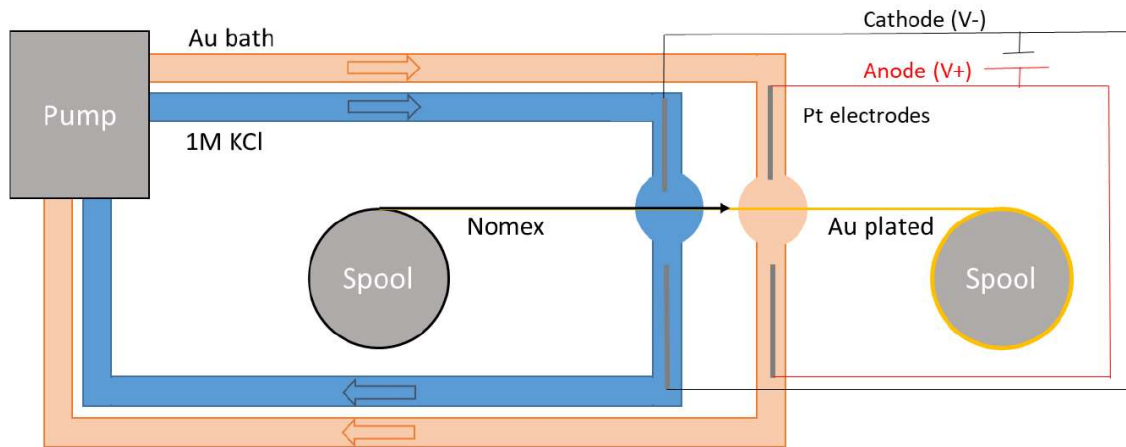
Figure 5.1. Schematic of a reel-to-reel electroplating setup for continuously coating PMIA nanofibers. (Figure Credit: Alex Couch, Draper)

Draper has built this prototype as show in Figure 5.2, and they tested it by plating much larger commercial metal wires (Figure 5.2). For the nanofiber spools, we have had some successful experiments where we prepared a spool with >1 m long nanofiber looped around as described in Section 5.2. Before PMIA nanofibers can be electroplated

using this setup, they need to be made conductive. So far, we have been relying on sputter coating the fibers with some gold, but for the ultimate rapid nanofiber coating process, this turns out to be too slow. The sample spool typically needs to be pumped down for some hours (unless we found a system with a much larger load lock chamber) before each sputtering, and once all the fiber handling procedures are in place, sputtering would be the significantly rate limiting step of this process. In Section 5.3, we describe our proposal to use localized electroless plating on the polymer nanofibers that could potentially deposit a conductive seed layer using a similar liquid bridge and be much faster than sputtering.
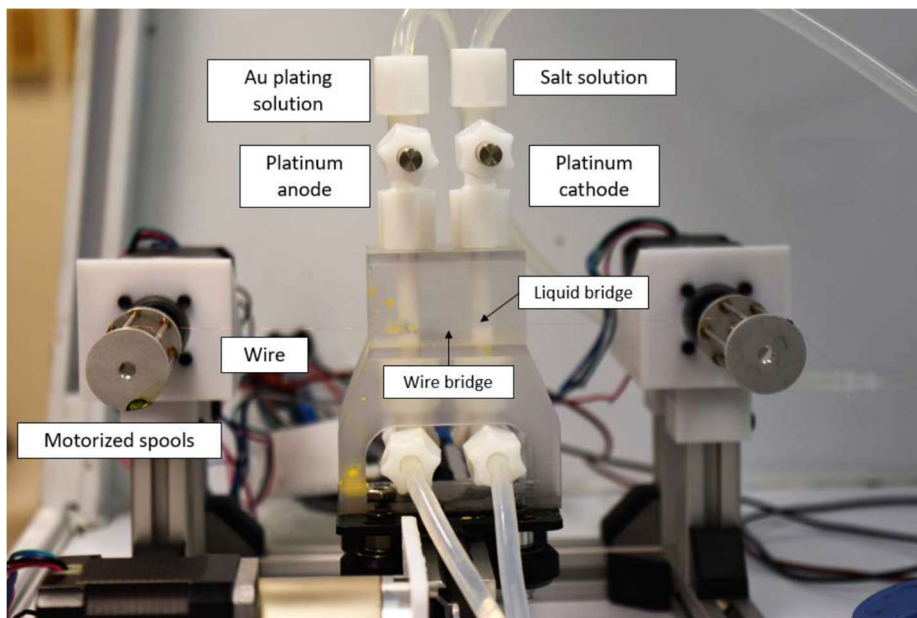
Figure 5.2. Reel-to-reel electroplating setup with liquid bridges. A 1 mil copper wire is shown getting coated for the test run. A saline solution with electrode is used to complete the circuit. (Photo Credit: Alex Couch, Draper)

5.2 Nanofiber Spool Preparation

After the PMIA nanofibers are spun onto the spoked-drum collector, they form a continuous spiral around and form the initial large spool that we leverage in this project. This spool is too large to bring into most sputtering chambers or routine transport between labs, so we decided to switch to using smaller cylindrical objects for spools. Earliest prototype we tried was a metal cylinder 1" in diameter for the spool. One end of the fiber was unwound from the large spool and attached to the smaller one using double sided tape. Handling the ~350 nm wide nanofiber at this step can be quite challenging, since it is only visible when the light hits at a perfect angle, but we have practiced it many times as of this writing. Then, we used a cake stand to rotate the large spool as we manually rotated the smaller spool that was attached to a shaft with a stand and transferred some fibers continuously.

Two problems were observed in the first transfer experiment: (1) As the fiber is unwound from the large holder, it gets taut for a while as it gets pulled off a spoke, then then it pops out and becomes very loose. While its loose, the fiber can wind around the second spoke in an uncontrolled fashion, instead of in a uniform spiral, and if it crosses over existing fibers, that would complicate unwinding in the next stage. Second, the fibers were not readily visible on the metal cylinder the same way they were not readily locatable on the large drum collector.

98

For the second experiment, we built a smaller (1" wide) spoked-drum to act as a spool to address the second issue, and Alex built a fully motorized setup to rotate the two spools (Figure 5.3). For the issue of fiber tautness, we introduced a fiber guide in the form of a water meniscus. This is achieved by having a small vial on a motorized plate between the two spools filled with water extending out of the vial. Once the fiber touches the water surface (Figure 5.3-d), it gets gently fixed in position along the length of the small spool, and this helped achieve a more uniform transfer process.
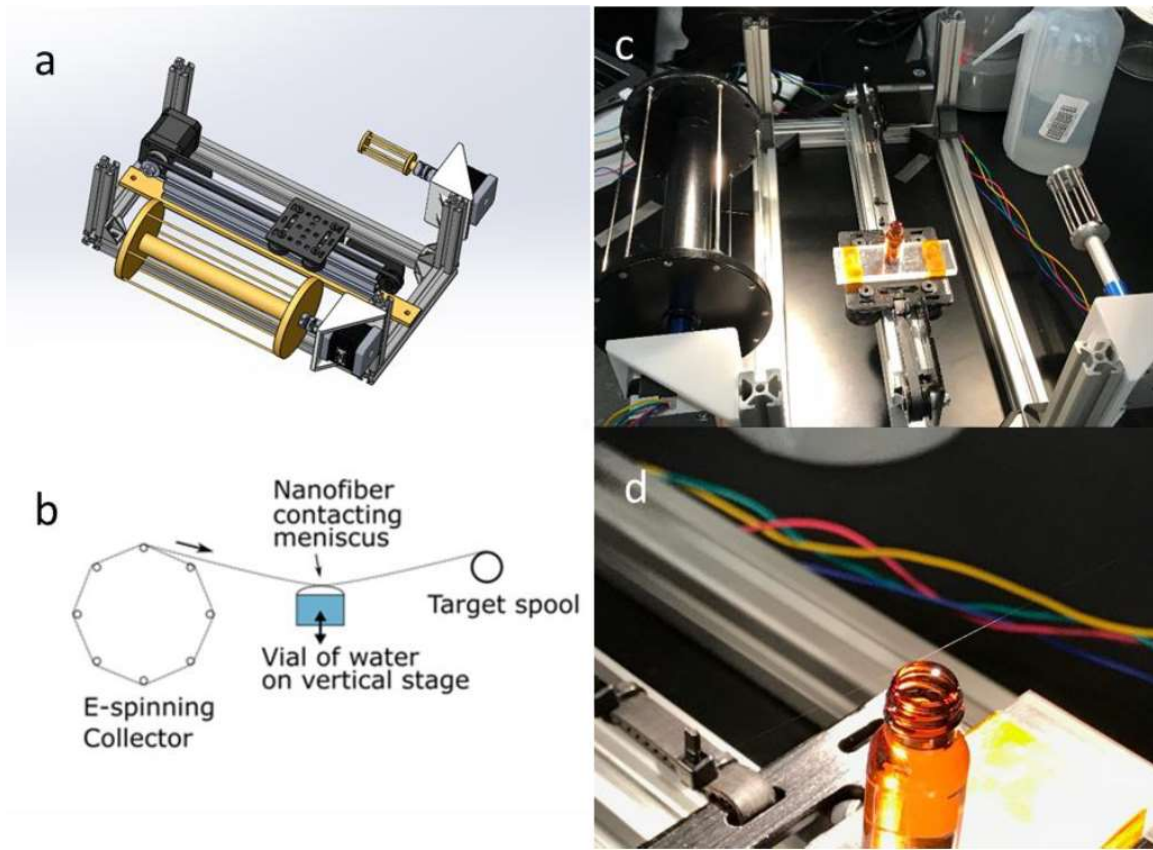
Figure 5.3. Motorized reel-to-reel spool transfer setup with water meniscus fiber guide. (a) Design of the reel-to-reel setup. (b) Sideview schematic of the transfer process. (c)

(Continued) Photos of the setup in action. (d) Closeup of the water meniscus guide holding the fiber. (Figure Credit: Alex Couch, Draper)

While Figure 5.3-c shows a configuration where the large spoked-drum having 6 spokes (the typical configuration we use for making nanowires to transfer on frames as in Chapter 2), we found that adding more spokes (to a total of 12) minimizes the looseness the fiber assumes after popping off from a spoke. In combination with the water meniscus-based guide, this strategy further improved transferred fiber positioning and minimized crossovers, and we were able to prepare one small spool with ~1.2 m long continuous PMIA nanofiber wrapped around in monotonously advancing fashion as shown in Figure 5.4.
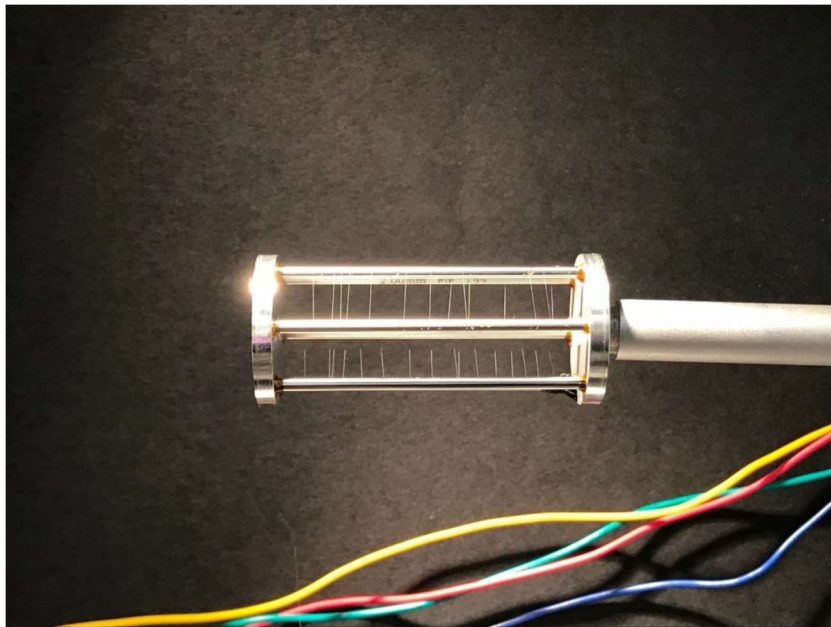
Figure 5.4. Image of the small spool with ~ 1.2 m PMIA nanofiber looped around. (In collaboration with Alex Couch.)

In collaboration with Dr. David J. D. Carter, Dr. Heena K. Mutha, and Peter Lewis, we are working on preparing small spools as the one shown in Figure 5.4 in a routine and reproducible way to support the electroplating efforts described in Figure 5.3. Most often the issues we find are related to keeping the fiber taut enough during the transfer to achieve such spiral with no crossovers. In addition to the irregularities in motion of the motors in the setup, the guide part as described above has some limitations. One problem that can occur is the fiber moving to the edge of the meniscus and touching the glass part (Figure 5.5). When that happens, the fiber gets stuck on the glass, and we need to stop the transfer and manually push the fiber back up. Otherwise, the adhesion to glass is strong enough to yank and break the fiber. Another issue is the positioning. The fiber wobbles back and forth on the droplet-air interface, so it inherently limits how densely we can pack the fibers in the second spoke without causing crossovers; and when the fiber moves to the rear side of the droplet (opposite from the direction of translation) and gets taut enough, it can pop off the guide and become uncontrolled. Efforts to improve the guide performance or come up with alternative fiber position control mechanisms are underway.

Translation Direction
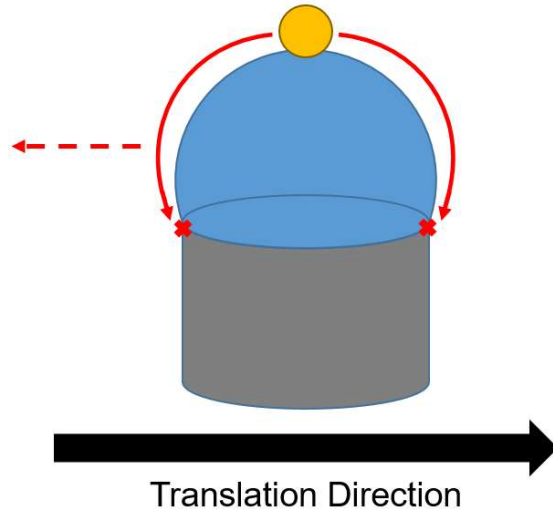
Figure 5.5. Illustration of the possible motions the fiber can do on the water meniscus. Yellow circle is the cross section of the fiber (running perpendicular to the paper plane), and the red arrows and marks show the possible motions it can do. If it touches the edges of the glass vial, it can get stuck and break the fiber. At the back of the droplet, with enough tension, it can pop off from the droplet and become uncontrolled.

5.3 Electroless Seed Layer Development

Sputter coating to add a conductive seed layer is the slowest step in this proposed scheme of making spools of nano- and microwires. Meanwhile, we could skip requiring a conductive layer altogether by using an electroless deposition, but that typically forms a less well-controlled, less conductive, and more brittle metal layer. Also, we are concerned the stability of an electroless plating solution and its potential to deposit elsewhere inside the reel-to-reel setup, clogging a tubing or damaging the pump. We have been looking at strategies to localize electroless deposition just on the surface of the fiber. There have

been some reports of localized electroless plating using light[1-3] or two-phase systems.[4-5] Inspired by the latter, we envisioned separating one of the components of an electroless plating solution and placing it in the nanofiber. The reactant-infused nanofiber could then be passed through a solution (in another liquid bridge in the reel-to-reel setup) and localized electroless plating could be achieved (schematically shown in Figure 5.6 for the case of reductant infusion).
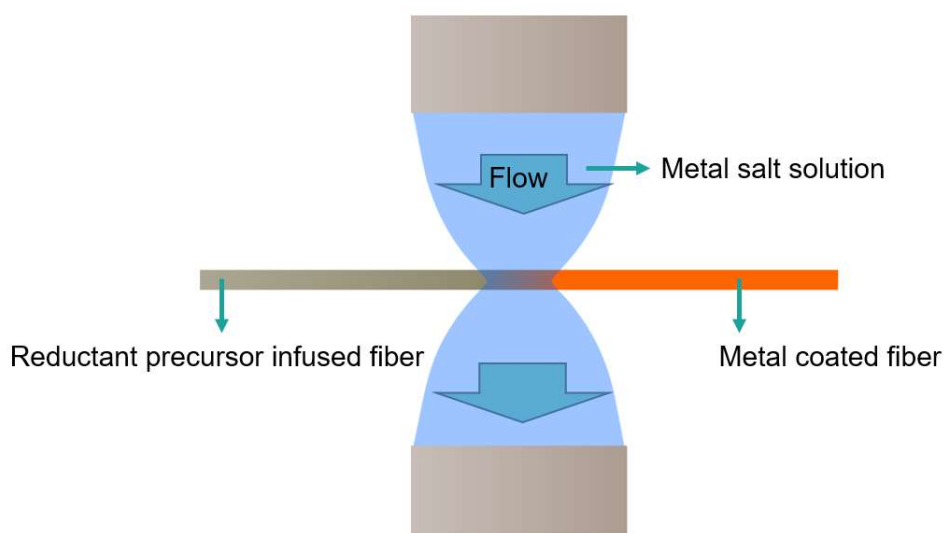
Figure 5.6. Localized electroless plating with reductant infused nanofiber.

We looked at copper and palladium as potential seed layers for the ensuant electrolytic deposition. A typical electroless plating solution for copper consists of: (a) a metal salt (e.g. copper (II) sulfate), a reducing agent, and some chelating agent.[6] For the case of the most commonly used reducing agent, formaldehyde, the solution is also made basic because that enhances the reduction potential of this reagent. We expected that a reducing agent in the form small organic molecule would be more soluble in our PMIA

solutions in DMAc/CaCl$_2$, and infusion of the nanofibers with reducing agents were considered first.

5.3.1 Reductant Infused PMIA Films and Nanofibers

First, we investigated adding a reducing agent into PMIA nanofibers by putting it into its solution. While formaldehyde is most commonly used as the reducing agent, a solid reagent is needed for doping the nanofibers. Adding sodium borohydride and sodium triacetoxyborohydride to previously prepared routine PMIA solutions (containing 17.5 wt. % PMIA and 8 wt. % CaCl$_2$ in DMAc) did not dissolve well or lead to clear solutions, but dimethylamine-borane complex is quite soluble in this solution system (shown up to ~5 wt. %). This reducing agent has been shown to work well for depositing electroless copper.[7-9]

For initial testing of the localized electroless plating, the reductant infused polymer solution was doctor bladed onto a Kapton film substrate, and a droplet of the metal solution was placed on top the check for deposition. All the components that would go into a conventional electroless plating solution minus the reducing agent were placed in this solution: Including the metal salt (CuSO$_4$ · 5 H$_2$O), chelating agent ethylenediamine-tetraacetic acid (EDTA), and some base (triethanolamine) that serves to lower the reduction potential of the reductant. No film became apparent at room temperature, even with exceedingly long wait times (at which point the solution droplet dried on the film). One of the references for using dimethylamine-borane includes an initial surface treatment with a PdCl$_2$ solution before applying the electroless solution did

not lead to conductive films, but we did see black particles form inside the solution droplet.

Removing the chelating agent, which normally serves to stabilize an electroless plating solution, afforded copper film depositions to occur, but only when the samples are heated to 70 or 80°C. We next attempted to cut pieces of our PMIA film on a PI support and dipping them into the copper precursor solution. We saw some copper-looking films form along with other dark deposits on the PMIA surface, but also color change within the solution and some copper deposits at the edges of the vial. Some of the tests yielded conductive coatings while others did not, and the system was complicated by the formation of additional copper particles that seem to form in it since copper catalyzes this reduction process. As the copper solution was too absorbing, a dilute $PdCl_2$ solution in HCl was used to demonstrate the reducing agent diffusion instead in (Figure 5.7): A reducing agent infused PMIA film (on a Kapton substrate) was placed within the metal solution (at RT). Immediately, black metal particles started forming throughout the solution. Since the reductant seems to readily diffuse outside the polymer before most of the deposition can occur, it seems this strategy does not work well in localizing the electroless plating solution.
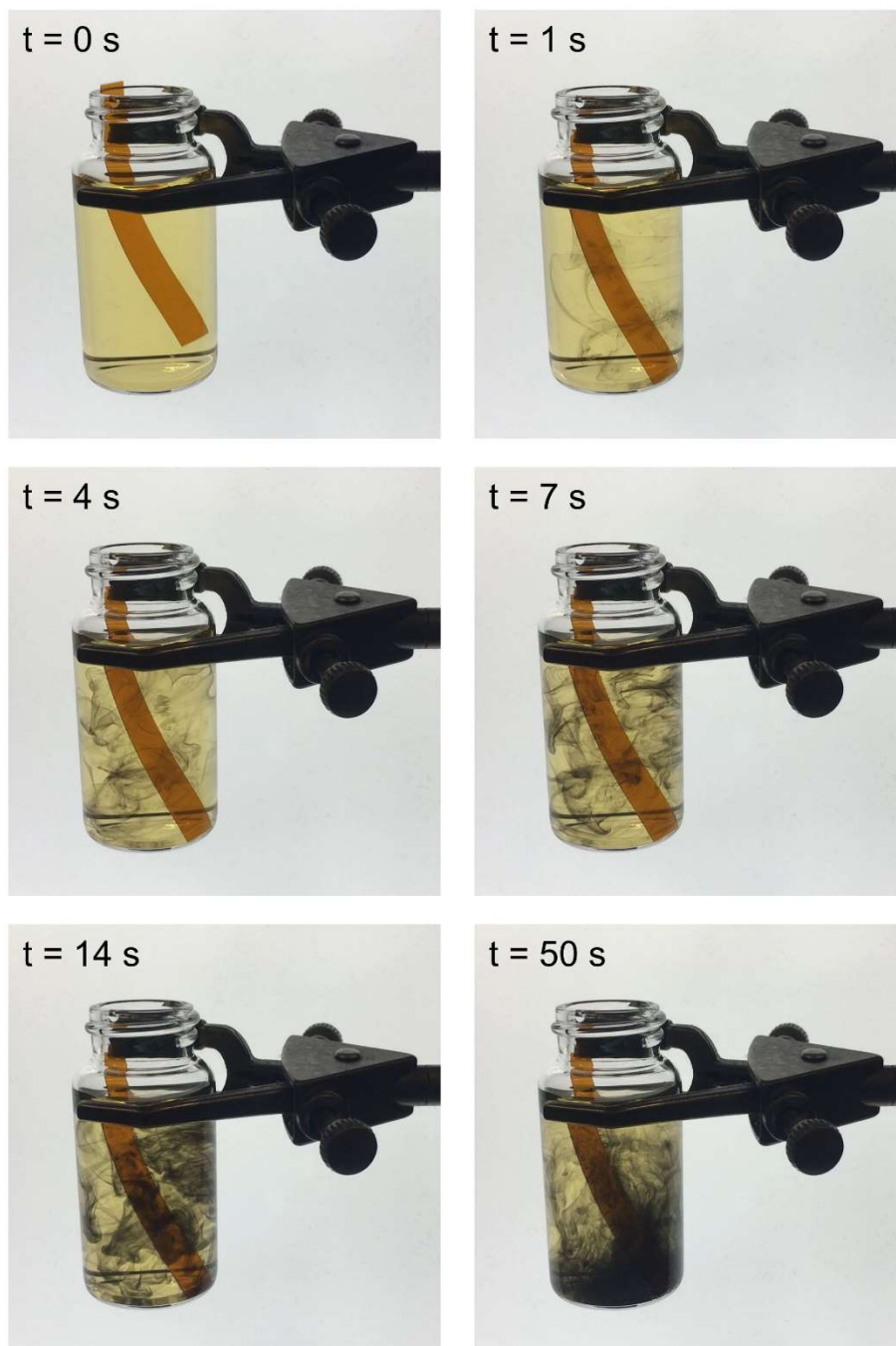
Figure 5.7. Reductant diffusion demonstration with $PdCl_2$ solution. Black particles start forming across the solution and eventually precipitate.

5.3.2 Metal Precursor Infused PMIA Films and Nanofibers
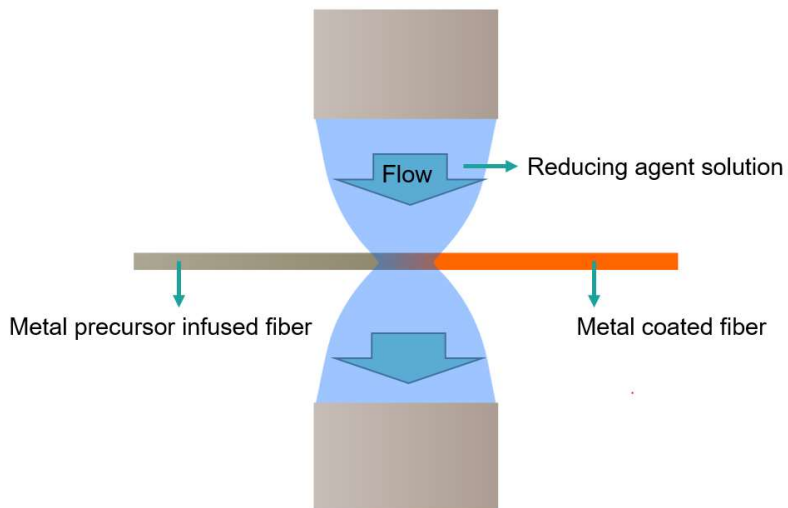
Figure 5.8. Localized electroless plating scheme with metal precursor infused fibers.

In this section, we inverted our original proposal and tried to add some metal precursor into the nanofibers (Figure 5.8). First, replacing part of $CaCl_2$ with $CuCl_2$ was investigated (Figure 5.9), but we found that we still need the full 8 wt. % of $CaCl_2$ to dissolve this concentration of PMIA.

17 wt. % PMIA
8 wt. % $CuCl_2$
DMAc

17.5 wt. % PMIA
4 wt. % $CaCl_2$
4 wt. % $CuCl_2$
DMAc

17.5 wt. % PMIA
7 wt. % $CaCl_2$
1 wt. % $CuCl_2$
DMAc

17.5 wt. % PMIA
8 wt. % $CaCl_2$
0.5 wt. % $CuCl_2$
DMAc
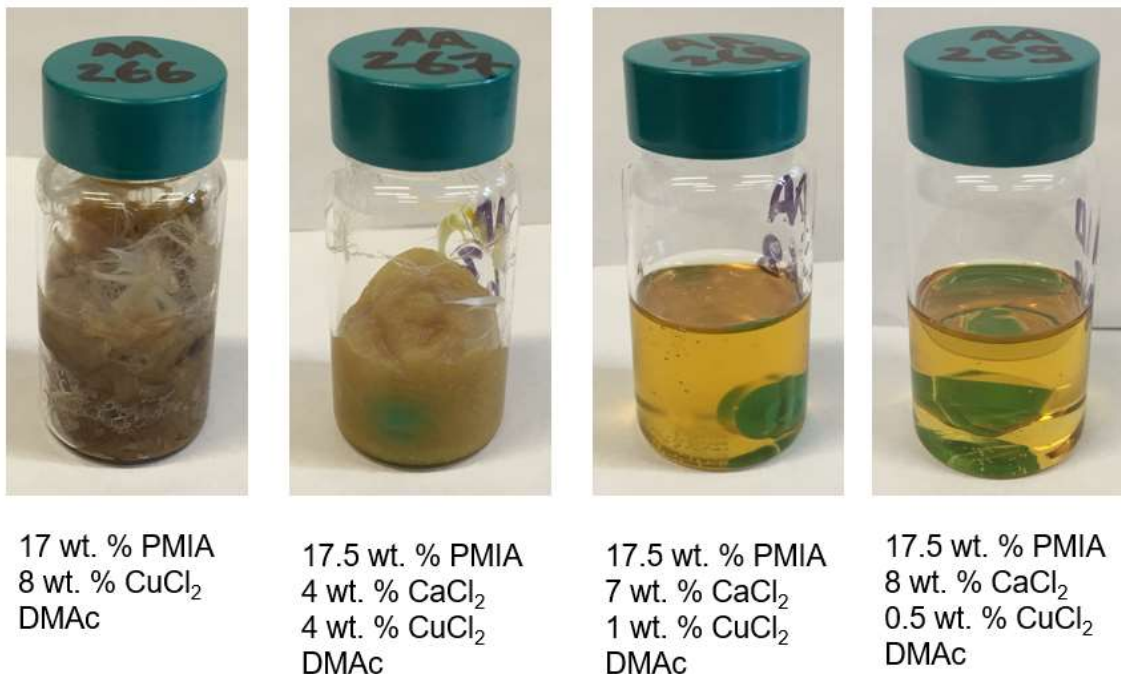
Figure 5.9. Attempts to replace $CaCl_2$ fully or partially with $CuCl_2$.

Next, films were blade cast on Kapton films as before and dried slowly (to minimize delamination). This time, a solution of reducing agent (still using dimethylamine-borane complex) in base (triethanolamine) was placed on top. At room temperature, no deposition was observed, but when the substrate was heated to >70 °C, immediate film formation was observed. The films looked semitransparent (Figure 5.10), and their thickness seemed to primarily depend on the $CuCl_2$ concentration in the polymer film.
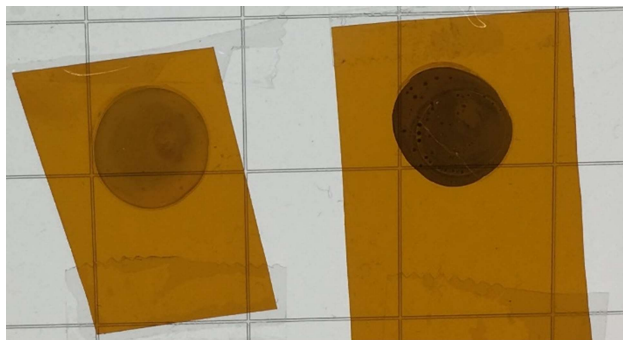
Figure 5.10. Localized copper depositions on CuCl$_2$ infused films. On the left, a lower CuCl$_2$ containing film lead to a thinner Cu film (37.9 Ω/sq). On the right, initial CuCl$_2$ concentration was about twice as high, and a thicker (cuprous and metallic looking) copper film was obtained (13.09 Ω/sq).

The electroless plated copper appears cracked under SEM, which explains the transparency. The thinner film has more frequent cracks, but the metal is still largely percolated.

a) Thinner Cu film from solution with 8 wt. % CaCl$_2$ and 0.5 wt. % CuCl$_2$:
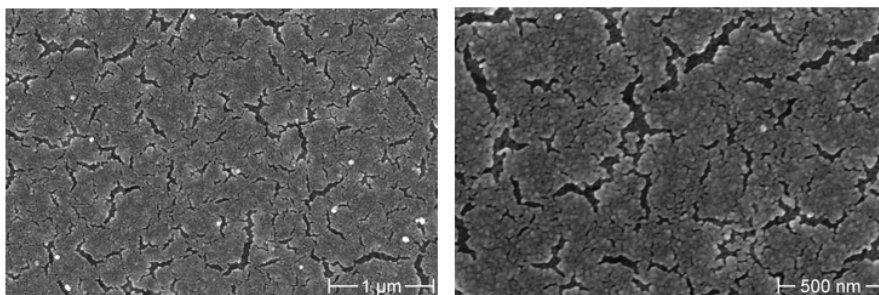
b) Thicker Cu film from solution with 7 wt. % CaCl$_2$ and 1 wt. % CuCl$_2$:
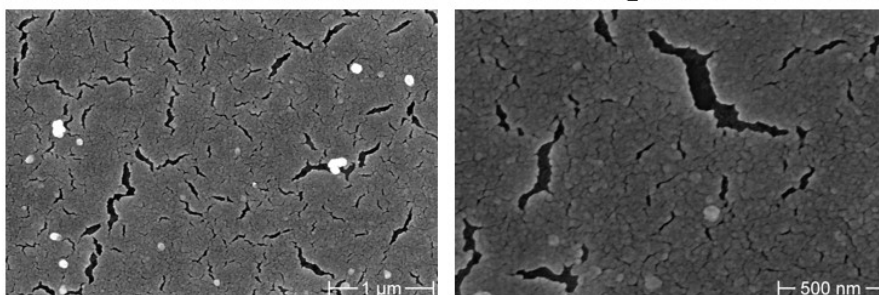
Figure 5.11. Electroless plated Cu on PMIA. (a) and (b) SEM image of the copper films from Figure 5.10.

The 0.5 wt. % CuCl$_2$ doped routine PMIA solution can be readily spun into nanofibers. Without any optimization, the routine PMIA nanofiber yielded some single fibers (Figure 5.12). To check if we can reduce them and obtain conductive nanowires, this solution was spun onto a polymer film substrate (on a rotating drum collector) for 30 minutes with the goal of making a nanofiber mat. The mat was reduced at 70°C and conductivity was tested along the fibrous mat, but we could not detect any conduction. Based on these concentrations, we expect on the order of one atomic layer to get coated around the wire at this concentration, which might be getting easily oxidized.
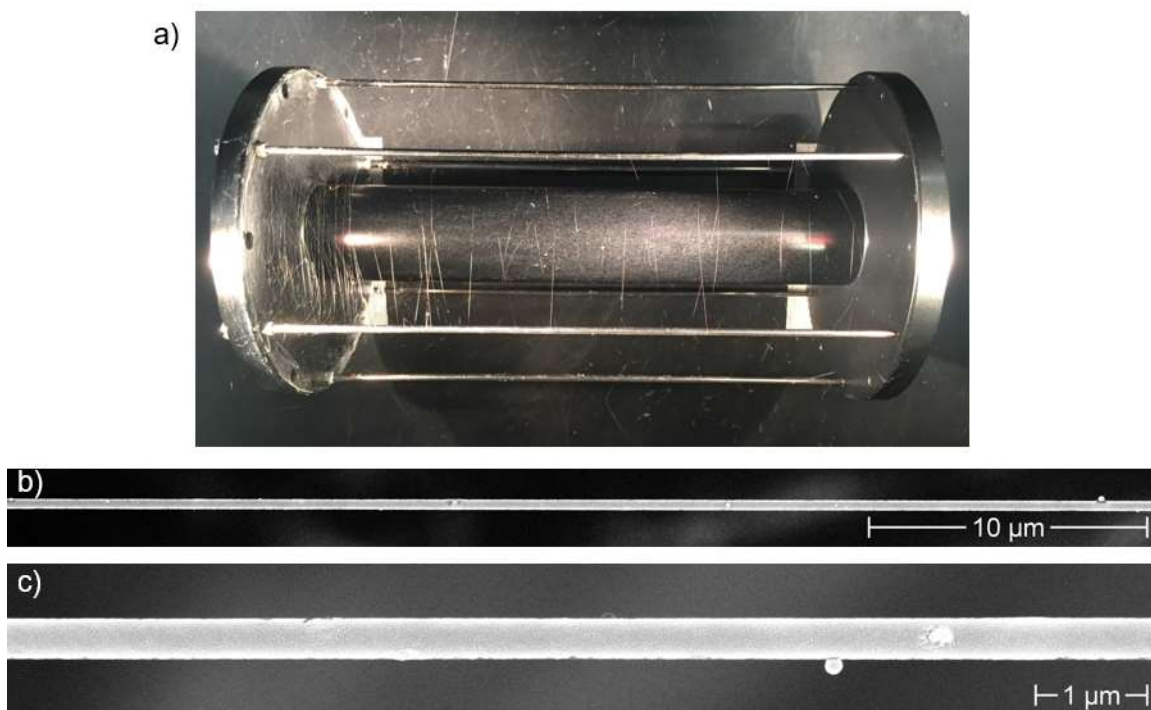
Figure 5.12. Electrospun $CuCl_2$ doped nanofibers. Photo of the fibers. (b - c) SEM images of the doped nanofibers.

For the regularly used PMIA solution, increasing concentrations of $CuCl_2$ were added to check their solubility with the goal of increasing the expected thickness for any localized deposition. We found that clear spinnable solutions are obtainable at 1.5 wt. % $CuCl_2$ addition, but not beyond 2.0 wt. %. Copper layer thickness could further be increased by electrospinning thicker nanofibers, e.g. by increasing the applied potential (Chapter 2). Further studies to show conductivity of these electroless plated wires is underway.

17.5 wt. % PMIA
8 wt. % CaCl$_2$
0.5 wt. % CuCl$_2$
DMAc

17.5 wt. % PMIA
8 wt. % CaCl$_2$
1.0 wt. % CuCl$_2$
DMAc

17.5 wt. % PMIA
8 wt. % CaCl$_2$
2.0 wt. % CuCl$_2$
DMAc

17.5 wt. % PMIA
8 wt. % CaCl$_2$
3.0 wt. % CuCl$_2$
DMAc
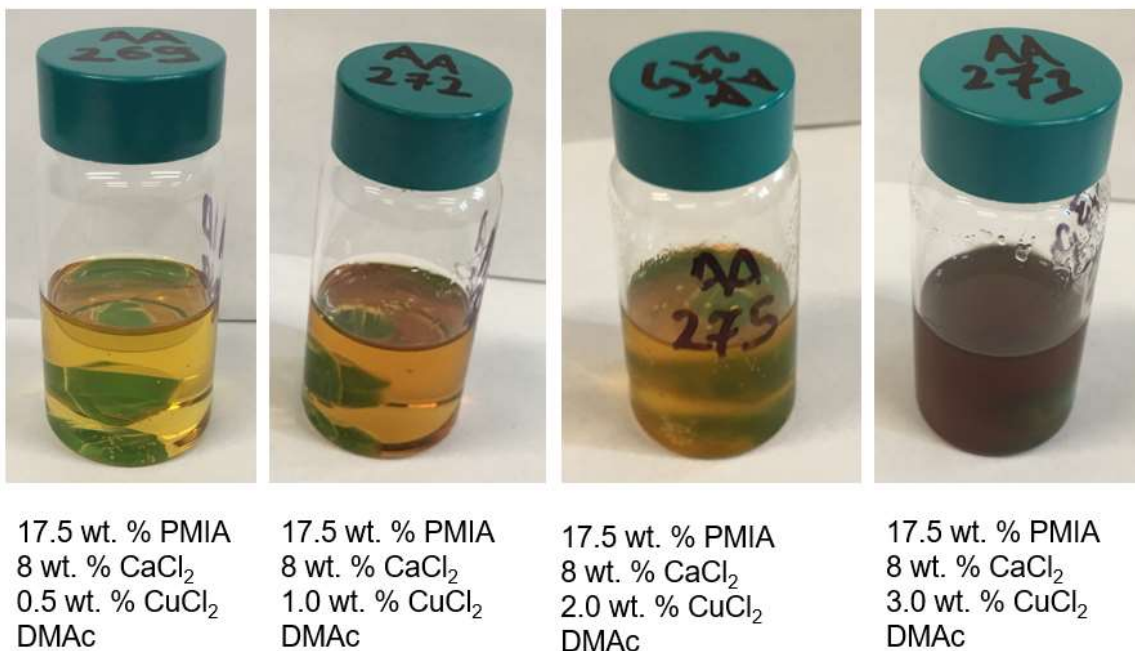
Figure 5.13. Increasing CuCl$_2$ concentration.

5.4 Conclusions

In this chapter, we describe the next stage of scaling up the polymer nanofiber scaffold-based nanowire production method: Reel-to-reel processing. Instead of cutting centimeter-scale fragments on frames, we can transfer a continuous nanofiber with > 1 m length, and we are building setups that would allow continuous coating of these long nanofibers.

In Section 5.1, we describe the setup developed at Draper for performing a high-throughput electrolytic deposition onto the nanofibers. In Section 5.2, we demonstrate our ability to transfer and handle nanofibers continuously and prepare a spool with over 1 m

long nanofiber. In Section 5.3, we describe our initial results towards developing a

localized electroless plating protocol for adding a conductive layer onto the nanofibers

using the reel-to-reel setup. This will be useful in replacing the currently used sputter

coated thin metal layer, since sputtering is too slow for an eventual large-scale nanowire

or microwire production process following this method.

5.5 References

1.   Ikeda, S.; Akamatsu, K.; Nawafune, H., Direct photochemical formation of Cu patterns on surface modified polyimide resin. *Journal of Materials Chemistry* **2001,** *11* (12), 2919-2921.

2.   Akamatsu, K.; Ikeda, S.; Nawafune, H., Site-Selective Direct Silver Metallization on Surface-Modified Polyimide Layers. *Langmuir* **2003,** *19* (24), 10366-10371.

3.   Akamatsu, K.; Kimura, A.; Matsubara, H.; Ikeda, S.; Nawafune, H., Site-Selective Direct Photochemical Deposition of Copper on Glass Substrates Using TiO2 Nanocrystals. *Langmuir* **2005,** *21* (18), 8099-8102.

4.   Tsuneyoshi, T.; Yohaze, Y.; Watanabe, T.; Ono, T., Free-Standing Metal Films Prepared via Electroless Plating at Liquid–Liquid Interfaces. *Langmuir* **2018,** *34* (44), 13183-13191.

5.   Garcia, A.; Polesel‐Maris, J.; Viel, P.; Palacin, S.; Berthelot, T., Localized Ligand Induced Electroless Plating (LIEP) Process for the Fabrication of Copper Patterns Onto Flexible Polymer Substrates. *Advanced Functional Materials* **2011,** *21* (11), 2096-2102.

6.   Deckert, C. A., Electroless Copper Plating A Review: Part I. **1995**, 8.

7.   Kulyk, N.; Cherevko, S.; Chung, C.-H., Copper electroless plating in weakly alkaline electrolytes using DMAB as a reducing agent for metallization on polymer films. *Electrochimica Acta* **2012,** *59*, 179-185.

8.   Plana, D.; Campbell, A. I.; Patole, S. N.; Shul, G.; Dryfe, R. A. W., Kinetics of Electroless Deposition: The Copper−Dimethylamine Borane System. *Langmuir* **2010,** *26* (12), 10334-10340.

9.   Ellsworth, A. A.; Walker, A. V., Role of the Reducing Agent in the Electroless Deposition of Copper on Functionalized SAMs. *Langmuir* **2017,** *33* (35), 8663-8670.

Chapter 6   Conclusions and Future Directions

6.1 Conclusions

Overall, this dissertation describes methods for electrospinning polymer nanofibers and coating them with functional materials to make submicron thick insulated cables. In chapter 2, we showed that PMIA is a particularly attractive polymer scaffold because of its favorable electrospinning behavior that can yield well-controlled fiber alignment and length. We also described some challenges related to humidity control in making these fibers reproducibly and storing them, and we described solutions to these challenges.

In chapter 3, we described our observations from depositing various materials onto the fibers. For PVD, we would coat the fibers from two opposite sites to improve conformality, which worked particularly well for sputtering Ag, but some other metals do not make as conformal coatings while causing the fibers to weaken and sag. We also showed that high-temperature ALD and CVD coatings can be applied onto the nanofibers. A sufficiently UV-blocking Al_2O_3/HfO_2 can be used to minimize the sputtering damage on the PMIA nanofibers, improving the metalized nanocable's tautness, strength, and coating conformality. Sputtering damage can be avoided altogether by switching to thermal evaporation of metals at the expense of coating conformality or to metal CVD depositions which are more limited in the choice of

metals. Finally, we showed one of our approaches for insulating the nanowires with a polysiloxane coating deposited by Prof. Karen Gleason's group.

The main goal of our work has been to develop a method to make insulated nanocables, and to supply our collaborators with these cables so that they can develop nanowire manipulation methods and make litz braids for GHz-frequency devices. We were successful in scaling up our nanofiber production as the demand for them increased. After we showed various strategies for getting metal coatings, most of the nanofibers were coated on an industrial scale sputter coater with a fixed thickness of ~350 nm (x2) of gold at Draper. The large sputter coater can coat more than 20 frames (outer dimensions: 3.5" x 1") at once. Draper required comparably high throughput depositions for the insulation layer such that they can coat many frames at once, and they realized this through the collaboration we initiated with Prof. Karen Gleason. Draper has then proceeded with successfully making hierarchical twists (twists of twists) that consist of 25 nanowires using a motorized setup submerged under water. In their method, small magnetic disks are glued onto each nanowire that allows their reversible attachment to a motorized arm which is then rotated and translated simultaneously to form a twist. Their method is readily scalable, such that they first make twists (consisting of 5 wires), then use the same method to make twists of twists (consisting of 5x5 wires), and they could presumably repeat to make higher order twists following the same method to make thicker wires (consisting of 125 wires etc.). Draper also continuously increased their

handling efficiency so that they can use most of the coated nanowires without breaking them.

The PMIA nanofibers are humidity sensitive because of the deliquescent $CaCl_2$ they contain. (Without this salt or LiCl, which is even more hygroscopic, the polymer cannot be dissolved in organic solvents.) In Chapter 2, we listed strategies for reducing this sensitivity, which would otherwise form protrusions on the fibers: (Section 2.4) Removing the $CaCl_2$ by washing it out or wiping off its solution droplets via contact, (Section 2.5) by vacuum packing samples with desiccant bags or storing them in various desiccators, and (Section 3.4) by coating them with a water diffusion barrier. For the most part, samples were simply preserved under low humidity, e.g. in a vacuum desiccator or vacuum packing with some silica gel packs, which was the main way samples for Draper were prepared.

In Chapter 4, results from electrospinning different materials are presented. This includes our earlier investigations before PMIA emerged as a sufficient system as well as our later efforts to make deliquescent salt-free nanofibers that do not require special handling or washing. We hope to replace with PMIA with another polymer to achieve that effect, and various solubilized polyimides look the most promising. Unfortunately, CP1 that was developed for space applications proved too fragile to coat readily (at least with sputtering), but P84 is quite promising in that regard. While we initially had issues with fiber morphology, we were able to make some uniform P84 nanofibers by adding some small amount NH_4SCN. While the presence of this salt might appear at odds with

our goals, its concentration is much lower than the $CaCl_2$ in PMIA nanofibers (such that it would cause less roughening), and it can be readily removed from the fibers via heating (NH_4SCN decomposes above 170 °C into NH_3 and HSCN). While we only discussed a few of the high temperature stable soluble polyimides, there are others we are looking at studying in the future: Matrimid 5218[1-2] and polybenzimidazole (PBI).[3-4] The latter polymer can be purchased from a vendor in solution form with reportedly high viscosity, which suggests this polymer will circumvent the low molecular weight related problems of the other polyimides we studied.

In Chapter 5, we describe our current efforts of scaling up the nanofiber production beyond the frames. Suspending fibers on frames has inherent length limitations that underutilize the multiple-meters long single nanofiber we are able to make, and the frame preparation protocol is manual intensive and not conducive to large scale nanowire fabrication. By preparing a spool of nanofiber that can be attached to different setups and facilitate reel-to-reel processing, we demonstrate some of the potential for commercializing this technology to large scale production. Draper is developing a high-throughput electroplating strategy that would dramatically increase metal deposition rate over PVD or CVD methods, and we are studying a localized electroless plating strategy to form a seed layer for that electroplating.

6.2 Future Directions

6.2.1 N-Substitution for Spinning Nomex and Kevlar

We are interested in making soluble versions of PMIA that do not require salt. One strategy we pursued at the beginning of the project is to make a co-polymer that is mostly PMIA with some para versions of the monomer mixed in, that was supposed to be soluble as such.[5] This strategy did not work well for us, as the polymer synthesis often left residual HCl which seem to contribute to polymer solubility. It seemed unclear if the co-polymer would still be soluble in the absence of the acid, and the acid contaminated co-polymer turned out to be too corrosive to utilize in our electrospinner.

Another strategy to solubilize polyaramids is to functionalize the N-groups.[6-8] Both for PMIA and para-aramid (Kevlar), the N-groups in the amide bonds can be alkylated by first reacting the amide with sodium hydride or sodium naphthalenide (or other reducing agents or strong bases), and then with the desired corresponding alkyl halide. More recently, this strategy was put to use for making para-aramid nanofibers by electrospinning.[9] The dissolution step apparently turned out to be more involved than what the original reports from the 1980s and 1990s would suggest, but they were able to make para-aramid nanofibers with propyl-functionalization with diameters 67.2 ± 21.5 nm to 1750 ± 377 nm by adjusting the polymer concentration. Although this modified para-aramid is likely less strong than unfunctionalized para-aramid mechanically, earlier reports suggest the thermal stability is often preserved with these alterations. We propose to test the preparation of such nanofibers and the optimization of their spinning

conditions for our controlled single nanofiber process. We could also try the same with meta-aramid (PMIA), which would likely be easier functionalize.[8]

6.2.2 Ligand Additives for Liberating Chloride Ions from CuCl$_2$ for making Highly Metal Doped Solutions

This proposal concerns the making of a highly CuCl$_2$ doped solution for electrospinning PMIA. As described in Section 5.3.2, such a solution would be quite advantageous for the electroless seed layer deposition for the reel-to-reel process. As described there, we can only dope up to ~1.5 wt. % CuCl$_2$ into the solution and need to maintain the full original concentration of CaCl$_2$ at 8 wt. %. CaCl$_2$ reportedly serves as a chloride source for interfering with the H-bonding in PMIA and allowing it to dissolve,[10] but CuCl$_2$ curiously does not provide the same effect (Figure 5.9, leftmost photo). In fact, we tested many other chloride salts, such as NH$_4$Cl, KCl, CoCl$_2$, BaCl$_2$, SnCl$_2$, and found that none of them lead to dissolution of PMIA, and the only other salt we are aware that has this solubility enhancement is LiCl. This is quite curious, as some of these salts, including CuCl$_2$, are readily and highly soluble in the solvent DMAc, whereas CaCl$_2$ is not nearly as soluble in DMAc by itself. 8 wt. % CaCl$_2$ we are using is quite above the solubility of this salt in neat DMAc (4.13 g / 100 g solvent at 25 °C),[11] and the salt only dissolves as much in the presence of PMIA.

It appears the solubility enhancement by CaCl$_2$ and LiCl is due to some free Cl$^-$ ions, but that the chloride ions are too closely associated with the cations for the other chloride salts. If that is the case, it might be possible to loosen up the chloride ions in

CuCl$_2$ by adding extra ligands that Cu^{2+} might prefer binding. By adding such ligands in a stoichiometric fashion, we could realize a PMIA solution with (~ 8 wt. %) CuCl$_2$ and no CaCl$_2$ that is spinnable. This would likely fulfill the increase in CuCl$_2$ we seem to need while also getting rid of the hygroscopic CaCl$_2$ in the fibers. We propose adding a ligand with a strong affinity to Cu^{2+} to bring prepare such a solution. We could try ethylenediaminetetraacetic acid (or its desired sodium salt) first and test other ligands as needed.

6.2.3 Conductive Polymer to Blend with PMIA or Coaxial Spinning

We are interested in making inherently conductive polymer nanofibers for electroplating by using conductive polymer nanofibers through different approaches: (1) We could blend one of the stronger polymers, e.g. PMIA or P84, with a conductive polymer in solution and spin that. We would check if the phase behavior of the polymer mixture is such that a conductive path can percolate through the nanofibers while maintaining enough of the high-strength phase to have handleable suspended nanofibers. (2) We could acquire a co-axial spinning nozzle and make nanofibers with a strong polymer core and a conductive polymer outer surface. (3) We could try to get oxidative-CVD conductive polymer coatings onto the nanofibers.[12-15] With facile access to such a setup, this would likely be fast enough to support the scaling-up for electroplated nanowires and microwires as it can be faster than sputtering.

6.3 References

1.   Chung, G. S.; Jo, S. M.; Kim, B. C., Properties of carbon nanofibers prepared from electrospun polyimide. *Journal of Applied Polymer Science* **2005,** *97* (1), 165-170.

2.   Gong, G.; Wu, J., Novel Polyimide Materials Produced by Electrospinning. In *High Performance Polymers - Polyimides Based - From Chemistry to Applications*, Abadie, M., Ed. InTech: 2012.

3.   Kim, J.-S.; Reneker, D. H., Polybenzimidazole nanofiber produced by electrospinning. *Polymer Engineering & Science* **1999,** *39* (5), 849-854.

4.   Jahangiri, S.; Aravi, İ.; Şanlı, L. I.; Menceloğlu, Y. Z.; Özden‑Yenigün, E., Fabrication and optimization of proton conductive polybenzimidazole electrospun nanofiber membranes. *Polymers for Advanced Technologies* **2018,** *29* (1), 594-602.

5.   Kakzau, A. Aromatic polyamide nanofiber and fiber structure containing the same. US20100288692 A1, 2010/11/18/, 2010.

6.   Takayanagi, M.; Katayose, T., N-substituted poly(p-phenylene terephthalamide). *Journal of Polymer Science: Polymer Chemistry Edition* **1981,** *19*, 1133-1145.

7.   Noh, S.-H.; Araki, K.; Seno, M., N-substituted poly (p-phenylene terephthalamide) film: surface characteristics and liquid-crystal alignment with high pretilt angles. *Journal of Materials Chemistry* **1993,** *3* (7), 755-759.

8.   Suzuki, K.; Ikeda, I.; Yamamoto, I.; Okubo, M., Homogeneous alkylation of poly (m-phenylene isophthalamide). *Polymer Engineering & Science* **1996,** *36* (10), 1410-1413.

9.   Yeager, M. P.; Hoffman, C. M.; Xia, Z.; Trexler, M. M., Method for the synthesis of para-aramid nanofibers. *Journal of Applied Polymer Science* **2016,** *133* (42).

10.   Yao, L.; Lee, C.; Kim, J., Fabrication of electrospun meta-aramid nanofibers in different solvent systems. *Fibers and Polymers* **2010,** *11* (7), 1032-1040.

11.   *Alkali metal, alkaline-earth metal, and ammonium halides. Amide solvents*. 1st ed ed.; Pergamon Press: Oxford ; New York, 1980; p 354.

12.   Tenhaeff, W. E.; Gleason, K. K., Initiated and Oxidative Chemical Vapor Deposition of Polymeric Thin Films: iCVD and oCVD. *Advanced Functional Materials* **2008,** *18* (7), 979-992.

13.   Allison, L.; Hoxie, S.; Andrew, T. L., Towards seamlessly-integrated textile electronics: methods to coat fabrics and fibers with conducting polymers for electronic applications. *Chemical Communications* **2017,** *53* (53), 7182-7193.

14.   Zhang, L.; Fairbanks, M.; Andrew, T. L., Rugged Textile Electrodes for Wearable Devices Obtained by Vapor Coating Off-the-Shelf, Plain-Woven Fabrics. *Advanced Functional Materials* **2017,** *27* (24), 1700415.

15.   Zhang, L.; Baima, M.; Andrew, T. L., Transforming Commercial Textiles and Threads into Sewable and Weavable Electric Heaters. *ACS Applied Materials & Interfaces* **2017,** *9* (37), 32299-32307.

Appendix A: Materials and Methods

Materials

Poly(m-phenylene isophthalamide) (PMIA) was purchased from Sigma-Aldrich (Product No: 446521-100g, MW $\approx$ 81,000). It was dried at 140°C in open air before making a solution. It comes in chopped fiber form. $CaCl_2$ (Product No: 746495-100g) and N,N-dimethylacetamide (DMAc) (Product No: D137510-500mL) were also purchased from Sigma Aldrich and were used without further purification.

Sputtering materials were provided by Harvard's Center for Nanoscale Systems. Copper thermal evaporation source was purchased from Kurt J. Lesker (99.99% pure, Product No: EVMCU40QXQD).

The Co DLE-CVD precursor used in this work is a cobalt amidinate, bis(N,N'-diisopropylacetamidinato) cobalt(II) ($CoC_{16}H_{34}N_4$) from Strem Chemical Company, which has been reported previously.[1] Tetradecane purchased from MilliporeSigma Chemical Co. was distilled from sodium to remove moisture before being used as solvent for the Co amidinate precursor.

For the ALD of $MnSi_xO_y$, tris-tert-pentoxysilanol (TPS) was purchased Sigma-Aldrich (Product No: 553441). Manganese (II) bis(N,N'-di-tert-butylacetamidinate) ($Mn(AMD)_2$) was acquired from Strem Chemical Company and was also previously reported.[1]

Nanofiber Sample Preparation

12.0 - 18.0 wt. % PMIA and 8.0 wt. % CaCl2 solutions in DMAc were prepared in 20 mL glass scintillation vials with stirring at 140°C for at least 24 hours. PMIA was typically dissolved within one hour after drying. Green Sm-Co stir bars (Sigma-Aldrich, Product No: Z671592) were used to stir the viscous solutions, and Teflon sealed caps (Qorpack, VWR Catalogue No: 16161-188) were screwed onto the scintillation vials to prevent leakage at this high temperature. 12.0 wt. % PMIA solution was used to generate fibers for the TGA experiments. Most of the optimized fiber processing was carried out with 17.5 wt. % PMIA solution.

Electrospinning was done with a commercial climate-controlled electrospinner system (EC-CLI, IME Technologies). The climate controller was connected to a compressed dry air line fitted with an additional dehumidifier (Fiber Dry Filter FMDR 301-03-AD, PISCO) that reduced the chamber humidity down to 2-3% and then re-humidified it to a controlled, preset level. Polymer solution was loaded into a plastic syringe and delivered to the nozzle via polytetrafluoroethylene tubing using a syringe pump. The nozzle-to-collector distance was varied between 4 and 12 cm. In general, PMIA fibers were spun from a single solution droplet at the nozzle without continuous pumping during the experiment. (For more continuous spinning of a yarn of fibers, one would need to pump the solution at about 120 µL/h based on our fiber generation rate.)

Electrospinning was initiated by applying a +12 kV voltage to the nozzle with respect to the grounded collector. After the jet was initiated, fiber diameter and alignment

were optimized by lowering the voltage to as low as 5-6 kV without stopping the jet. Once the voltage was turned on at 12 kV, a droplet at the nozzle typically grew and ejected after a few seconds, to form a continuous jet. A rotating drum collector (EM-RDC, IME Technologies) covered with aluminum foil was used to prepare mats of aligned fibers or a rotating spoked-drum collector (EM-RTC with EM-PSD, IME Technologies) with custom windshields was used to prepare single fibers with rotation speeds up to 2500 rpm. (The spoked-drum collector originally comes with 12 spokes, and every other spoke was removed to only have 6 spokes with increased separation.) For making single fibers, the jet was initiated at one end of the collector, and once the jet was stabilized at a selected lower voltage, the nozzle was translated to the other end of the collector (using EM-TNS, IME Technologies) to separate the fibers along the collector. Voltage was manually turned off as soon as the nozzle reached the end of the collector. (If the jet was allowed to continue beyond one pass over the collector, more fibers got deposited that typically crossed and/or stuck to the existing fibers.) A typical experiment lasted under one minute. There was a messy region of fibers around where the jet is initialized on the collector, while the aligned single fibers covered the rest of the collector. The area of the messy fiber region decreased with decreasing nozzle-to-collector separation.

After initial optimization, most fiber samples were spun while keeping the chamber around 10% relative humidity (RH) and 24°C. A 17.5 wt. % PMIA and 8.0 wt. % $CaCl_2$ solution in DMAc was used for most of the experiments. Nozzle-to-collector

126

distance was typically kept at 8.0 cm. After the collector was brought up to speed at 2500 rpm, the jet was initiated at 12 kV, then brought down to 10 kV. The translating nozzle was then rapidly scanned along the collector at up to 300 mm/s, and once it arrived at the end of its motion, the voltage was manually turned off.

Electrospinning was initiated by applying a +12 kV voltage to the nozzle with respect to the grounded collector. After the jet was initiated, fiber diameter and alignment were optimized by lowering the voltage to as low as 5-6 kV without stopping the jet. Once the voltage was turned on at 12 kV, a droplet at the nozzle typically grew and ejected after a few seconds, to form a continuous jet (Video S2). A rotating drum collector (EM-RDC, IME Technologies) covered with aluminum foil was used to prepare mats of aligned fibers or a rotating spoked-drum collector (EM-RTC with EM-PSD, IME Technologies) with custom windshields was used to prepare single fibers with rotation speeds up to 2500 rpm. (The spoked-drum collector originally comes with 12 spokes, and every other spoke was removed to only have 6 spokes with increased separation.) For making single fibers, the jet was initiated at one end of the collector, and once the jet was stabilized at a selected lower voltage, the nozzle was translated to the other end of the collector (using EM-TNS, IME Technologies) to separate the fibers along the collector. Voltage was manually turned off as soon as the nozzle reached the end of the collector. (If the jet was allowed to continue beyond one pass over the collector, more fibers got deposited that typically crossed and/or stuck to the existing fibers.) A typical experiment lasted under one minute. There was a messy region of fibers around where the jet is

initialized on the collector, while the aligned single fibers covered the rest of the collector. The area of the messy fiber region decreased with decreasing nozzle-to-collector separation.

Thin Film Depositions

Fibers were transferred onto fixtures for deposition as described in the Supporting Information. Sputter coating was performed on a variety of different systems: Orion 3 and ATC (AJA), or EMS300T D and EMS150T ES (EMS). Thermal evaporations were done with Sharon thermal evaporation systems. Aluminum oxide and hafnium oxide layers were deposited in a Savannah ALD S-200 system (Cambridge Nanotech).

Cobalt metal direct-liquid-evaporation chemical vapor deposition (DLE-CVD) was conducted using a homemade deposition system. The DLE deposition process followed the same procedures and conditions previously reported by our group.[2-3]

Manganese silicate ($MnSi_xO_y$) deposition via ALD was previously reported by our group.[4] We deposited MnSixOy using a custom-built hot-walled ALD reactor. Purified nitrogen gas was used for delivering precursors and purging between precursors. Each ALD cycle consisted of 1 s $Mn(AMD)_2$ vapor and 3 s TPS vapor with 30 s purging between each precursor cycle. The substrate temperature was 350 °C.

Instruments

FEI Helios NanoLab 660 DualBeam SEM and FIB was used for imaging and cross sectioning of the samples. Images were obtained by attaching fiber or nanowire samples to an SEM stub using multiple strips of double-sided carbon tape. Nanowires were often imaged at locations where they are suspended between two strips of carbon tape to attain blurred or dark background. For cross-sections, the sample was tilted to 52° at which point the FIB in this system becomes perpendicular to the surface of the sample, allowing a straight cut of the wire. After the wires were cut using FIB, SEM images of the cross-sections were collected at this 52° tilt angle. Thermogravimetric analysis was performed with TA-Instruments Q50 under nitrogen atmosphere. Electrical characterization was performed on a Signatone S-1160 Probe Station. Image analysis was performed on MATLAB (version R2017b).

Appendix A References

1.   Lim, B. S.; Rahtu, A.; Park, J.-S.; Gordon, R. G., Synthesis and Characterization of Volatile, Thermally Stable, Reactive Transition Metal Amidinates. *Inorganic Chemistry* **2003,** *42* (24), 7951-7958.

2.   Yang, J.; Li, K.; Feng, J.; Gordon, R. G., Direct-liquid-evaporation chemical vapor deposition of smooth, highly conformal cobalt and cobalt nitride thin films. *J. Mater. Chem. C* **2015,** *3* (46), 12098-12106.

3.   Feng, J.; Gong, X.; Lou, X.; Gordon, R. G., Direct-Liquid-Evaporation Chemical Vapor Deposition of Nanocrystalline Cobalt Metal for Nanoscale Copper Interconnect Encapsulation. *ACS Applied Materials & Interfaces* **2017,** *9* (12), 10914-10920.

4.   Gordon, R.; Sun, L.; Chen, Q.; Park, J.-S.; Kim, S. In *ALD of Manganese Silicate*, 2015; 2015; pp 1-20.

Appendix B: Molecular Weight Determination of PMIA

Recognizing that molecular weight is a key parameter in improving the reproducibility of our results, we carried a molecular weight determination for the Nomex batch we have been using based on viscosity measurements. Since the rheometer we had access to does not have a humidity-controlled housing, and the polymer would often precipitate over the course of measurements, and we were only able to get reliable data now that the weather is dry. We prepared five Nomex solutions with varied concentrations in 5 wt. % LiCl/DMAc and measured their viscosity (Figure B-1). Considering the shear rate window where the readings were stable, we calculated the intrinsic viscosity as 1.42 dL/g. For these solution conditions, K and α coefficients for the Mark-Houwink equation of the form

$$[\eta] = K \overline{M}_w^a$$

have been reported as 3.7 x 10-4 and 0.73, respectively,[1] which gave a molecular weight of 81,000. Being able to report this value will improve the reproducibility of our electrospinning results.
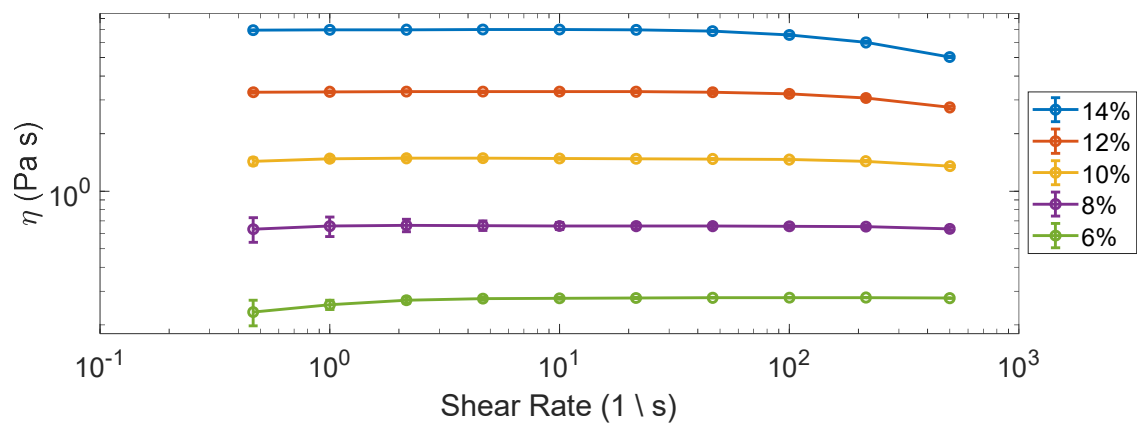
Figure B-1. Viscosity of PMIA solutions with varied concentrations in 5 wt. % LiCl

DMAc. Each point is the average of three measurements.

References

1.   Harwood, D. D.; Fellers, J. F., Imposed Polyelectrolyte Behavior of Poly(m-phenyleneisophthalamide) in LiCl/Dimethylacetamide. *Macromolecules* **1979,** *12* (4), 693-697.

Appendix C: Humidity Content in PMIA Solutions

Solution preparation in Appendix A points out that PMIA bulk fibers are dried at 140 °C before preparing a solution. This step was added because of some discrepancies observed while dissolving undried PMIA in the DMAc/CaCl$_2$ solvent system as well as the final solution's electrospinning performance. When the polymer solution is prepared from undried PMIA bulk fibers during a humid weather, the polymer solution has more moisture in it to begin with, which seems to promote ribbon formation. In one extreme case, the concentrations that regularly yielded a clear solution before even resulted in a partially cloudy suspension. This was caused by the PMIA starting material being hygroscopic itself, containing about ~6 wt. % humidity which increases with air humidity. When a partially wet solution is used for the spinning, its clouding point becomes lower. We have characterized the water content in these solutions with ATR-FTIR and found stronger water peak intensities for solutions prepared during the a more humid season (Figure C-1). We found that this peak intensity can be brought back down by drying the PMIA bulk material before preparing solution. This improves the reproducibility of the nanofiber making process and the resulting fiber morphology.
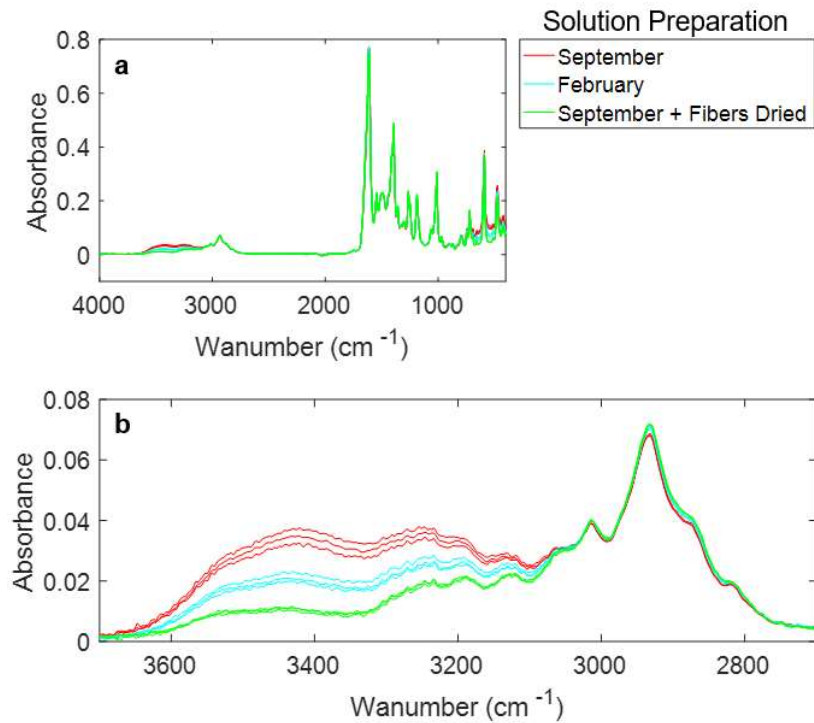
Figure C-1. FTIR spectra of the PMIA electrospinning solutions. (a) Overview of the whole spectrum. (b) Zoom in of the region showing the aliphatic C-H stretching and water peaks. Red lines correspond to a solution prepared in September of 2017 when the outside humidity was higher. Blue lines correspond to a solution prepared in February of 2017 under a dryer environment, showing reduced intensity from the water peaks. Green line corresponds to a solution prepared in September of 2017 after the polymer starting material is first dried, showing the lowest moisture content in the solution.

Appendix D: Notes on Fiber Handling

We used custom frames of varied dimensions for taking the fibers off the spoked collector and holding them during depositions. The spoke-to-spoke separation was 4.5 cm (after we removed every other spoke to increase this separation, Figure 1.7-a) on the collector. For getting the highest yield, we placed acrylic frames of matching width on three sides of the collector first (Figure 1.6-b). Then, narrower frames with double-sided tape along their long edges were brought into contact with the fibers to collect them. Without adding the larger holders that press onto the fibers at their points of contact with the spokes, harvesting fibers from one side of the collector often causes fibers to get pulled from adjacent faces of the 6-sided collector.

It is best to break the fibers away from the frames forcibly during transfer, as merely bringing the holder with tape in contact with the fibers and then pulling away may leave fibers behind; i.e., the strength of the adhesive (for a tape that is often ¼" wide) is often not enough to break the fibers when pulled away.

For PVD, we either added another top frame to the existing double-sided tape, or we added screws on four corners of a frame where we had threaded holes (Figure 1.7-c). This was done so that the holder can be flipped between two PVD depositions to improve conformality without bringing the fibers in contact with a surface to which they might possibly adhere. Qualitatively, we found that the fibers can be brought into contact and lifted back from smooth Si wafer or glass surfaces, but if they get into contact with a

plastic surface, they often strongly adhere to it and break off the holder. Most of the holders and screw caps we used are 1/8" thick, but we also used 1/16" thick top and bottom frames for certain sputtering experiments that required thinner samples.

We used double-sided Kapton tape (McMaster-Carr, Product Numbers 7361A11 or 7361A12) for most of our deposition experiments. Especially during dry seasons, Kapton tape often becomes non-sticky, in which case we revived its adhesiveness by wetting it with isopropanol before starting to collect fibers. For parts that did not need to go into a deposition chamber (transfer holders, fixing holders to surfaces, etc.), we used a fiber glass reinforced cloth masking tape (McMaster-Carr, Product Number 7577A1) which is more conveniently handled and can be removed from most surfaces without leaving a residue.

Between experiments, we kept the frames in petri dishes that we often stored in a desiccated environment or vacuum sealed in a plastic bag with some silica gel packs. When first placing the fibers into a petri dish, it is important to get rid of static charging by applying an anti-static gun. Both the insides of the bottom and top components of the petri dish need to be thoroughly neutralized; otherwise fibers sag and become slack. Brief tests show this sagging is reversible, but if left sagging, the fibers can slip on the tapes from the sides and sag permanently; this adds a complication to the conformality of a CVD coating. Especially when using wide gapped (Figure 1.7-c) or thin (1/16") holders, this sagging can cause the fibers to touch the bottom of the plastic dish, at which point they become strongly attached and eventually break.

136

For ALD and CVD processes operating at high temperatures, we needed to use a mechanically clamped holder without glue, as discussed in the main text. Our clamped holder design consists of 3.5"x1" frames with a central gap of 0.52" with three holes along the long edges that are threaded for the bottom part and through holes for the top part. More holes increase grasping efficiency at the cost of potentially breaking fibers in their vicinity. We found it necessary to add a layer of Kapton film (typically by attaching it to the bottom frame with double-sided tape on the edges) that serves as a gasket. Without that, we more commonly observe fibers breaking during depositions – especially for the CVD processes that operate at a larger flow rate of gases. Fibers were first transferred onto an acrylic frame with a gap that is larger than the mechanical holder. We used the same acrylic holders with a width matching the spoke separations that we described above for fixing the 6 sides. The bottom part of the clamped holder is fixed on a surface (using large pieces of double-sided tape). The intermediate holder is then placed so the fibers stretch along the bottom part of the holder, and the intermediate tape is also fixed on the same surface. The top frame is then lowered gently onto the bottom part, sandwiching the fibers in the middle (Figure 1.6-c), and screwed in place. Afterwards, the transfer holder can be removed, breaking fibers outside the clamped region seemingly without affecting the fibers within. If the fibers are held strongly, we can avoid fibers breaking during CVD. Figure 1-d shows a mechanically clamped holder with fibers after being coated with CVD. Apart from serving as a pliable gasket layer, the polymer film might also be enhancing grasping efficiency due to strong van der Waals forces with the fibers. We found that after depositions, if the top frame is gently removed, many fibers

often remain suspended and attached to the Kapton film on both sides (though they certainly break in the absence of a Kapton film).